DEVELOPMENT OF A GOLD NANOPARTICLE BASED COLORIMETRIC SENSOR KIT FOR THE ANALYSIS OF SODIUM CHLORIDE LEVELS IN SEAWATER

by

Andile Truelove Mbambo

Dissertation submitted in fulfilment of the requirement for degree

MASTER OF APPLIED SCIENCES

in

CHEMISTRY

In the

FACULTY OF APPLIED SCIENCES

of the

DURBAN UNIVERSITY OF TECHNOLOGY

Supervisor: Dr LAWRENCE M. MADIKIZELA

Co-supervisor: Dr PHUMLANE S. MDLULI

2018

DECLARATION

I hereby declare that this dissertation, which I herewith submit for the research qualification

MASTER OF APPLIED SCIENCES IN CHEMISTRY

to the Durban University of Technology, Department of Chemistry, is apart from the recognized assistance of my supervisors, this is my own work and has not been previously submitted by me to another institution to obtain a research diploma or degree.

_____ on this **11** day of **April 2019**

Ms. A. T. Mbambo *(Candidate)*

_____on this **11** day of **April 2019**

Dr. L. M. Madikizela *(Supervisor)*

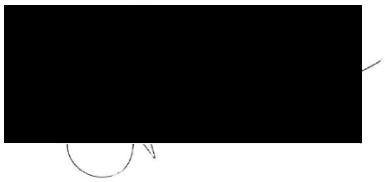

_____on this **11** day of **April 2019**

Dr. P. S. Mdluli *(Co-supervisor)*

ACKNOWLEDGEMENTS

I would like to state my gratitude and sincere thanks to my prestige supervisor Dr. Lawrence M. Madikizela, for his exemplary guidance and encouragement throughout the project. Special thanks to my co-supervisor Dr. Phumlane S. Mdluli for allowing me to learn a lot of new things about nanochemistry and for the accommodation to grow and learn from the mistakes I made in the project in order to successfully complete it. I would like to acknowledge National Research Foundation (NRF) of South Africa through post-graduate collaboration funding between Durban University of Technology and University of KwaZulu-Natal for financial support of this project.

I am very thankful to Durban University of Technology, in particular Department of Chemistry's spectroscopic and chromatographic laboratory staff for permitting me to access their research instruments. Assistance from Mrs Devrani "Avy" Naicker and Mr Sandile Majola is highly appreciated. I also like to express my sincere gratitude to Mrs. Maureen Msimango from Mangosuthu University of Technology, who permitted me to carry out the FTIR analysis in her laboratory. I am also thankful to Dr. Michael M. Shapi from Mangosuthu University of Technology for his advice and support throughout my studies and career in Chemistry.

Ms Lethiwe D. Mthembu a PhD student at Durban University of Technology, thank you for your support and for being more than a friend, I would not have made it this far if it was not for your help. Many thanks to Mr S'busiso M. Nkosi for the valuable discussions, association and generous suggestions. Mr Syabonga Gumede thank you for the support and everything you have done for me may God bless you abundantly. Ms Slungile Nxumalo (MAppSc student) and PhD student (Mr. Stanley Onwubu) are acknowledged for their help. I would also like to extend my thanks to the Durban University of Technology for allowing me to pursue my studies. I cannot forget to thank my family, my friends especially Ms Vuziwe Siyotula who were of great moral and practical support during my studies. However, if it were not for God Almighty none of it all would have been a success, Lord, I thank you for the strength and patience through it all.

DEDICATION

This dissertation is dedicated to:

- My mother, **Dumazile Harriet Mbambo,** who always believed in me and understood who and what I wanted to be in life.
- My sister, **Lisa Mbambo,** who is my source of strength.
- My late sister, **Sheryl "Shie" Mbambo (1979-2017),** who was the loudest and free-spirited person in the family, may her soul rest in peace.
- My late father, **Thembelani Nqabeni (1950-2005),** hope you are proud wherever you are dad and may your soul be at peace Ngcitshane!

ABSTRACT

In this study, colorimetric assay was used to develop a gold nanoparticle enabled optical sensor for the analysis of sodium chloride in seawater. Sodium chloride has a major effect in the seawater's salinity level, thus, this has led to the design of a colorimetric device that is selective to sodium chloride, which can be used for both seawater and the nearby estuarine water. Flocculation assay based on gold nanoparticles was used to optimise the colorimetric response of the selected sodium chloride concentration range (5-40 ppT) for the developed kit. Polydispersed and stable gold nanoparticles were synthesized via the Turkevich method using tri-sodium citrate as a reducing and capping agent. The optical properties of the as-synthesized gold nanoparticles were characterized by Ultra-Violet- Visible spectroscopy where the existence of the Surface Plasmon Resonance (SPR) absorption peak was observed at 525 nm. Transmission Electron Microscopy (TEM) image revealed the morphology of the gold nanoparticles to be isotropic/ spherical with a calculated average size of gold nanoparticles which was found to be 7 nm. The introduction of sodium chloride to gold nanoparticles solution resulted in aggregation which was indicated by the change of colour from red to blue.

Scanning Electron Microscopy (SEM) images confirmed the spherical morphology of the gold nanoparticles. The gold nanoparticles with sodium chloride image showed crystals of the salt covering the aggregated gold nanoparticles inferring that the tri-sodium citrate barrier on the surface of the nanoparticles had been broken. In the Fourier-transform Infrared Spectroscopy spectrum (FTIR), the existence of hydroxyl was observed in the gold nanoparticles solution at 3540 cm^{-1} due to the deionised water used in preparation of all solutions. The carbonyl groups observed at 1782 cm^{-1}, 1520 cm^{-1} and 1290 cm^{-1} in the gold nanoparticles spectrum were due to the citrate capping the nanoparticles. Ultraviolet-Visible Spectroscopy (UV-Vis) spectroscopy was also used to validate the colorimetric method as the application of gold nanoparticles is based on solution colour convergence from wine red to blue upon analyte introduction. The colorimetric assay of the sodium chloride concentration range gave distinguishable colour shades which were visually observed. The intensity of the colour in standard solutions increased as the concentration of NaCl was

increased. A red shift was observed in the UV-Vis spectrum due to the increase in sodium chloride concentration. A decrease in the 525 nm SPR peak was observed with an increase of another SPR peak at longer wavelengths around 660 nm. Images of the colorimetric assay were analysed using the Colorgrab application. Results of this analysis showed that the colour intensities in the Greyscale percentages were decreasing with increasing sodium chloride concentration and were in the range of 42.33-57.66%. The red green blue (RGB) colour model analysed by ImageJ software revealed that the red colour of the gold nanoparticles gradually disappeared with the development of the blue colour as the concentration of sodium chloride was increased in solution. *Commission Internationale d'Eclairage* (CIE) Lab colour management method validated the colour similarities and differences of the sodium chloride colorimetric assay. The sodium chloride quantification colour wheel/disk was then fabricated using the RBG colour model values.

The developed colorimetric device was applied to screen the level of salinity along the coastal seawater and estuaries of Durban in KwaZulu-Natal. Results of this colorimetric method had a linearity value of 0.9980, a detection and quantification limits of 1.18 ppT and 3.57 ppT, respectively. The concentrations of NaCl in the tested seawater and estuary samples were in the ranges of 30-35 ppT and 5-30 ppT, respectively. The measured concentrations of sodium chloride in water samples using the proposed colorimetric method were in agreement with those observed when using the traditional methods such as ion chromatography and titration. Overall, gold nanoparticles based colorimetric sensor used for the analysis of sodium chloride in seawater and estuarine water was rapid, cost effective, accurate, precise, sensitive, and selective.

TABLE OF CONTENTS

List of figures

List of tables

List of abbreviations

AuNPs - gold nanoparticles

SPR - surface plasmon resonance

LSPR - localised surface plasmon resonance

UV-Vis – Ulta-violet- Visible spectroscopy

ppT- parts per thousand

ppt - parts per trillion

*u*PAD – microfluidic paper analytical device

SEM - scanning electron microscopy

TEM - transmission electron spectroscopy

FTIR - Fourier transform infrared region

IC - ion chromatography

NaCl - sodium chloride

SWRCB - State Water Resources Control Board

SMCL - secondary maximum contaminant level

Cl^- - chloride ion

Na^+- sodium ion

Ca^{2+} - calcium ion

K^+ - potassium ion

Mg^{2+} - magnesium ion

SO_4^{2-} - sulphate ion

$AgNO_3$ - silver nitrate

$KCrO_4$ – potassium chromate

EWA - egg white albumin

App - application

RGB - red, green, blue

CIE - Commission Internationale d’Eclairage

WHO – World Health Organization

ANNEXURES

Annexure A: Lovibond results for the quantification of NaCl in standard solutions and samples.

Annexure B: Typical ion chromatograms for NaCl standard 40 ppm, seawater sample and estuarine water sample.

Annexure C: Map and sampling locations

Annexure D: Sampling No. 2; map of sample locations in Durban city in South Africa.

Chapter 1: Introduction

1.1. General introduction

Different coastal activities provide important economic and ecological facilities to humanity (Kildow *et al.* 2014; Sutton-Grier, Wowk and Bamford 2015). The ocean economy allows society to harness the functions of ecosystems and the services they provide (van Wyk 2015). This has caused an expansion in coastal populations, economic activity and coastal settlement growth in South Africa (Petersen *et al.* 2012). As a result, the South African government has invested approximately R24,569 billion to support and further improve the ocean economy through state development projects (Zuma 2014; Dorrington *et al.* 2018). Operation Phakisa a project that deals with ocean economy and aquaculture transformation has created thousands of job opportunities in various sectors for low and lower middle-income households in coastal areas of South Africa, through trading different edible fish species, abalone, mussels, shrimp, oysters etc. (van Wyk 2015; Sink 2016).

The coastal areas are at the forefront of climate change leading to the vulnerability of the poor populations living in the low-elevation coastal region. The coastal areas of KwaZulu-Natal, Western Cape and Eastern Cape in South Africa have been reported to be experiencing sea floods (Hoogendoorn, Grant and Fitchett 2016). This was assumed to be due to climate change elevating sea level rise, which in turn caused unusual height of tidal water (Bornman *et al.* 2016; Yang and Chui 2017). Salinity the composition of seawater (usually expressed as sodium chloride/Chloride concentration in the water) was reported to influence evaporation rates which contributed to sea level rise (Vineis, Chan and Khan 2011; Girjatowicz and Świątek 2016). Long-term climatic changes with adverse impacts, such as sea-level rise, saline intrusion and erosion also lead to the disappearance or degradation of the coastal and near-shore ecosystems (Rasmussen *et al.* 2013; Yang and Chui 2017) . These include estuaries, mangroves, marsh, coral reefs, oyster reefs, seagrass beds and barrier islands (Bornman *et al.* 2016). For example, mangroves provide an important natural barrier that protect against hazardous events from sea floods (Wells and Ravilious 2006). In many remote and rural coastal areas, they may be the only form of protection against storms/floods available for the poor (Wells and Ravilious 2006). The rise of

sea levels will likely pose the risk of the further penetration of salt water with more severe intensity in coastal areas (Rasmussen *et al.* 2013). As sea level rise gradually, it will likely pose the risk of the further penetration of salt water with more severe intensity in coastal areas (Yang and Chui 2017), therefore, salinity becomes an important parameter to measure in seawater due to its negative effects on the environment. Highly saline water from sea floods is responsible for the deterioration of groundwater quality in numerous coastal rivers worldwide and create a serious threat to local groundwater resources, as well as to the provincial economy of coastal areas (Han, Post and Song 2015a; Knüppe and Meissner 2016). Developing countries like South Africa are facing challenges in producing enough clean drinking water for its residents, therefore, to assist alleviate these negative effects associated with seawater intrusion, a well-designed method for assessing and monitoring could be implemented. The implementation of the method is associated with substantial benefits for the environment and the local economy. In this perspective, the present study develops a gold nanoparticle based colorimetric sensor for the analysis of sodium chloride which represents salinity levels in seawater. The device can be used to assess any indicative changes in salinity prior to seawater flooding.

1.2. Description of sodium chloride and its analysis

NaCl makes up about 86% of seawater salinity level, as a result, any fluctuations in its concentration was reported to change the salinity of seawater (Pawlowicz 2012). A report by Castro and Huber had a pie graph which is shown in **Figure 1.1**, it illustrated the percentage distribution of all ions involved in the composition of seawater salinity (Castro and Huber 2005). The pie graph in their work showed that there was a high salinity compared to river or tap water due to high salt content in the water (Han, Post and Song 2015b). Changes in sodium chloride concentration in seawater has been reported to have a potential of promoting seawater flooding through sea level rise (Hoggart *et al.* 2014). As a major component of salinity, NaCl was perceived to play a significant role in the sea level rise, as a result, it was responsible for high tide waves that could lead to flooding (Buchori *et al.* 2018). Fluctuation in NaCl levels within the seawater environment has been showed to affect certain marine species and it was as well demonstrated that it could limit their life span in the water (Bielmyer-Fraser *et al.* 2018). Apart from these challenges, removal of NaCl in seawater is currently one

of the augmented processes to produce fresh drinking water for many countries situated along the coastal areas of the oceans (Wu *et al.* 2018).

Desalination techniques however are complicated as they involve removal of high quantities of NaCl in water and the use of expensive membranes (Meng *et al.* 2018; Wu *et al.* 2018). Efficient removal of NaCl from water needs to be monitored using suitable analytical methods. A report by Robaina has showed that NaCl could be quantified with relation to the concentration of chloride ion. Thereafter, the concentration of the ion could be used to calculate the concentration of the whole compound (Robaina *et al.* 2016). There are other reported methods that are based on titration and ion chromatography (IC) for analysis and quantification of NaCl (Silveira, de Caland and Tubino 2014; Robaina *et al.* 2016; Asakai 2018). These methods, however involves long complex calculations not to mention the toxic waste generated from titration and the technical personnel required for IC operation along with its high maintenance and time-consuming analyses. In this study, the colorimetric method was developed. The developed method involved the synthesis and application of gold nanoparticles (AuNPs) as colour enhancers and detecting sensors for different sodium chloride concentrations in seawater. This was a better approach for identification and quantification of NaCl as it offered the overall concentration of NaCl in water. Furthermore, human and systematic errors were limited and the analysis method did not use any toxic chemicals.

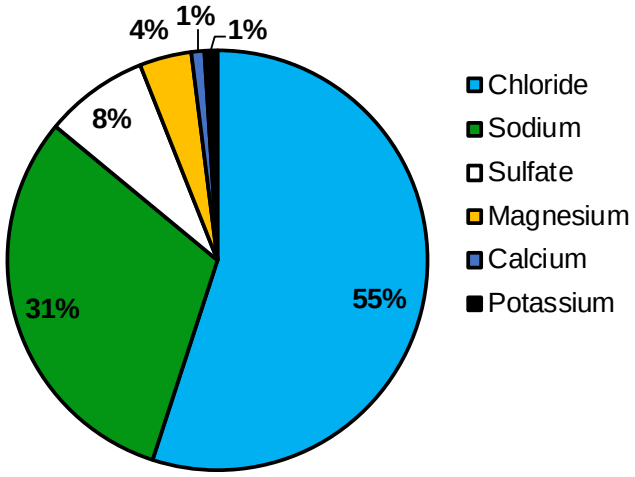

Figure 1. 1 : Pie graph of the distribution of ions for salinity composition in seawater (Castro and Huber 2005).

1.3. Gold nanoparticles and their selection in colorimetric assays

Nanoparticles are nanomaterial that are reduced to nanometer size range of less than 100 nm. Nanoparticles have improved physical, chemical and optical properties compared to that of the material in its bulk state. The application of nanoparticles in scientific research have received great attention in vast technological applications in chemical industry, medicine, food industry, etc. (Alim *et al.* 2018; Chen, Zhou and Zhao 2018). Nanoparticles are renowned in the chemical industry for providing easy and practical solutions for complex analysis. They have been applied as colorimetric detecting sensors for different organic and inorganic compounds (Lazarus and Fedder 2014; Lai, Chang and Wang 2017). They have provided a solution for simple, rapid, reliable and cost-effective analysis. Due to less-toxic nature of gold and its inert core, gold nanoparticles have been the environmental cautious choice amongst other nanoparticles, as a result they have been used to various studies such as drug delivery, catalytic studies, biological and chemical sensors etc. (Martínez-Barrera *et al.* 2018; Thambiraj, Hema and Ravi Shankaran 2018).

The solution of gold nanoparticles is red in colour due to the Surface Plasmon Resonance (SPR) as it scatters light in visible and near IR region. For this reason, gold nanoparticles have been deemed to be an ideal candidates in the colorimetric assay development (Aldewachi *et al.* 2017). The characteristic change of the aggregation of gold nanoparticles was observed with the red-shift of the Localised Surface Plasmon Resonance (LSPR) peak to longer wavelengths in the spectrum (Bonyár *et al.* 2018). Li and co-workers have shown that in order to have an improved application of the gold nanoparticles, it was desirable that the majority of the nanoparticles are in the same size and shape in solution. This was to ensure that the strength and nature of interactions between nanoparticles and the target compound are unaltered (Li *et al.* 2018).

1.4. Characterization of gold nanoparticles

Gold nanoparticles of different morphology, size and chemical properties can be synthesized by the use of chemical reduction method. Apart from the size and radius of the metal nanoparticles, there are many other factors such as chemical condition of

environment and temperature of system which were reported to alter the size and shape of the nanoparticles produced (Dube *et al.* 2018; Kusumawati, Nishio-Hamane and Sasaki 2018). Therefore, it is important to determine the size and shape of the gold nanoparticles to assess the effect of the above-mentioned conditions, to confirm a successful synthesis and the applicability of the nanoparticles in the study. Different techniques can be used to characterize the synthesized gold nanoparticles, these involve Ultraviolet-Visible Spectroscopy, Fourier-transformer Infrared Spectroscopy, Scanning Electron Microscope and Transmission Electron Microscope. These techniques were applied in this study.

1.5. Analytical methods for quantifying sodium chloride

Array-based sensors featuring AuNPs provides ideal platform for inorganic compounds detection in environmental samples. Optical sensor for detection of NaCl has been developed and demonstrated by variation of the concentration (Fang *et al.* 2017). AuNPs and NaCl reactions have been demonstrated to effect the ionic strength in the detection of various chemical compounds (Kusumawati, Nishio-Hamane and Sasaki 2018). The array sensor was evaluated to show a distinctive colour pattern of each analyte due to the analyte interaction on the surface of AuNPs, leading to distinguishable identification of diverse analytes (Wei *et al.* 2017). The aggregation of the nanoparticles in solution is an indicator of a loss of dielectric environment on the surface of AuNPs, thus, resulting in a total colour change of solution from red to blue. Das and co-workers observed that the red-shift of the SPR absorption peak of AuNPs in the UV-Vis spectrum was increasing with increasing the optical density (Das *et al.* 2012; Seh *et al.* 2012). Currently, our literature survey found that there are limited published reports for the determination of NaCl in environmental seawater samples using AuNPs as colorimetric sensors, normally intensive laboratory-based procedures such as chromatographic and titration techniques are used.

In ion chromatography, the chloride or sodium ion is separated in the chromatographic column and quantified using the conductivity detector (Paull 2004). This analysis can be costly due to the expensive ion chromatographic parts such as the column. Precipitation titration is also used for the analysis of NaCl. In precipitation titration, sodium chloride content is measured by titrating and precipitating chloride with silver

ions (Ellwood, Hunter and Cunninghame 2003). In addition, both ion chromatographic and precipitation titration methods are time-consuming and require strong labour. AuNPs sensing, however, offer the advantages of simplicity, rapidness, cost effectiveness, reliable, and short analysis times. Moreover, analyte recovery in water samples is high even in the presence of interfering ionic species.

1.6. Problem statement

Sodium chloride is the fresh water-contaminating compound as it is the major constituent of seawater salinity (Li *et al.* 2017a; Gupta 2018). Changes in salinity contribute to sea level rise that cause high tidal waves. Sea level rise causes floods that penetrate the land and fresh water systems through estuaries, resulting into affecting the seawater and estuary ecosystem (Velez *et al.* 2016; Yang and Chui 2017; Senner *et al.* 2018). This may affect the country's economy as a result of the cost that government would incur in the rehabilitation process of the affected areas. It has been reported that salt intrusion by strong tidal waves into river systems could lead to mortality of different fresh water species as most of them are not used to high saline waters and the degradation of the estuary (Kijewska *et al.* 2016; Santos, Ramos and Bonecker 2017; Senner *et al.* 2018; Souid *et al.* 2018). Forbes and Demetriades (2008) have shown that the degraded estuaries had no balance in their ecosystem which resulted in the decline of ecotourism (Forbes and Demetriades 2008).

The importance of monitoring sodium chloride levels in seawater includes giving an indication whether there are any potential threats building up in the seawater (Al-Shammiri 2002; Millero *et al.* 2008; Girjatowicz and Świątek 2016). The lack of frequent monitoring of the seawater environmental parameters at field level and the devices associated with the evaluation processes is another major problem. Therefore, this raises a need for devices and convenient techniques that are applicable at a point-of-need, which are easy to use and interpret. Such methods are very vital for onsite detection of the salinity levels, especially during the desalination processes. The desalination process is vital in producing potable water to relieve the stress of the Southern African countries to meeting the demand for drinking water (Schoeman and Steyn 2003).

1.7. Justification

Various Laboratory-based analytical approaches have been reported for NaCl determination in seawater, these include ion chromatography and titration as the most popular analysis (Laux, Hemminger and Finlayson-Pitts 1994; Laikhtman, Riviello and Rohrer 1998). Prior to the analysis in ion chromatography, sample pre-treatment is required for isolation of target compound. IC technique is based on the separation of chloride through a low capacity ion-exchange stationery phase and a conductivity detector for continuous monitoring of the eluted ion (Robaina *et al.* 2016). Silver nitrate is used to quantify NaCl by relating the mole ratio of Ag^+ to that of Cl^- in solution at equivalence point of the precipitation titration (Ellwood, Hunter and Cunninghame 2003; Asakai 2018). The main disadvantages of this method are; the use of large volumes of highly toxic, expensive reagent ($AgNO_3$) which can lead to unmanageable and expensive waste disposal. Reports has shown that this method maybe subjected to human error leading to inaccurate results (Silveira, de Caland and Tubino 2014; Asakai 2018).

Therefore, development of a simple calorimetric device that is easy to use for the detection of sodium chloride in seawater is reported in this study. Such device had to meet certain expectations including high accuracy and precision, cost-effective, sensitivity, reliability, portability, robustness and shorter analysis times. In addition, the colorimetric technique is easy to use, does not require highly skilled personnel to perform analysis and the interpretation of results, and the visual colour indicator of the detected samples can be visually observed without the use of the sophisticated equipment. Moreover, the samples do not require any pre-treatment or dilution of water matrix. The Lovibond colorimetric device fabricated in this study is not limited to measure sodium chloride concentration in seawater only but it is applicable in estuarine and river water analysis as well. Additionally, the proposed procedure could play a vital role in environmental monitoring and management. It could assist in the collection of satellite reports and data modelling information for prediction of potential seawater disasters and identify the extent of salt intrusion into estuaries.

1.8. Aim:

This research is aimed at developing a colorimetric kit based on gold nanoparticles for the detection of sodium chloride in seawater and estuarine water.

1.9. Objectives:

- To synthesize gold nanoparticles using the Turkevich method and perform characterization using SEM, TEM, FTIR and UV-Vis spectrophotometer.
- To develop and fabricate a colour scheme disk that changes the colour intensity of the gold solution as the concentration of sodium chloride varies.
- To determine the concentrations of NaCl in seawater and estuaries using a fabricated disk alongside the traditional methods such as ion chromatography and precipitation titration.

1.10. Dissertation outline

This dissertation is presented in five chapters as described below:

Chapter 1

This chapter covers the introduction, problem statement, justification, aims and objectives of this study.

Chapter 2

This chapter outlines a literature review of the relevant reports that informs this study. Detailed literature related to sodium chloride and its analysis, gold nanoparticles and their different synthetic methods, sampling and sample preparation techniques. This chapter also include the background information of the characterization techniques used in this study.

Chapter 3

The detailed experimental procedures for the synthesis of gold nanoparticles, characterization techniques of the synthesized nanoparticles and the evaluation of sodium chloride in seawater as well as estuary water are outlined.

Chapter 4

This chapter outlines the results and discussion obtained from this study. These range from synthesis of gold nanoparticles and their characterization together with their application for the determination of sodium chloride in seawater as well as estuary water samples. The results on characterization of the synthesized gold nanoparticles, optimization of the optical measurements, that uses gold nanoparticles as sensors, selectivity, validation of the method and quantitatively determination of sodium chloride in water samples and statistical validation of gold nanoparticles are presented and discussed in this chapter.

Chapter 5

In this chapter the conclusions from the study was drawn, furthermore the recommendations are outlined as well.

Chapter 2: Literature review

2.1. Environmental concerns

A risk factor such as climate change is not only placing more people at risk of disasters, but the number of events giving rise to disasters are also increasing. Global statistics showed that the number of geophysical and hydrological events occurring each year continue to fluctuate within a relative narrow band (Jonkman 2005; Wei *et al.* 2018). Ocean related floods globally, and indeed in South Africa have been on the rise recently posing a threat to both society and the environment. The coastal areas of South Africa have been experiencing seawater flooding due to high sea-level rise which causes uncontrollable high tides that have penetrated into the land and nearby estuarine water outlets (Cooper 2001). Sea level rise has been suspected to be aggravated by changes in temperature and salinity levels. As sea level continues to rise due to fluctuations in key water parameters such as salinity, seawater-flooding events are expected to occur more frequently (Hoggart *et al.* 2014; Gingerich, Voss and Johnson 2017).

Previous studies conducted on the transience of different significant species in different estuaries proved that seawater is the primary source of sodium chloride contaminants, as a result, there is an extinction of some species (Velez *et al.* 2016; Zhang *et al.* 2016). Few reports have shown that in some instances the communities are affected by seawater flooding of the coastal surface, the freshwater supply can be rendered temporarily non-potable for a several months elevating the scarcity of water (Hoggart *et al.* 2014; Gingerich, Voss and Johnson 2017). These adversities prompted salinity to become an important factor to be monitored as it affects key quality parameters of water.

2.2. Effects of salinity

Salinity includes many different ions; however, relatively few ions make up most of its composition in seawater. The most common ions in seawater are chloride, sodium, calcium, magnesium, and sulfate (Mondal, Singh and Saxena 2010; Little, Wood and Elliott 2017; Lv *et al.* 2018). The concentration of other trace ions (bicarbonate, boron, bromide etc.) in seawater can be rendered insignificant. The ocean depth is hundreds

of feet and ocean water has a very high salinity (35 ppT), while water in rivers can have low salinity of about 0.2 ppT (Agency 2006). Salinity of the sea is of great importance for the marine ecosystem. Some marine species require certain levels of salinity during their life stages. Studies conducted on cod eggs have revealed that, these eggs need a minimum salinity of 11.5 ppT to survive (Hinrichsen *et al.* 2016; Kijewska *et al.* 2016). Moorman *et. al.* (2014) have investigated the effects of salinity on tilapia species in the Mozambique Sea. They found that the species could not survive at salinity levels above 5 ppT, as osmoregulation of the respiratory system is affected (Moorman *et al.* 2014). Saltwater intrusion can also change the species abundance, diversity of terrestrials and estuarine aquatic ecosystem, due to a loss of suitable habitat for them (Zhang *et al.* 2013; Mazzei and Biber 2015; Pereira *et al.* 2015).

Seawater intrusion has been widely recognized as a widespread environmental problem which greatly affects the groundwater reserves of numerous coastal areas throughout the world. A study conducted by Perera *et. al.* (2018) in Bentota river of Sri Lanka showed that the penetration of high tides from the nearby sea into the river had subsequently rose up from 0.6 to 1 m above the sea level. This was the highest seawater intrusion noticed in the area with a total distance of 25 km affected lengthways in the river from Bentota estuary. The total annual economic loss in the coastal community was estimated to be 7 million USD per year and was directly due to the seawater intrusion, which affected agriculture, fishing, tourism and quality of drinking water sources of surrounding areas (Perera *et al.* 2018). Oceanic landmasses such as islands have freshwater rivers that lead to estuaries which connect to the sea. However, such places are subjected to long-term salinization from seawater flooding. Often, the freshwater is the sole-source water supply for inhabitants. Terry and Falkland (2010) monitored the water recovery in the Northern Cook Islands after seawater flooding. Their results showed that the saline contamination rendered the freshwater river non-portable for nearly a year (Terry and Falkland 2010).

The poor rural coastal populations are highly affected by sea-level rise and coastal hazards, such as salt-water intrusion (Roberts 2008). Since they lack resources to help them either to adapt or protect themselves against these disasters, the losses

caused by coastal floods impact directly on livelihoods of many rural coastal households which depend mostly on agriculture and fishing to survive (Fisher *et al.* 2017). Many of the operation wells, as the critical water supply sources in these communities become salinized causing a challenge to accessibility of drinking water (Park *et al.* 2005; Gopinath *et al.* 2016). This leads to poor health as there is not enough food or clean drinking water to sustain these communities. A study conducted by Barbier (2015) showed that in most developing countries millions of people in the low elevation coastal zones lived in areas with high infant mortality and malnourished children due to climate change effects such as sea level rise resulting in inland salt intrusion (Barbier 2015).

Intrusion of sea water is known to cause barriers and restraints for existing agricultural practices for most coastal communities. Nhung *et. al.* (2019) reported that the projection of saline simulation on nearby farms showed that sea level rise will facilitate for increasing salt concentration and making salinity boundaries move further up the Hau river in Vietnam, which will cause damage for freshwater agricultural activities, such as rice farming (Nhung *et al.* 2019). When salinity is beyond the salt tolerance of crops, the growth of plants is affected, the yield becomes very low (Katerji *et al.* 2003). The main impact of salinity when it exceeds the tolerance of plants results in the increasing of osmotic pressure of the soil solution causing a reduction in both the rate of water absorption by the plants and the soil water availability resulting in plant wilting (Sadak, Abdelhamid and Schmidhalter 2015). The reduction in size of the produce; change in colour and appearance; and change in the composition of the produce are all problems associated with salt intrusion from sea floods (Ventura *et al.* 2011).

With all these problems associated with salinization affecting human health, agriculture, marine and estuarine ecosystem alterations and portable water, assessment and long-term monitoring methods for salinity levels are significant. To measure salinity variations in seawater along the seacoast areas, weather satellite tracking is typically used and data can be found mostly in monographic treatments on hydrological and meteorological conditions (Salman and Al-Shammiri 2007; Hinrichsen *et al.* 2016; Wiegman *et al.* 2018). This method is very expensive and requires the use of highly sophisticated machinery and is based on theoretical climate-

change and seawater-flooding scenarios (Gingerich, Voss and Johnson 2017). This study reports on the development of a device for basic understanding of salinization through on-site monitoring of sodium chloride concentration levels as a representative of salinity in the water.

2.3. Sodium chloride as the compound of interest

Seawater has a high electrical conductivity due to conducting ions such as Na^+ and Cl^- which function as electrolytes. NaCl can have adverse effects on the environment should the compound exist in excess in seawater and estuarine water. High concentrations of NaCl in water can affect marine plants growth, estuarine ecosystem upstream and sometimes degrade drinking water resources (Gossett, Millhollon and Lucas 1994; Khan, Singha and Panda 2002). Excess NaCl in ground water can be persistent and uneasy to be naturally reduced. Reports has shown that the economic impact of increased NaCl in groundwater can result in environmental issues such as famine of fresh water species and human beings (Kennish 2002; Wolanski *et al.* 2006). The California State Water Resources Control Board (SWRCB) is a board that is responsible for the establishment of NaCl concentration secondary maximum contaminant level (SMCL) in drinking water standards for public water supplies. SMCLs range set by SWRCB for salinity/sodium chloride is 500 mg/L (recommended) and the upper SMCL is 1,000 mg/L (Pereira *et al.* 1996). According to literature, the 1937 standard indicated that, chloride was the only variable with the ability to describe the salt concentration in seawater as a result of the other ions associated with salinity being too small in composition (Pawlowicz 2015).

2.4. Gold nanoparticles as colorimetric sensors

In the past twenty years, gold nanoparticles (AuNPs) based colorimetric sensors have attracted more attention as an excellent platform for colorimetric assays which offer naked eye-distinguishable signals, simplicity, rapidness, convenience and inexpensive way for determination of analytes (Liu *et al.* 2012; Zohora *et al.* 2017). Therefore, gold nanoparticles have been applied as a detection tool for inorganic compounds in various samples. Chemical colorimetric sensors for the detection of inorganic compounds such as hydrogen peroxide and hydrogen sulfide amongst

others in environmental samples have been developed based on AuNPs (Rivero *et al.* 2017; Zhang *et al.* 2017). For anion detection, Fang *et. al.* (2017) reported the determination of harmful anion (F^-), toxic contaminants (CN^- and AsO_3^{3-} /AsO_4^{3-}) and anionic fluoro-surfactants in water samples using AuNPs-based optical sensor (Fang *et al.* 2017). Similarly, modified AuNPs have been widely used in colorimetric sensors to determine heavy metal ions.

Recently, Du *et. al*. (2018) reported a colorimetric detection of silver cation (Ag^+) using a Plasmonic AuNPs sensor based on synergistic coordination of two biomolecules with Ag^+ on AuNPs surface (Du *et al.* 2018). Report by Li *et. al*. (2011) designed a gold nanorods based colorimetric probe which could be applied for chromium (VI) detection in lake water sample with a detection limit of 8.8×10^{-8} M (Li *et al.* 2011). AuNPs were able to detect chromium (VI) in solution by giving individual colour intensity corresponding to the prepared concentration ranges (Liu *et al.* 2012). AuNPs in their application has surpassed the existing traditional analytical methods by providing enhanced sensitivity and selectivity of the target compound even in the presence of interfering ions (Sivaraman, Kumar and Santhanam 2011; Qin *et al.* 2018). This is due to gold nanoparticles feature, a phenomenon called Surface Plasmon Resonance (SPR) (Esfahani *et al.* 2016; Khodaveisi *et al.* 2017).

This phenomenon occurs when the conductive electrons in the metal nanostructures collectively oscillate due to their interaction with an incident electro-magnetic radiation (Rivero *et al.* 2017; Nirala, Saxena and Srivastava 2018). The report by Doyen and co-worker showed that resonance condition was satisfied at visible wavelengths, thus, this was attributed as a contributor of AuNPs intense red colour (Doyen, Bartik and Bruylants 2013). The change in the red colour to blue upon analyte introduction can be easily identified upon the change of surface properties of AuNPs. Herein, a colorimetric sensor based on AuNPs for the detection of NaCl in seawater is developed. Apart from the expensive, time consuming and toxic waste generating analytical methods such as ion chromatography (IC) and precipitation titrations to quantify NaCl, silver nanoparticles have been applied as colorimetric sensors for the chloride ion in water samples (Ellwood, Hunter and Cunninghame 2003; Gros 2013; Yakoh *et al.* 2018). Although this was a simpler and less costly procedure in

comparison to IC and titration methods, synthesis of the desired shape of silver nanoprisms is cumbersome. Another disadvantage is the toxicity levels of silver nanoparticles compared to the less-toxic and inert AuNPs (Ray, Yu and Fu 2011; Starnes *et al.* 2015). In this study, the synthesis of AuNPs was based on chemical reduction of gold (III) chloride trihydrate salt using tri-sodium citrate that act as stabilizing and capping agent. The colorimetric assay array to quantify NaCl based on AuNPs is illustrated in **Figure 2.1**. **Figure 2.1** is a schematic illustration of a flocculation-based assay for increasing concentration of sodium chloride for the AuNPs sensor. Citrate capped gold nanoparticle solutions are unstable with respect to precipitation and flocculate rapidly upon addition of electrolytes (Xie *et al.* 2003). The chemical reaction between the cation and AuNPs leads to aggregation of particles that causes the appearing of the blue colour patterns for each NaCl concentration (Liu and Lu 2004).

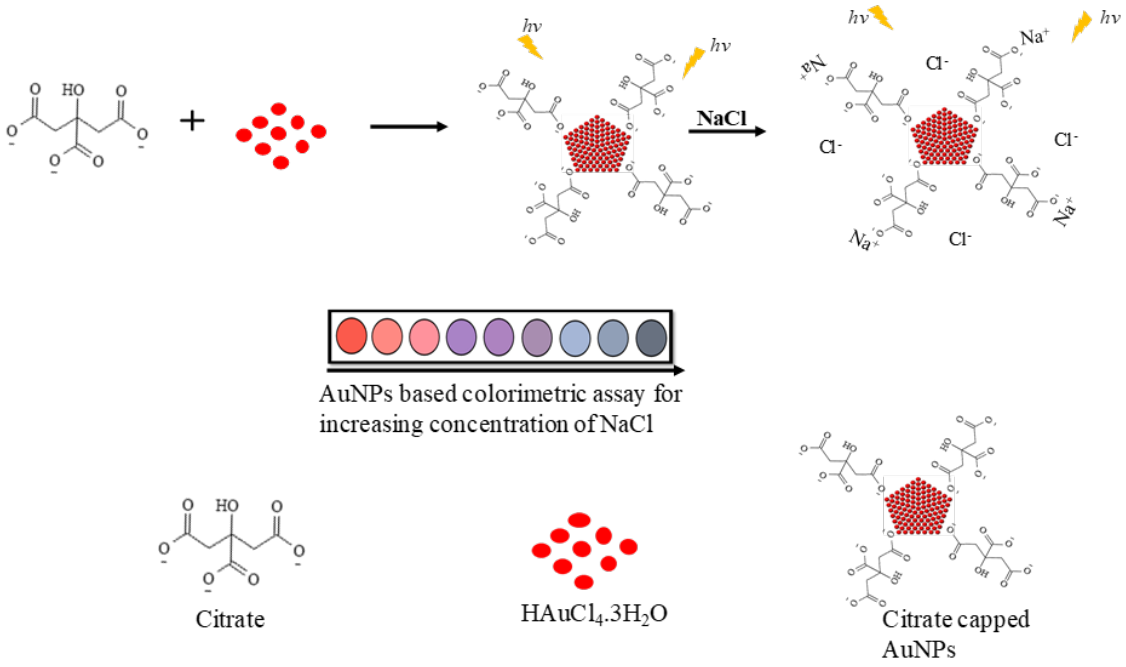

Figure 2. 1: Schematic illustration of the gold nanomaterial enabled colorimetric sensor.

2.5. Turkevich method for synthesis of gold nanoparticles

This method was the first and moderately systematic method to synthesize AuNPs and was established by Turkevich *et. al*. in 1951 (Turkevich, Stevenson and Hillier 1951). The method involves the reaction of boiling gold (III) chloride trihydrate solution with small volume of warm sodium tri-citrate solution under thorough stirring that leads to a series of colour change from light yellow (to purple or black which fades in seconds in solution) and finally to wine red. The main principle is that the gold ions (Au^{3+}) of chloroauric acid in solution are reduced to gold atoms (Au^0) by the reducing agent tri-sodium citrate leading to the formation of well-dispersed spherical nanoparticles (Lin *et al.* 2004). The mechanism for stepwise formation of AuNPs was reported to be based on three stages after citrate reduction: nucleation, gold adsorption growth and aggregation as can be observed in **Figure 2.2** (Doyen, Bartik and Bruylants 2013; Kim *et al.* 2017). This by far is the most used method to produce highly stable monodispersed nanoparticles ranging from 5-30 nm in average diameter in the aqueous phase (Sivaraman, Kumar and Santhanam 2011). This method has an advantage of flexibility to modify the concentration ranges for the reagents used in the synthesis to produce even bigger stable nanoparticles without changing the spherical morphology of the particles.

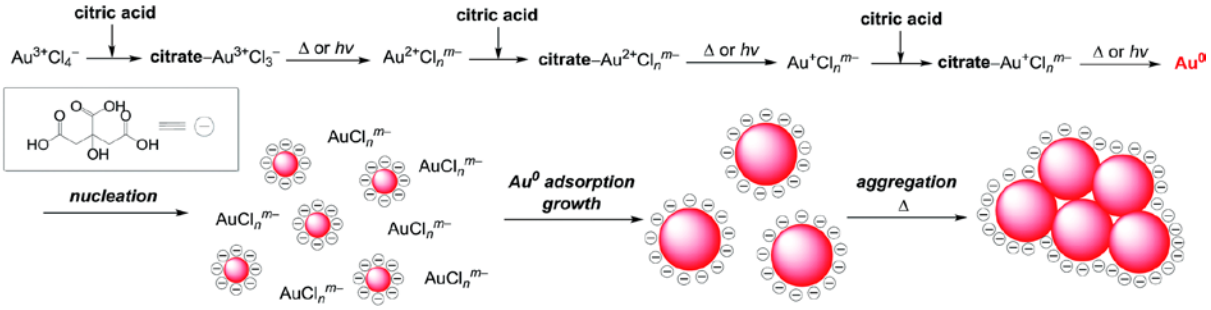

Figure 2. 2: A schematic representation of the synthesis of citrate-stabilized gold nanoparticles by Turkevich method (Shiraishi *et al.* 2017).

2.6. Analysis of sodium chloride in seawater

Small gold nanoparticles in both dispersed and aggregated forms have strong extinction coefficients to facilitate colorimetric determinations even by naked eyes (Takatsuji, Ikeno and Haruyama 2012). Due to the alterations of SPR properties of the particles, the red colour of gold nanoparticle turned from wine red to blue when the

nanoparticles aggregate in solution (Qin *et al.* 2017). These aggregation processes are induced by the changes of solution compositions or particle surface properties to minimize the electro static or hydrogen bonding interactions between the nanoparticles and their surroundings (Khezri, Bahram and Samadi 2018). In this study the use of an electrolyte sodium chloride to react with the gold nanoparticles induces aggregation of the nanoparticles. The subsequent various colour changes produced from the colorimetric assay were used to fabricate the Lovibond comparator device. This acted as the concentration level guide for the quantitative determination of NaCl levels in seawater as shown in **Figure 2.3**. The visual colour of the analysed sample was compared with the optimised NaCl concentrations range engraved on the colorimetric disk.

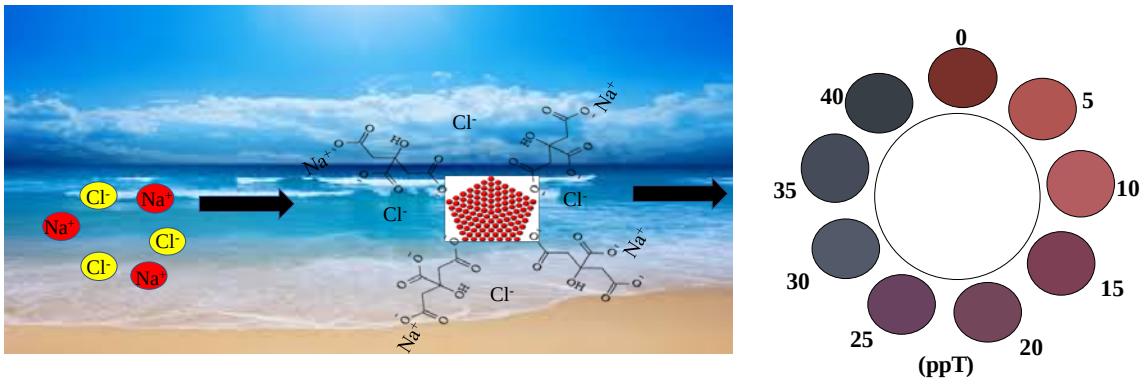

Figure 2. 3: Schematic illustration of the gold nanoparticle based colorimetric response of the fabricated device for the analysis of NaCl concentration.

2.7. Characterization of gold nanoparticles

2.7.1. Ultra Violet-Visible spectroscopy

The SPR absorption peak was reported to depend on the following factors: particle size, shape and the dielectric constant of the surrounding medium affecting the electron charge density of the nanoparticle (Daniel and Astruc 2004b). A weak peak (transverse peak) corresponding to gold nanoparticles can be observed in the visible region and a strong absorption peak (longitudinal peak) in the near IR region corresponding to electron oscillations along the long axis in the spectrum (Nehl, Liao and Hafner 2006; Nehl and Hafner 2008). The SPR peak was applied as an indication

of nanoparticles size and stability. Spherical gold nanoparticles were reported to have a SPR peak ranging from 520 nm to 550 nm, these nanoparticles were typically in the range of >5 – 60 nm in size (Habib, Tabata and Wu 2005). Tan and co-workers showed that gold nanoparticles with rod or cubic shape usually had a SPR peak from 600 nm – 800 nm, these were in the range of 80 –100 nm in diameter (Tan *et al.* 2016). The optical properties of AuNPs is the main fixture that has prompted their various applications in the field of portable colorimetric sensors (Takatsuji, Ikeno and Haruyama 2012).

2.7.2. Transmission Electron Microscopy

Transmission Electron Microscopy is a technique where an electron beam interacts and passes through a sample. The electrons that are elastically scattered consist of the transmitted beams, which pass through the objective lens form the image in the microscope (Mohanraj and Chen 2006). The formed image is shown either on a fluorescent screen or in a monitor. Through a sequence of buttons, adjustments of focus and brightness of the beam morphology of the sample can be obtained. TEM is widely employed for AuNPs morphology and size illustrations in samples (Welch and Compton 2006).

2.7.3. Scanning Electron Microscopy

Scanning Electron Microscopy is used to image and characterize materials. The working principle of SEM involves the acceleration of electrons by the potential difference between cathode and anode (Mohanraj and Chen 2006). The accelerated electrons penetrate into the sample within a small depth, for proper surface topology and imaging (Hondow *et al.* 2012). SEM is also used for chemical composition of the sample's surface since the brightness of the image formed by backscattered electrons is increasing with the atomic number of the elements. SEM is a good microscopic technique for characterization of AuNPs where different morphologies and sizes in can be observed.

2.7.4. Fourier-Transform Infrared Spectroscopy

Spectroscopic methods are used to provide information on a large variety of chemical processes in solids or liquids (Wulandari *et al.* 2008). Infrared spectrum contains large

number of bands, the possibility of the two compounds to have the same infrared spectrum is extremely small (Gene Chong *et al.* 2018). FTIR is an effective tool in detecting the relationship between the nanoparticles and its capping agent. The functional groups of the capping agent are compared with the synthesized nanoparticles spectrum for any resonance and confirmation of the encapsulation of the AuNPs with the capping agent.

2.8. Image processing

The colour is a psychophysical quantity, acting as an impression during the stimulation of our visual system (Livingstone and Hubel 1988). The dependence on external factors like lighting, background and individual human characteristics have a significant influence on the perception and comparison of colour experiences (Kandel *et al.* 2000). With the aid of smartphone applications, computer software's and mathematical models, the description of colours is accurately and precisely defined by fixed values which are easy to interpret (Cox 1996; Celik 2010).

2.8.1. Colorgrab analysis

Colorgrab is a typical colour picker that is used to select and adjust colour values. It is a simple method for measuring the different colour intensities produced when colours are mixed (Montangero 2015). Colorgrab is used for images or to practically measure colour variation. For solution evaluation, colours are selected via an interface with a visual representation of a colour pre-arranged with perception relevant to lightness and saturation of objects (Hossain *et al.* 2015). Colour appearance depends on comparison of neighboring colours, therefore, many interfaces attempt to clarify the intensity relationship between colours prior red green blue (RGB) colour model.

2.8.2. Red Green Blue colour model

The (RGB) colour model is used for sensing representation and display of images in an electronic system. A comparison is done between computer colour space using appropriate applications and software (i.e. ImageJ) which are based on naked eye perception (Kumar and Verma 2010). The RGB values can be used as a colour reference in the fabrication of colorimetric sensors. These RGB values produce clear

colour relations to the optimised standard ranges. RGB colour model is easy to use with the reliability to produce highly efficient colorimetric schemes. RGB measurements from AuNPs colorimetric assays are used to interpret the distinguishable colour signals given by AuNPs in reaction solutions (Cheng *et al.* 2014).

2.8.3. CIELab colour system

In 1931, the Vienna based international standards body, the International Commission on Illumination (***CIE**: Commission Internationale d'Eclairage*), developed a mathematical model for the purpose of numerically describing all colour differences (delta E) using the calculated *L*a*b values (Leon *et al.* 2006). The *L is for the lightness, *a and *b for the green–red and blue–yellow colour components. CIELab became the basis of several successive refined colorimetric systems for the measurement and specification of colour. CIELab is the reference colour model used by the paper making and graphic arts industries (Kuehni 1990; Žiljak *et al.* 2012). **Figure 2.4.** illustrates the CIELab colour management system, solutions with lower intensity values (moving towards the 0) are more intense in colour compared to solutions with high intensity values (moving towards 100) in their respective colours (Ajlouni *et al.* 2018). The CIELab system is the universally accepted colorimetric reference system for quantifying and communicating colours (Gong *et al.* 2005).

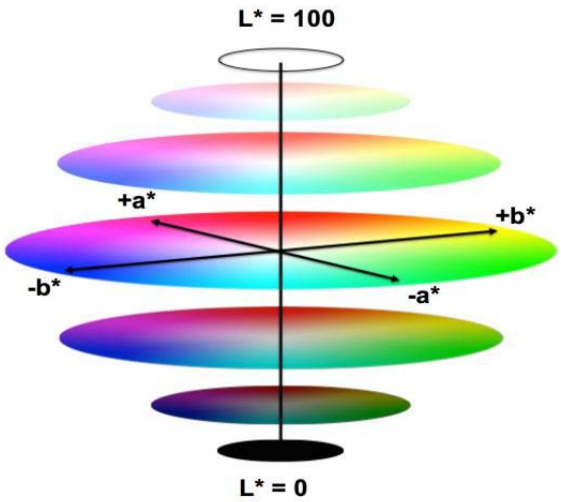

Figure 2. 4: Schematic representation of colour distribution along the x and y axis with lighter colours moving towards 100 and darker towards 0 (Sappi 2013).

Chapter 3: Research methodology

3.1. Chemicals

Gold chloride trihydrate (>99.9%) was purchased from Leap Chem (Hangzhou, China) through DLD Scientific (Durban, South Africa). Other chemicals used were tri-sodium citrate dehydrate (>99%) from Merck (Pty) Ltd (Durban, South Africa) and NaCl from Associated Chemical Enterprises (Johannesburg, South Africa). Inorganic salts ($CaCl_2$, KNO_3, $MgSO_4$, NaOH and $KCrO_4$) were purchased from Merck (Pty) Ltd and Na_2SO_4 was purchased from Associated Chemical Enterprises. $AgNO_3$ (≥99.0%), HPLC grade acetone (≥99.9%) and phthalic acid (≥99.5%) were purchased from Sigma-Aldrich (Johannesburg, South Africa). HCl was purchased from Laboratory Supplies (Durban, South Africa).

3.2. Synthesis of gold nanoparticles

The standard method, reported in literature (Turkevich, Stevenson and Hillier 1951), was used for the synthesis of gold nanoparticles with slight modification. For the synthesis of tri-sodium citrate capped AuNPs, gold chloride trihydrate solution was prepared by dissolving 0.02 g of the salt in 100 mL deionized water to give a concentration of 0.01 mM. This solution was placed on a hot plate and vigorously stirred using Teflon-coated magnetic bar. The solution was allowed to boil under constant stirring until it reached the temperature of 96-98 °C. Thereafter, 5 mL of 0.04 mM warm tri-sodium citrate solution was rapidly added into the boiling solution. A noticeable colour change from pale yellow to wine red was observed within 20 minutes which indicated the formation of AuNPs. The reaction flask was then removed from the hot plate to allow the reaction solution to cool at room temperature.

3.3. Characterization of gold nanoparticles

3.3.1. UV-Vis spectrophotometer

A UV-Vis spectrophotometer Cary UV 50 from Varian (Cape Town, South Africa) was used to perform the measurements. All LSPR spectra were recorded from 400 to 800 nm and experimental absorbance measured at 525 and 660 nm on the UV-Vis at room

temperature. Baseline correction of the spectrophotometer was carried out by using deionised water as a blank reference.

3.3.2. Transmission Electron Microscopy

Transmission electron microscopy was used to characterize the morphology and size distribution of the gold nanoparticles. Samples for TEM imaging were prepared by drop-casting the AuNPs solution onto the carbon coated copper grid. TEM observations were carried out with a TEM CM 120 model from Philips (Johannesburg, South Africa). A Leica microtome was used to place a drop of gold nanoparticles samples on top of the 400 Mesh copper grid. The TEM was operated and images processed at 120kV under room temperature environment. The particle size distribution of AuNPs were analysed using ImageJ software (National Institute of Health USA, http://imagej.nih.gov./ij). This was done by selecting sufficient number (100) of spherical nanoparticles from the TEM image (Hondow *et al.* 2012).

3.3.3. Scanning Electron Microscopy

SEM was carried out with an EVO 15 HD from Carl Zeiss (Durban, South Africa) accessed at Durban University of Technology and an S-3000N-Carl Zeiss (Durban, South Africa) from University of KwaZulu-Natal to characterize the nanoparticles morphology using a solid gold nanoparticles sample. The solid samples were obtained by centrifuging the AuNPs containing solutions for 20 minutes at 10000 rpms using a Hettich Universal II (model D72) centrifuge machine. The colloidal gold settled at the bottom of the centrifuge tube. The liquid part was then discarded and the AuNPs were deposited onto the filter paper and dried at room temperature. A double-sided carbon tape was used to transfer the AuNPs onto the SEM sample holder for analysis. The measurements for the respective SEM instruments were performed at 20.00 KX and 49.64 KX magnification resolution power under electrical signal of 3.00 kV and 20.00 kV.

3.3.4. Fourier-Transform Infrared Spectroscopy

To study the structural resonances between the synthesized gold nanoparticles and capping agent, a FTIR spectrometer equipped with attenuated total reflection (ATR)

from Perkin Elmer (Johannesburg, South Africa) was used. The synthesized AuNPs and tri-sodium citrate salt were placed in the ATR crystal and characterized. For the liquid sample, two drops of the solution were dropped onto a secured ATR and the transmittance of the solution was measured. The solid sample was analysed by depositing a small amount of the salt onto the ATR crystal and pressing with the knob to secure the solid material and the transmittance was measured. Spectra of the reagents were recorded in the range of 400-4000 cm^{-1}.

3.4. Preparation of sodium chloride standard solutions and their treatment with gold nanoparticles

For the UV-Vis spectrophotometric analysis and image processing, stock solution of 100 ppT of sodium chloride was prepared by dissolving 10 g of the salt in 100 mL deionised water. The working standard solutions were prepared by dilution of the stock solution with deionised water to get a concentration range of 5 to 40 ppT. In a 2 mL AuNPs solution, 400 μL of each NaCl standard solution was added. The collected water samples were treated likewise.

3.5. Fabrication of Wax-patterned paper

Circular areas with a diameter of 0.7 cm were designed by Adobe illustrator CS4 software (Adobe Systems, Inc.). The wax printing method was used for the fabrication of microfluidic paper analytical device (μPAD). The black wax colour was to be used as a complementary to the colorimetric reaction. The process to fabricate μPAD consisted of two steps: (1) printing the wax pattern on the surface of normal white printing paper by a commercial wax printer (Xerox Colour Qube 8570, Japan) and (2) melting the wax printed paper at 175 °C for about 60 seconds on a hot plate. The printed wax can penetrate the paper and generate complete hydrophobic barrier and hydrophilic channels within the paper. **Figure 3.1** shows the schematic diagram for the preparation of the *u*PAD.

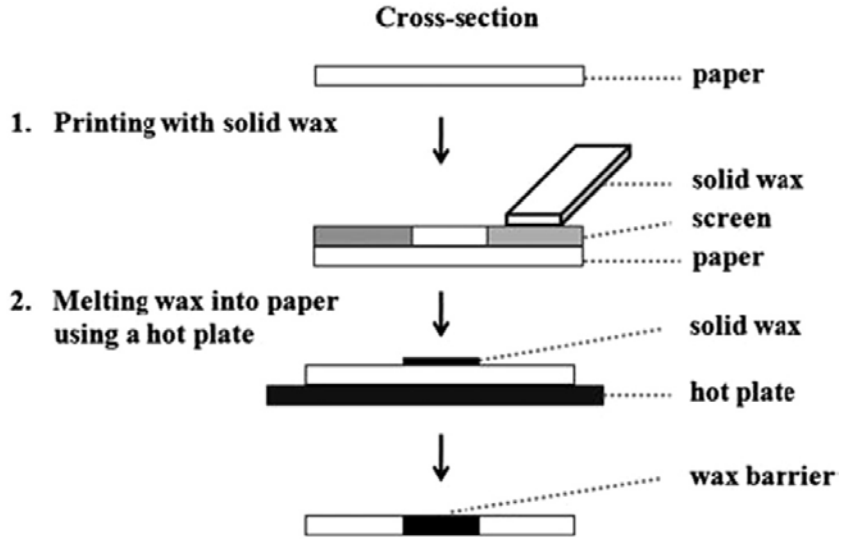

Figure 3. 1: Schematic diagram of fabrication step for wax screen-printing method (Kang and Kim 2018).

3.6. Analytical procedure and image processing

For colorimetric assay of NaCl, 80 µL of the AuNPs was firstly added onto the hydrophilic test zone on the μPAD. This was followed by adding 20 µL of either sample solution or NaCl standard solution onto the test zone. The colour change of AuNPs was rapidly visualized after 2 minutes through the naked eye. After that, the test zone of μPAD was captured with a smartphone (Blackberry Z10 model with 8 mega pixels' rear camera) under normal laboratory in-house lighting. The JPEG format image was then imported to ImageJ software (National Institute of Health, USA) for measurement of the mean colour intensity. The image colour threshold was set to remove the light background colour by adjusting the hue. The colour signal of each zone was measured as the mean RGB colour intensity and then imported into a computer software (Lenovo G400 model) for analysis.

3.6.1. Colorgrab intensity measurements

The intensity of the NaCl calibration standards was measured using a smartphone (Samsung J1 smartphone, Samsung Electronics Co., Korea) and analysed by the Colorgrab intensity-processing mobile application (app) developed using the Greyscale percentage platform. Upon clicking on the 'capture' button, the smartphone

camera measures the intensity of each solution. Triplicate measurements were taken for each point.

3.6.2. RGB colour analysis

Photograph of the NaCl calibration ranging from 5-40 ppT was analysed using ImageJ software (National Institute of Health USA, http://imagej.nih.gov./ij). The picture was processed by firstly eliminating the background light effect to highlight the actual colours of solutions in the cuvettes. The RGB values output was measured for each colour and recorded. The RGB values were then transferred into the “More fill” colour tab on the computer for further processing. The resultant colour hues were used to create the circular colour patterns on the fabricated Lovibond device colour wheel. Image processing was done in triplicate for mean RGB values.

3.6.3. CIELab colour analysis

Quantified colour differences are computed as the relative distance between two reference points (between two mathematically specified colours) within a colour space (CIELab). This difference is typically expressed as delta E (ΔE) and is calculated by comparing reference and sample *L*a*b values to pinpoint how far apart two colours reside within a colour space. In case of the *L*a*b space, ΔE difference between two colours is calculated by the following formula:

$$\Delta E_{Lab} = \sqrt{(\Delta L)^2 + (\Delta a)^2 + (\Delta b)^2}$$ (Robertson 1977)

Colour differences based on (ΔE) calculations for a standard observer can be quantified as follows, when:

• 0 < ΔE < 1 - observer does not notice the difference,

• 1 < ΔE < 2 - only experienced observer can notice the difference

• 2 < ΔE < 3:5 - unexperienced observer also notices the difference,

• 3:5 < ΔE < 5 - clear difference in colour is noticed,

• 5 < ΔE - observer notices two different colours.

3.7. Fabrication of Lovibond comparator disk

The Lovibond device was fabricated using transparent plastic slide with 210 x 297 mm dimension using the Xerox Colour Qube 8570, Japan printer. The device was cut into a wheel shape and had an overall size of 88 mm in diameter, containing 9 round colour channels with dimensions of 17 mm in diameter. The colour channel patterns had the optimised colorimetric response from the NaCl calibration standards in the range of 5-40 ppT. The device was then mounted inside a black box with a square shape with an open right-hand side space allowing for easy rotation of the colour wheel to match the optimised concentration of NaCl. Near the bottom of the black box there was an open gap where the corresponding concentration of the matched colour can be observed at 90 degrees angle from each other as shown in **Figure 3.2** below.

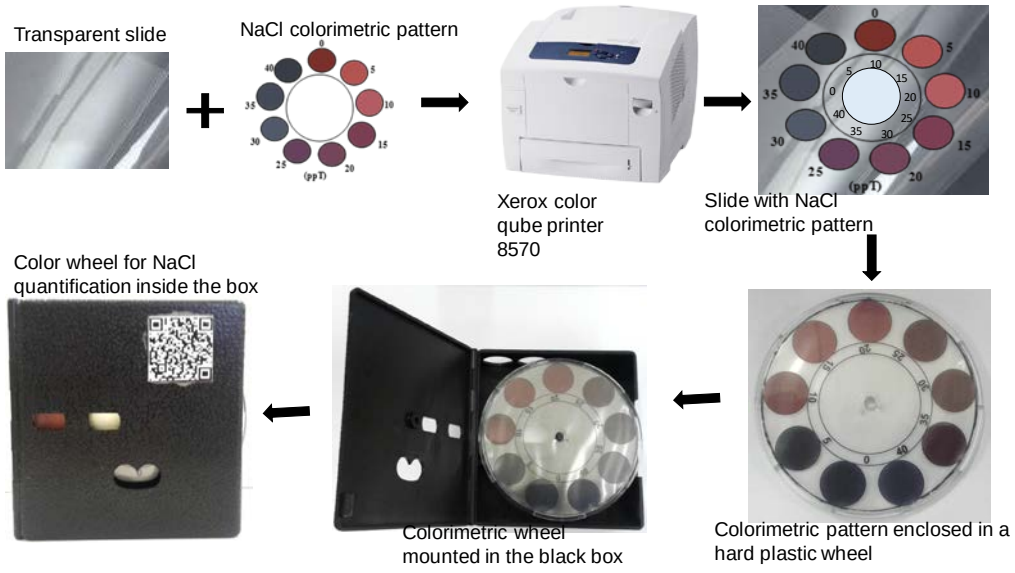

Figure 3. 2: Summary of the fabrication steps involved in the fabrication of the Lovibond colorimetric device.

3.8. Method validation

The proposed method was validated using linearity, precision, accuracy, repeatability, robustness as well as limits of detection (LOD) and quantification (LOQ). The linearity was determined by plotting concentration of NaCl against the corresponding absorbance. The calibration curve was constructed by plotting absorbance versus the concentration of NaCl standard solutions (5-40 ppT).

3.8.1. Limit of detection and limit of quantification

LOD and LOQ were calculated from the data obtained from the slope linear calibration studies. LODs and LOQs were calculated using equations (1) and (2), respectively (Martins and Mainardes 2017):

$$LOD = \frac{\sigma}{S}\ x\ 3 \quad (1)$$

$$LOQ = \frac{\sigma}{S}\ x\ 10 \quad (2)$$

Where σ = standard deviation of the response; S = slope of the calibration curve.

3.8.2. Statistical evaluation of AuNPs

A one-way analysis of variance (ANOVA) was used to compare the concentration of NaCl in the samples using SPSS statistical tool (IBM SPSS Statistics v23; IBM Corp). Significant main effects of NaCl concentration were followed up by the Tukey and Bonferroni multiple comparison test (α=0.05). Data was expressed as means ± SD.

3.8.3. The effect of interferences on the analysis of sodium chloride

The selectivity of AuNPs was investigated by spiking seawater with the interfering ions such as, Ca^{2+} (0.15-0.35 ppT), K^{+} (0.15-0.35 ppT), Mg^{2+} (0.125-1.5 ppT) and SO_4^{2-} (1-3 ppT), all these ions co-exist with NaCl in seawater. This was done by spiking the in-house simulated seawater sample containing sodium chloride (30 ppT) and other ions that included Ca^{2+} (0.35 ppT), K^{+} (0.35 ppT), Mg^{2+} (1.5 ppT) and SO_4^{2-} (3 ppT). Thereafter, the method used for the analysis of NaCl in collected water samples was applied for the evaluation of AuNPs selectivity towards the analyte in spiked seawater.

3.8.4. Recovery studies

Accuracy of the proposed method was evaluated based on the recovery studies from the standard addition method. The recovery study was conducted on two laboratory prepared seawater different in composition which were prepared by adding accurately weighed amount of NaCl (3 g) dissolved in 100 mL deionized water. A mass of 3.5 g of iodated table salt dissolved in 100 mL of tap water for a more complex matrix (Tsolaki, Pitta and Diamadopoulos 2010) along with a set of NaCl spiked deionized

water with a concentration of 10, 20 and 30 ppT was added as well. The percentage recoveries were calculated for AuNPs sensor device, titration and ion chromatography methods. To determine the precision of the method the relative standard deviation percentage (%RSD) was calculated.

3.9. Sample collection and treatment

The GPS co-ordinates for the different sampling locations are provided in **Tables 3.1 & 3.2** which is the coastal part of Durban and Amanzimtoti. The samples were collected on the same day using a grab sampling approach. Prior to the analysis, samples were filtered for removal of any suspended materials using a Whatman qualitative filter paper, Grade 1 (diameter of 70 mm**,** pore size 11 µm). For on-site detection of NaCl, samples were analysed with Lovibond device without any pre-treatment step. The physicochemical properties (pH, conductivity, dissolved oxygen (DO), total dissolved solids (TDS), oxidation-reduction potential (ORP), salinity and resistivity of all collected samples were measured by the multi-channel portable apparatus (Bante 900P).

Table 3. 1: Sampling No.1 (March 2018) GPS co-ordinates.

Sample	Location	GPS Co-ordinate
Blue Lagoon Beach	Durban, South Africa	29◦48’45.6” S 31◦02’27.9” E
Suncoast Beach	Durban, South Africa	29◦50’09.3” S 31◦02’15.5” E
Umgeni estuary	Durban, South Africa	29◦48’44.3” S 31◦02’27.2” E
Umgeni estuary 405 m upstream	Durban, South Africa	29◦48’41.6” S 31◦02’12.6” E
Amanzimtoti estuary	Amanzimtoti, South Africa	30◦03’35.8” S 30◦53’01.1” E
Amanzimtoti estuary 253 m upstream	Amanzimtoti, South Africa	30◦03’35.8” S 30◦53’01.1” E

Table 3. 2: Sampling No. 2 (August 2018) GPS co-ordinates.

Sample	GPS Co-ordinate
Blue Lagoon Beach	29◦48’49.7” S 31◦02’21.1” E
Suncoast Beach	29◦50’09.1” S 31◦02’16.5” E
Durban South Beach	29◦51’15.8” S 31◦02’28.6” E
Harbour Sample 1	29◦51’47.7” S 31◦01’42.5” E
Harbour Sample 2	29◦51’45.8” S 31◦01’18.0” E
Umgeni estuary	29◦48’44.4” S 31◦02’25.5” E
Umgeni estuary 100 m upstream	29◦48’44.3” S 31◦02’21.9” E
Umgeni estuary 200 m upstream	29◦48’42.0” S 31◦02’19.1” E
Umgeni estuary 300 m upstream	29◦48’41.6” S 31◦02’15.5” E
Umgeni estuary 400 m upstream	29◦48’41.6” S 31◦02’11.7” E

3.10. Analysis of sodium chloride in water samples

3.10.1. On-site Lovibond device detection

The untreated water samples were analysed on-site using the AuNPs, deionized water as a reference and the fabricated Lovibond disk. 2 mL of AuNPs solution was added to the tube and 400 μL of samples was added to the AuNPs. The tube was shaken to thoroughly agitate AuNPs and then it was placed in the sample holder of the Lovibond device. After 1 minute the resultant colour of the sample was compared with the optimized colours engraved on the Lovibond disk. The best matching colour and concentration were recorded. All analysis was performed in triplicate for the detection of sodium chloride concentration. **Figure 3.3** illustrates the steps involved in the quantification of sodium chloride in seawater and estuarine water using the fabricated Lovibond device.

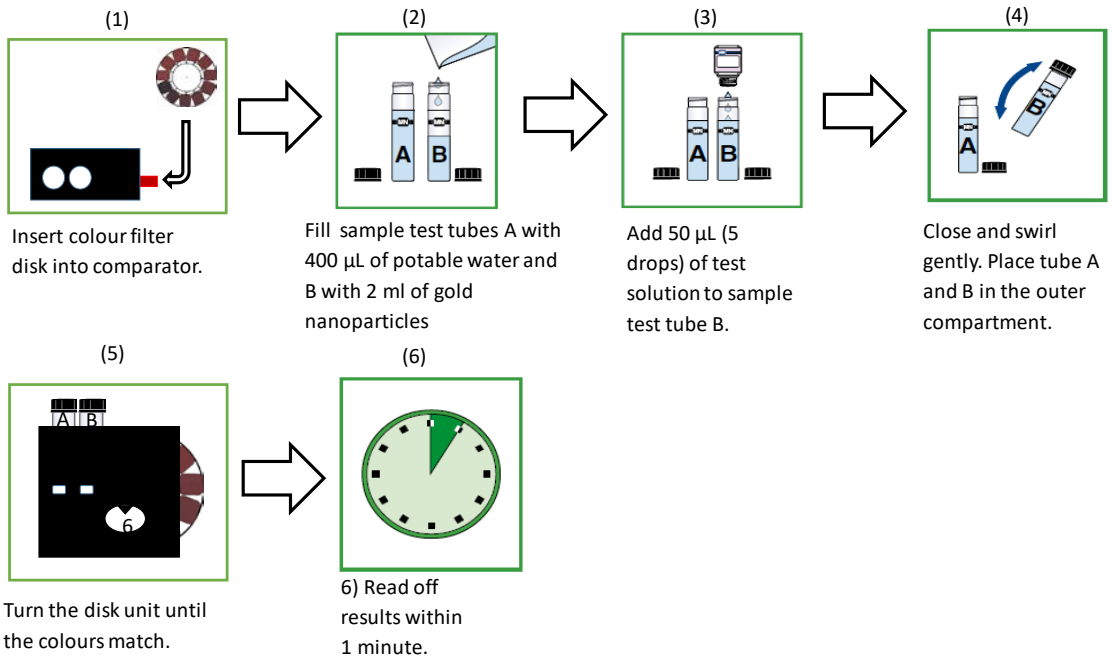

Figure 3. 3: Schematic representation of how the AuNPs colorimetric kit is used to quantify sodium chloride.

3.10.2. Titration (Mohr method)

$AgNO_3$ solution (0.1 M) was prepared by weighing 17g in 1000 mL deionized water. This solution was standardized before use by accurately weighing 0.25 g of NaCl salt and diluting in a 100 mL with deionized water. Each NaCl solution was titrated against the prepared $AgNO_3$ standard and the final concentration of the standardized $AgNO_3$ was 0.1008 M. The seawater samples were prepared by pipetting 20 mL of each sample and diluting to the mark with deionised water in a 100 mL volumetric flask (dilution factor of 5). From these solutions, 10 mL aliquots were pipetted into a conical flask containing 50 mL of deionized water and about 4 drops of indicator (5% potassium chromate) were added. The sample solutions were titrated against the standardized $AgNO_3$ solution. Calculations of NaCl were based on the reaction between chloride ions and $AgNO_3$ which resulted into a formation of a white precipitate of AgCl as follows:

$$AgNO3 + NaCl \rightarrow AgCl_{(s)} + NaNO_{3(aq)} \quad (1)$$

$$Cl^- + AgNO_3 \rightarrow AgCl_{(s)} + NO^{3-}{}_{(aq)} \quad (2)$$

$$AgCl_{(s)} \rightarrow Ag^+{}_{(aq)} + Cl^-{}_{(aq)} \quad (3)$$

Ratio 1:1

Therefore, moles of Ag^+ = moles of Cl^-/NaCl

The initial and final volume of $AgNO_3$ were recorded and the concentration of Cl^-/NaCl was calculate using the equation:

[NaCl (mg/L] = (A x N x 35.45 $g.mol^{-1}$) x1000/V_{sample}

where A= volume of titrant used, N is the normality of silver nitrate and V_{sample} is volume of sample used. Blank average volume was found to be 0.1 mL.

3.10.3. Ion Chromatography

A stock solution of 1000 ppm was prepared by dissolving accurately weighed 0.1684 g of NaCl in a 100 mL volumetric flask with deionized water. NaCl standard solutions ranging from 5 to 50 ppm were prepared by dispensing (0.5, 1, 2, 3, 4 and 5 mL) of the stock solution from a burette and diluting with deionized water in a 100 mL volumetric flask. The collected samples were diluted by pipetting 10 µL into 10 mL using deionized water. The mobile phase for Cl^- analysis was prepared by accurately weighing 0.3333 g of phthalic acid, this mass was transferred into a 1000 mL beaker and 700 mL deionized water was added. The solution was placed on a hot plate at low heat (70 °C) and stirred until all the phthalic acid had dissolved, the solution was allowed to cool to room temperature and the pH of the solution was adjusted to 5.03 with 6 M NaOH. Analysis was carried out using an ion chromatography instrument, Waters Division of Millipore, model 430 Liquid chromatograph, pump model 590 with a conductivity detector operating at 196 μS. The column was a Hamilton PRP-X100 anion separator (Bischoff chromatograph). A stable base line was obtained within 1 hour of start-up of the instrument. The injected sample size was 20 µL and the flow rate of the mobile phase was set at 2 mL/min.

Chapter 4: Results and discussion

4.1. Synthesis and Characterization of synthesized gold nanoparticles

4.1.1. Synthesis

The experimental results show that gold nanoparticles were successfully synthesized following the chemical reduction method with tri-sodium citrate as a capping and reducing agent. The final wine-red colour of the synthesized AuNPs solution confirmed the presence of the metal nanoparticles in solution. This colour was due to the reduction of gold (III) from the gold (III) chloride trihydrate to metallic gold (0) (Doyen, Bartik and Bruylants 2013; Nirala, Saxena and Srivastava 2018). **Figure 4.1** shows the colour of the synthesized AuNPs solution.

Figure 4. 1: Image of the synthesized AuNPs solution through Turkevich method.

4.1.2. UV-Vis spectroscopy

The result of the synthesized AuNPs using UV-Vis spectrophotometer for SPR peak location is shown in **Figure 4.2**. **Figure 4.2**, showed the existence of a SPR peak at a well-defined wavelength position of 525 nm which was associated with spherical AuNPs (Mdluli *et al.* 2009; Li *et al.* 2017b; Shrivas, Maji and Dewangan 2017). The SPR absorption peak at 525 nm was due to collective oscillation of the surface electrons of AuNPs due to their interaction with electromagnetic radiation (Doyen, Bartik and Bruylants 2013; Rivero *et al.* 2017; Shi *et al.* 2017). The result is in agreement with the previous studies where synthesized AuNPs gave the SPR peak at

525 nm for spherical nanoparticles (Mdluli *et al.* 2009; Li *et al.* 2017b). The observed SPR peak at 525 nm where a red-shift can be observed, suggests that the size of the synthesized spherical nanoparticles is in the range of <3.5 nm - 20 nm (Shi *et al.* 2017). Furthermore, a study conducted by Daniel et. al. (2004) showed that the mobile electrons trapped within the gold metal colloids had a characteristic collective oscillation frequency giving rise to SPR peak observed near 530 nm were in the range of 5 - 20 nm diameter range (Daniel and Astruc 2004a).

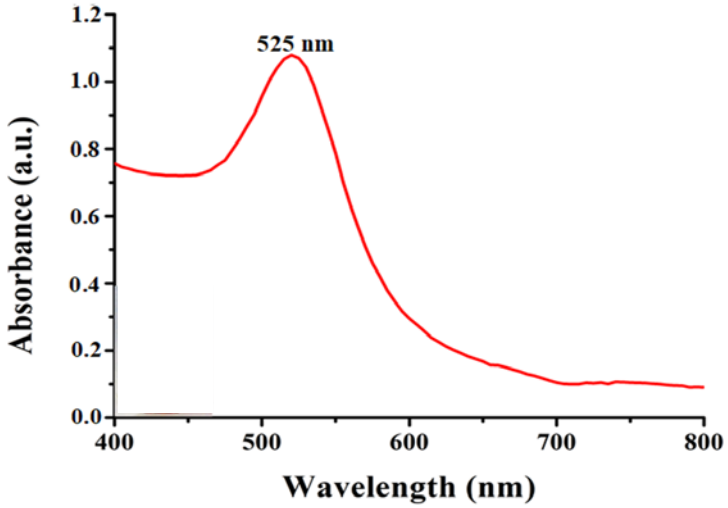

Figure 4. 2: The UV-Vis absorbance spectrum of the synthesized AuNPs and the corresponding image of the colour of the analysed AuNPs solution.

4.1.3. Transmission Electron Microscopy

In the present study, the shape of AuNPs was evaluated using TEM. As shown in **Figure 4.3a**, the TEM image revealed the presence of isotropic AuNPs. The isotropic AuNPs are commonly synthesized using Turkevich method (Sivaraman, Kumar and Santhanam 2011; Doyen, Bartik and Bruylants 2013; Shi *et al.* 2017). In **Figure 4.3a** image 100 random particles were used to assess the size of the synthesized AuNPs and the average particle sizes was calculated to be around 7 nm as shown in the particle size distribution histogram in **Figure 4.3b**. The 7 nm synthesized AuNPs are within the nanomaterial range (>2 nm), that do not suffer from quantum effect in solution (Daniel and Astruc 2004a). The TEM image in **Figure 4.3c** showed the size distribution of AuNPs in the presence of NaCl. It can be observed that gold nanoparticles have extremely aggregated in solution upon the introduction of the

electrolyte solution, implying the formation of larger particles as compared to **Figure 4.3a**. This is due to a reduction in the electrostatic repulsion of the citrate capped AuNPs in the presence of NaCl solution, as a result, the surface charge of nanoparticle is decreased and high aggregation of nanoparticles was observed. Similarly, a study conducted by Yuan *et. al.* (2015) to evaluate the effect of NaCl on colloidal gold revealed that when gold nanoparticles are mixed with a highly concentrated NaCl solution, this action led to Na+ and Cl− ions attacking the surface electric potential of the AuNPs. As a result, the nanoparticles lose their mutual repulsion and agglomerate (Yuan *et al.* 2015). The majority of the nanoparticles in the presence of NaCl had an average diameter of 13 nm as can be observed in **Figure 4.3d** in the particle size distribution histogram. The increase in the size of the nanoclusters was consistent with previous studies conducted for the reactions of AuNPs with different inorganic compounds as conjugates (Tang 2016; Zhang *et al.* 2017).

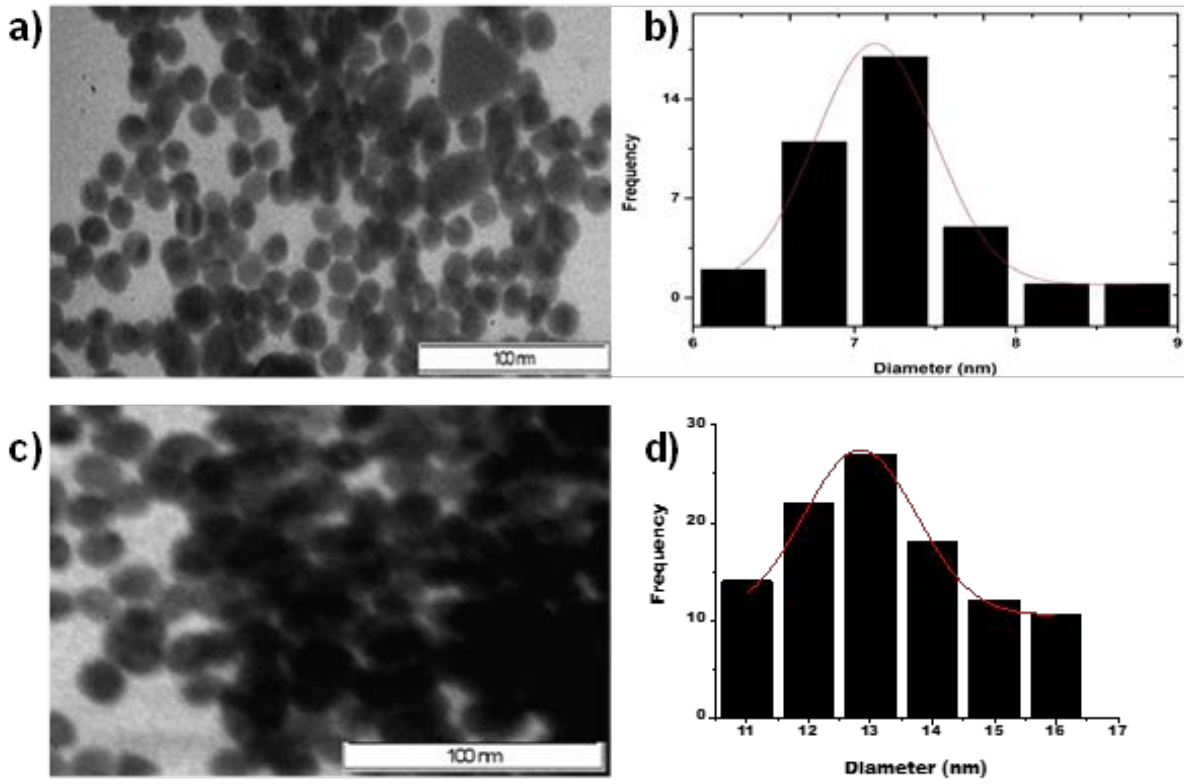

Figure 4. 3: TEM image of; (a) the synthesized AuNPs. (b) the average particle size histogram from analysing several nanoparticles from the TEM image in Figure 4.3a. (c) the AuNPs in the presence of 30 ppT NaCl. (d) the average particle size histogram from analysing several nanoparticles from the TEM image in Figure 4.3c.

4.1.4. Scanning Electron Microscopy

The synthesized gold nanoparticles were analysed for their morphology and interaction of particles with sodium chloride using SEM. The resulting image of the AuNPs solid sample revealed a lot of agglomeration as observed in **Figure 4.4**. However, it was observed that the morphology of the nanoparticles is spherical in shape with some of the particles taking other shapes as observed in the image in **Figure 4.4**. In this study, the agglomeration of the nanoparticles did not affect the objective of the developed colorimetric sensor as its application is based on flocculation of the nanoparticles and alteration of the SPR. From **Figure 4.5**, it can be observed that the AuNPs are closely packed due to aggregation of nanoparticles in the presence of NaCl. The presence of NaCl decreases the steric hindrance around the AuNPs hence, breaking the capping agent barrier and attaching to the surface of the AuNPs. NaCl, which is whitish crystals, can be observed covering the surface of the aggregated solid AuNPs denoting adsorption on the surface of gold nanoparticles.

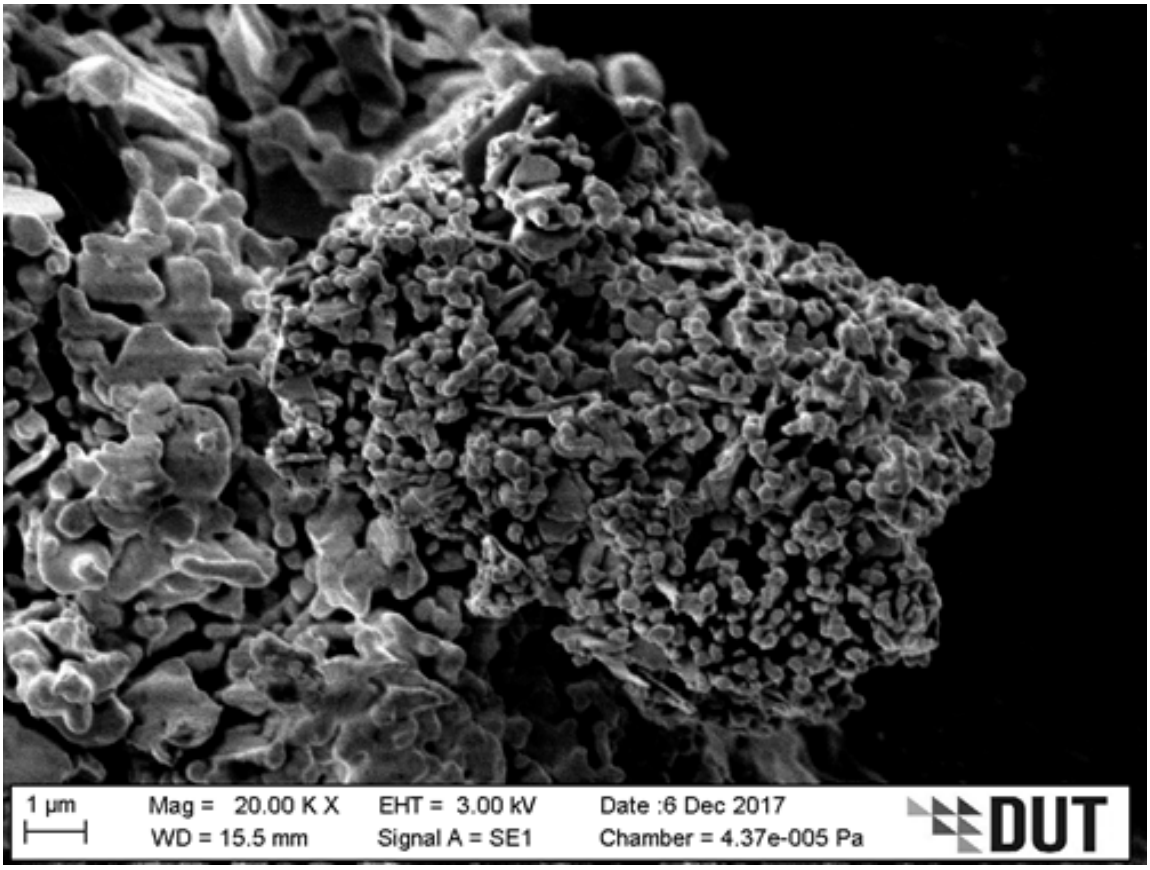

Figure 4. 4: SEM image of the synthesized AuNPs in solid form.

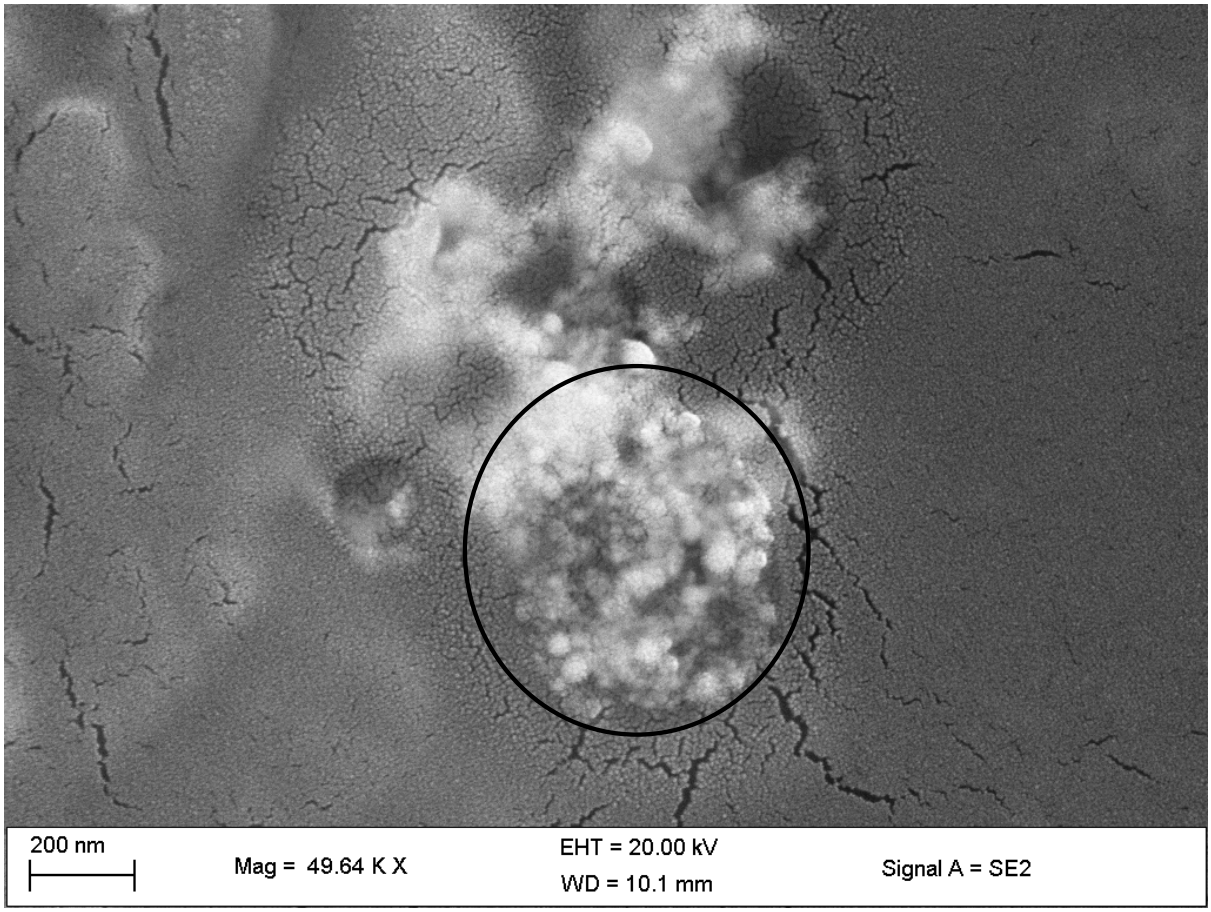

Figure 4. 5: SEM image of the AuNPs in the presence of 30 ppT NaCl in solid form.

4.1.5. Spectroscopic analysis

Figure 4.6 shows FTIR spectra of citrate capped AuNPs taken in the wavelength range of 4000 cm^{-1} - 400 cm^{-1}. Generally, in the synthesis of AuNPs, ligands bind on their surface then stabilize the nuclei and large nanoparticles against aggregation by electrostatic repulsive force (Sapsford, Berti and Medintz 2006). Hence, FTIR was used to confirm a successful synthesis of the stable citrate capped AuNPs in solution by comparing with the FTIR spectrum of tri-sodium citrate salt (**Figure 4.6a**), the synthesized AuNPs solution (**Figure 4.6b**) and AuNPs with NaCl (**Figure 4.6c**). In the region of 3700-3100 cm^{-1} in both spectrums, the peak at ≈3540 cm^{-1} is mainly due to O-H stretching absorption of COOH and water molecules present in the sample (Gene Chong *et al.* 2018). In the fingerprint region, the characteristic peak at 1782 cm^{-1} is for the carbonyl stretch in carboxylic-acid dimers (Gene Chong *et al.* 2018). The sharp band at ≈1614 cm^{-1} in the citrate spectrum that slightly shifted to ≈1520 cm^{-1} in the AuNPs spectrum was assigned to the stretching vibrations of $\nu(C{=}OO^{-})$ from the

carboxylate group in citrate (Park and Shumaker-Parry 2014). Citrate symmetric/asymmetric carboxylate COO^- stretching are characteristics vibrations when bonded with AuNPs surface (Wulandari *et al.* 2008; Park and Shumaker-Parry 2014) . The peak at ≈1290 cm^{-1} in both spectrums was assigned to the C–OH stretching vibration frequency from the carboxylic acid group in citrate (Gene Chong *et al.* 2018). The peak resonances found in both spectrums indicate that the citrate molecules are bound to the surface of the synthesized gold nanoparticles. In **Figure 4.6c**, the peak observed ≈1520 cm^{-1} where stretching vibrations of $\nu(C{=}OO^-)$ occur might be due to traces of tri-sodium citrate in solution. The differences in the three spectrums showed the encapsulation of AuNPs with citrate molecules was achieved (**Figure 4.6b**) and the reaction of AuNPs with NaCl (**Figure 4.6c**) broke the capping agent barrier during ligand exchange and the Na^+ ions attached themselves on the surface of the AuNPs in solution.

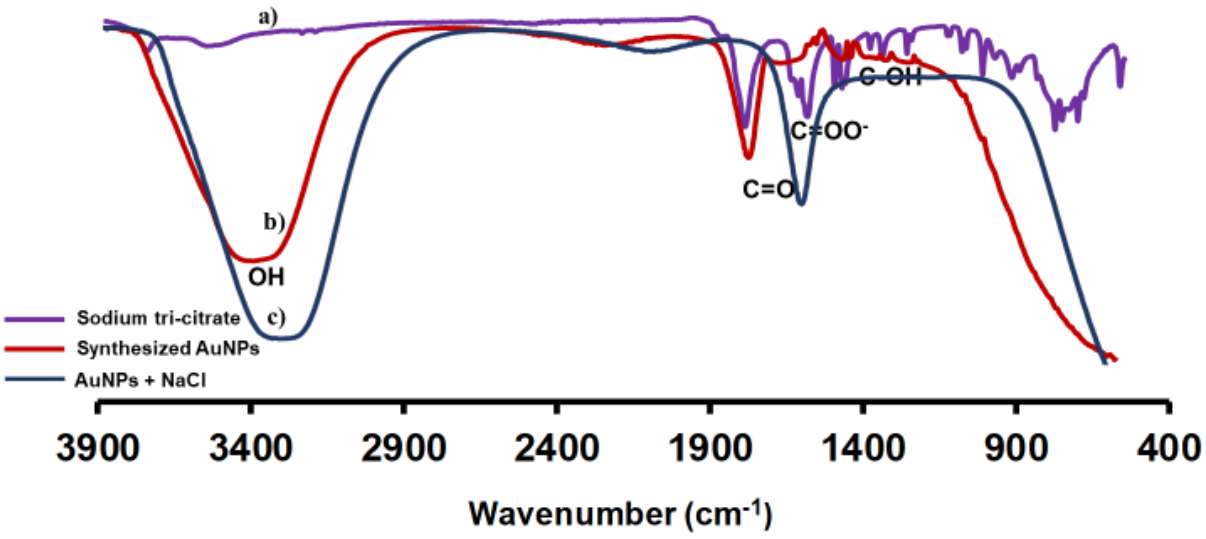

Figure 4. 6: FTIR spectra of (a) solid tri-sodium citrate, (b) synthesized AuNPs solution and (c) a solution of AuNPs with NaCl.

4.2. Effect of AuNPs-NaCl volume ratio

The absorbance of AuNPs solution was recorded after the addition of different volumes of AuNPs into NaCl solution to establish a suitable ratio where maximum aggregation can be observed. The volume ratio of AuNPs to NaCl had to produce a clear colorimetric response and provide adequate volume that fits in the sample holder colour viewer of the developed AuNPs colorimetric kit. **Figure 4.7a**, displays the effect

of AuNPs volume on the sensor and from the results it was observed that the absorbance increased sharply with the increase of AuNPs volume from 500 to 3000 µL. When AuNPs volume was higher than 2000 µL, the absorbance approached a stable condition. Thus, 2000 µL was selected as the optimum volume of AuNPs for the on-site detection of NaCl. **Figure 4.7b**, shows the curve of absorbance vs the volume of NaCl added to 2 mL AuNPs solution. It was observed that the absorbance increased upon the addition of NaCl from 100 to 400 µL, after 400 µL, the trend of the curve became slowly stable. Therefore, 400 µL was selected as the optimum volume of NaCl added to the 2 mL AuNPs solution.

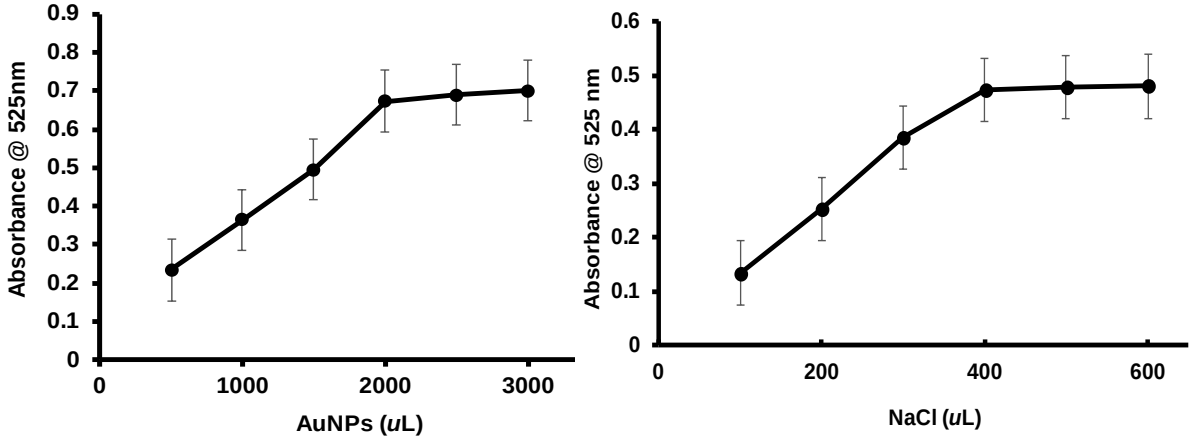

Figure 4. 7: The effect of AuNPs and NaCl amount in the analysis of the developed and fabricated sensor was tested using different volumes of (a) AuNPs and (b) NaCl.

4.3. The effect of ionic strength

It can be observed **in Figure 4.8a** and **4.8b** that the critical point of the stability of AuNPs was achieved with 30 ppT NaCl concentration which was the point of intersection at the flocculation study. The citrate capped AuNPs were able to interact with a cation of the analyte (NaCl), thereby resulting in destabilization of the negative surface charge of AuNPs. This interaction of the cation with the AuNPs led to flocculation, which depends on the concentration of NaCl. The addition of NaCl induced changes to the surface of the gold nanoparticles causing alterations of particle surface Plasmon resonance properties. The gradually increased NaCl concentration induced aggregation of the nanoparticles, resulting in the red shifting of a peak at 525 nm to a longer wavelength to 660 nm (Rivero *et al.* 2017; Zhang *et al.* 2017).

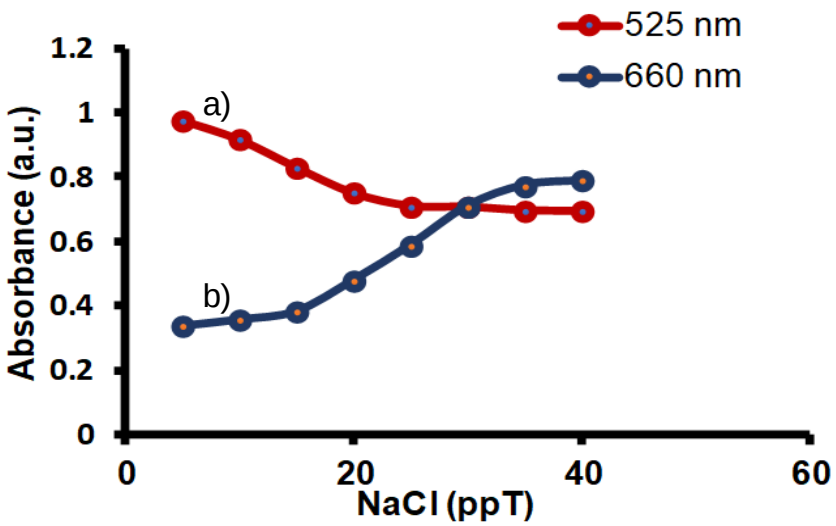

Figure 4. 8: UV-Vis analysis resultant plot for the evaluation of ionic strength on the performance of AuNPs as efficient sensors for the detection of NaCl concentration measured at (a) 525 nm and (b) 660 nm.

4.4. Optical measurements

Colorimetric assay based on the colour properties of gold nanoparticles was conducted for NaCl in the concentration range of 5-40 ppT. As shown in **Figure 4.9**, the introduction of various standards of NaCl into AuNPs resulted in a colour change from wine red to blue. It was observed that the colour (wine red) of AuNPs started to fade as trace amounts of NaCl were added. As the concentration of NaCl was increased, the blue colour started to appear. Therefore, each colour corresponded to the amount of NaCl added, a shift was seen as the colour moves from the deep red of AuNPs to light red for the lower concentration (5-10 ppT), then to purple for the intermediate concentration (15-25 ppT) and finally to blue for the highest concentration range (30-40 ppT). This change was due to the flocculation of AuNPs in solution by aggregation that facilitated optical changes that was visually observed (Rivero *et al.* 2017; Zhang *et al.* 2017). These results agreed with study conducted by Liu and co-workers (2012) where a similar colour trend was observed in a colorimetric assay using AuNPs with increasing NaCl concentration (Liu *et al.* 2012).

Figure 4. 9: Photograph of the AuNPs in the presence of 5-40 ppT NaCl range, the volume ratio of AuNPs and NaCl within each hydrophobic circle barrier of the *μ*PAD is 80 µL: 20 µL.

4.5. UV-Vis spectroscopy analysis

The change in UV-Vis spectra of the AuNPs upon the addition of NaCl solutions in the concentration range of 5-40 ppT was recorded in **Figure 4.10**. Two well-separated SPR peaks were observed in the spectra. The introduction of NaCl into AuNPs solution resulted in a decrease of SPR intensity at 525 nm with an increase of the peak 660 nm. This was due to the aggregation of AuNPs that occurred during the addition of NaCl solutions. This resulted in the red shift of the maximum absorption of AuNPs. The UV-Vis spectra were in agreement with the colorimetric assay array given in **Figure 4.9**. The colour of AuNPs solution changed from wine red to blue, hence the SPR peak shifted to longer wavelengths.

Furthermore, it was observed that when NaCl concentration was 30 ppT, the variance to the intensity was starting to reach maximum indicating that aggregation of AuNPs. This transformation behaviour of AuNPs demonstrated by LSPR absorption bands displayed in **Figure 4.10**, showed that the developed sensor works efficiently in the concentration range of 5-40 ppT. This was an indication that the developed sensor could be applied in the quantitative determination of NaCl in seawater and estuaries where the typical NaCl levels are expected to be in the ranges of 28-33 ppT (Strickland and Parsons 1972; Kolesar *et al.* 2018; Papaslioti *et al.* 2018) and 0.5-10 ppT (Meade 2003; Feng *et al.* 2017), respectively.

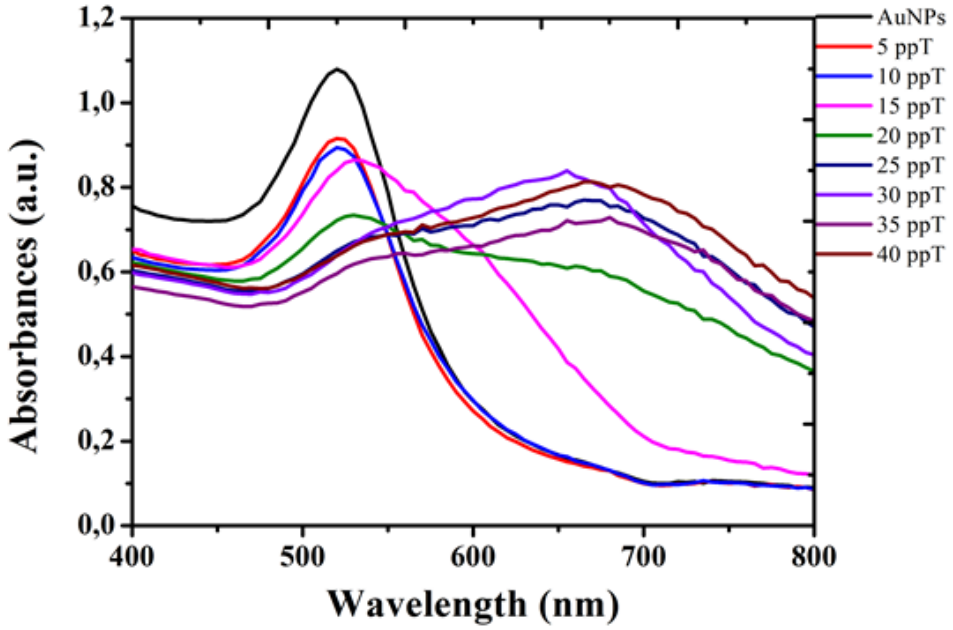

Figure 4. 10: UV–Vis spectra of the AuNPs after the addition of different concentrations of NaCl in the range of 5-40 ppT.

4.6. Effect of sample pH

The pH of water is an essential factor in environmental water samples. For practical application, the developed AuNPs sensor must possess the ability to adapt in different pH levels of the tested water samples. The evaluation of pH effect on the detection of NaCl was done using NaCl spiked solutions in the range of 10-30 ppT (**Figure 4.11**). The initial pH of the spiked solutions with 10, 20 and 30 ppT of NaCl was found to be 9.14, 8.27 and 7.32 respectively. The pH was then adjusted to 3, 6 and 9 where necessary with 6M NaOH or 6M HCl. The pH range represented both alkali and acidic forms that may be encountered in real samples. For 10 ppT the recoveries were 103.2%, 104.9% and 99.7%, for 20 ppT were 100.6%, 101.8% and 99.15%, for 30 ppT were 100.3%, 99.7% and 101.3% for pH 3, 6 and 9 respectively. The calculated recoveries of NaCl in the studied pH range indicated that there was no change in the behaviour of the AuNPs upon exposure to these various pH levels and that the developed colorimetric sensor was not affected by the acidity or alkalinity of the system. These results are similar to the behaviour of AuNPs in this pH range reported for other colorimetric sensors (Li *et al.* 2017b).

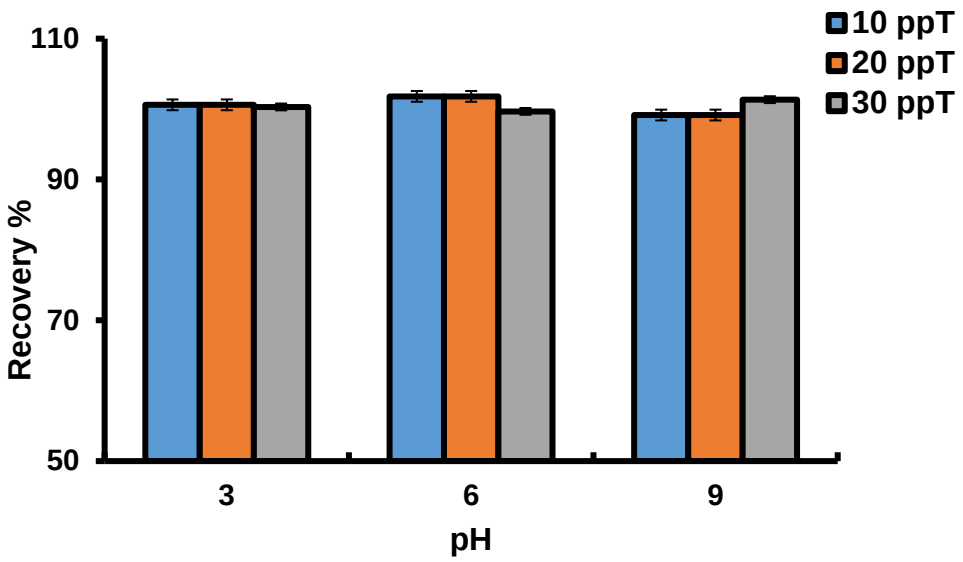

Figure 4. 11: Recoveries of NaCl in various pH levels (3, 6 and 9), for spike solutions with NaCl concentration of 10, 20 and 30 ppT.

4.7. AuNPs contact time

The relationship between mean intensity and analysis time ranging up to 24 minutes was studied using 30 ppT NaCl solution. As shown in **Figure 4.12,** the experimental results showed that the mean colour intensity in greyscale percentage remained constant from 0 to 6 minutes and gradually increased from 8-14 minutes, after 14 minutes the colour intensity increased at a faster rate until it reached 24 minutes. The results suggested that the aggregation of the AuNPs was highest between 0 to 6 minutes and gone under completion in this period hence the darker colorimetric intensity response of solutions. The intensity percentage increased as the solution colour was fading over longer exposure time. In **Figure 4.12** picture insert, the blue colour response began to fade after 6 minutes, indicating less aggregation of AuNPs from this point forward hence, the high greyscale percentages. Therefore, the response time for the colorimetric sensor can be taken from 1 to 6 minutes, where aggregation of the nanoparticles is highest thus producing visual colorimetric responses. This time is enough to the technician when conducting field samples to process the results by comparing the right sample colour with the corresponding concentration in the Lovibond device before colour fading occurs. The mean RGB values of the solution at each time interval were analysed and can be seen in **Table 3**, it was observed that the B values are larger than the R and G values in each row.

In the RGB colour model when one component increases, the colour will go more towards that component and become lighter, hence the lighter the blue colour as time increased.

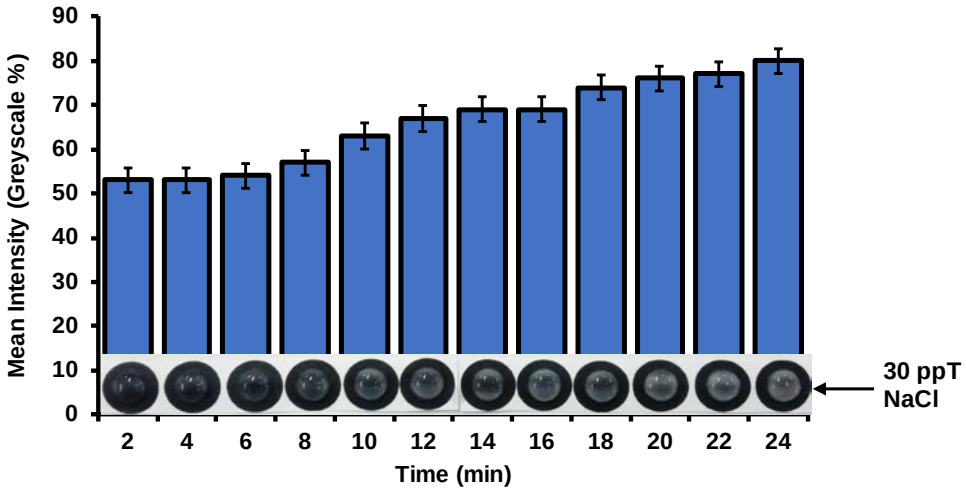

Figure 4. 12: Bar graph of the mean intensity measured for a 30 ppT NaCl solution at different time intervals to evaluate the effect of response time for AuNPs, insert is the corresponding image of the analysis.

Table 4. 1:Mean RGB values with corresponding intensity of the 30 ppT NaCl solution at different time intervals to study the response time of AuNPs (N=3).

Time (min)	Mean R	Mean G	Mean B	Mean
2	38	40	53	53
4	39	43	54	53
6	37	46	53	54
8	42	53	57	57
10	39	48	58	63
12	45	56	62	67
14	43	50	68	69
16	58	67	72	69
18	54	59	76	74
20	65	75	79	76
22	75	86	90	77
24	66	73	92	80

4.8. Negative control

Negative control experiments were conducted using egg white albumin (EWA), a protein. The AuNPs solution was added to the EWA and to EWA containing NaCl in the concentration range of 5-40 ppT. As can be observed in the UV-Vis spectra in **Figure 4.13a**, the absorbance of the AuNPs solutions showed no obvious decrease in all different concentrations of NaCl concentrations added and all the mixtures had the SPR peak at 525 nm along with that of the AuNPs solution. This was due to the EWA stabilizing the AuNPs preventing functionalization of all active sites on the metallic surface hence preventing any possible alterations to the SPR and aggregation of the AuNPs in the mixtures (Wei *et al.* 2017). The EWA also lowers the affinity of NaCl to the AuNPs as a result the NaCl ions remain suspended outside the EWA layer (Lai, Chang and Wang 2017). The image in **Figure 4.13b** revealed that there was no change in colour of the mixtures, this was also evident in the UV-Vis spectra results. The environmental samples analysed in this study (estuarine and seawater) do not contain any protein like EWA, therefore, the AuNPs will be able to detect the NaCl levels in the water with no apparent difficulty.

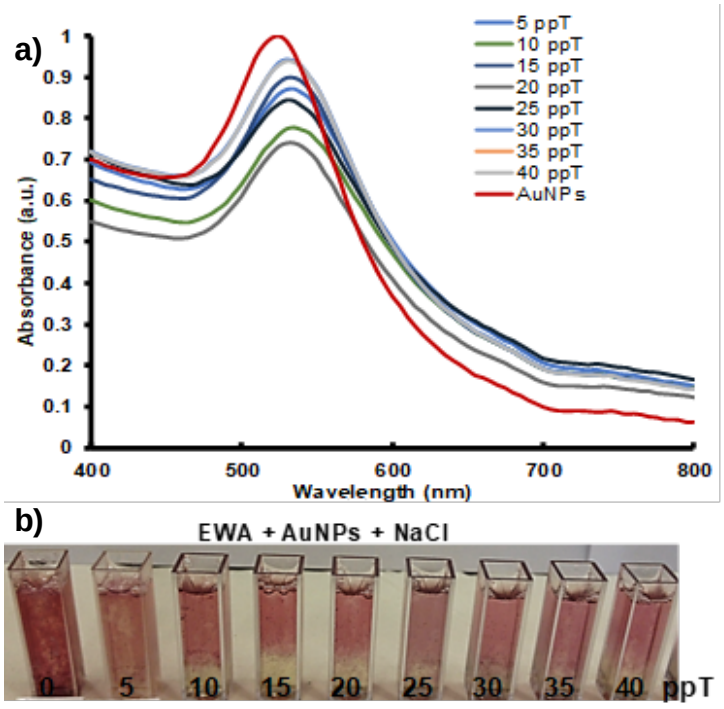

Figure 4. 13: (a) Negative control test results of UV-Vis analysis of the mixtures. (b) Corresponding image for the AuNPs colorimetric assay for the mixtures.

4.9. Colorgrab intensity measurements

Light can affect the colour of solutions, too much light can make solution appear paler than usual while the absence of light makes solutions appear more intense in colour (Langer 2001). Using the smartphone-based intensity detection, the colour change can be monitor by recording the greyscale % values. To perform the analysis, the mobile App (Colorgrab) was downloaded online in the Samsung J1 and the change in intensity values of the cuvettes containing AuNPs solutions in the presence of different concentrations of NaCl were measured by using the back camera. This colorimetric analysis by smartphone provides a simple solution to measure variations in intensity by providing % values of each AuNPs-NaCl reaction even when the naked-eye observation is not sufficient for further analysis.

Advantages of using this App include rapidness and the ability to compensate for background under or over lighting (Abbasi-Moayed, Golmohammadi and Hormozi-Nezhad 2018; Yusufu and Mills 2018). **Figure 4.14a** demonstrates how this App was applied using a smart phone camera to measure the intensity. The intensities of the calibration standards from 5-10 ppT increased. This was due to the solution of AuNPs (0 NaCl added) becoming paler as the intermediate colour (purple/violet) appeared from 15-25 ppT. From the 15 ppT concentration, the intensity gradually decreased. This was due to the increased aggregation of AuNPs in solution leaning towards the blue colour conversion as the NaCl concentration continued to increase. The mean intensity was in the range of (42.33-57.66%) in Greyscale percentages. Therefore, the results of the measured intensity using Colorgrab were substantial to save time by confirming the differences in colour intensity before ImageJ colour processing. **Figure 4.14b**, shows the bar graph of the measured mean intensity, insert: photograph of a smart phone equipped with Colorgrab application measuring the intensity in the NaCl calibration standards.

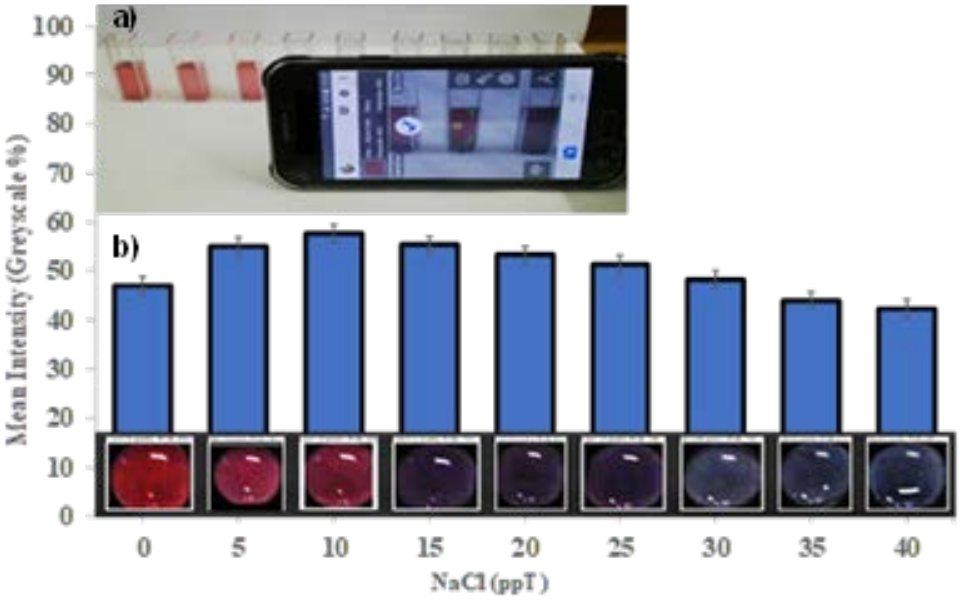

Figure 4. 14: (a) Mobile smartphone equipped with Colorgrab application for intensity measurements (b) Bar graph of the mean intensity of the NaCl calibration standards, insert images of the colorimetric assay of NaCl standard solutions using AuNPs.

4.10. Image processing

ImageJ software was used to measure the colour dynamics between the reaction of NaCl and AuNPs. A photograph of standards was uploaded to the ImageJ application software as observed in **Figure 4.15a**. This action properly exposed the colour shades and their corresponding intensities visually in the form of RGB values. **Figure 4.15b**, shows the picture of the calibration standards, the background effect was eliminated revealing the true uncompromised colour hues of solutions. The resultant colours in the processed image in **Figure 4.15b,** were duplicated to produce solid colours as shown in **Figure 4.15c**.

Figure 4. 15: Colour formation using ImageJ image processing. (a) Actual image uploaded to ImageJ. (b) Image with background separation mode. (c) Resultant duplicated colours for RGB analysis.

To apply the color change of AuNPs in the presence of NaCl for on-site detection application, the changes in RGB values when the wine red color of AuNPs changes to blue upon addition of NaCl must be established. The standard RGB scale is represented by whole-number value system for each of the three colors, the red, green and blue from 0 to 255. In that scale, the number [255,255,255] corresponds to pure white whereas [0,0,0] to absolute black (Leon *et al.* 2006). The mean RGB values of the solid colours in **Figure 4.15c** were measured in ImageJ by analysing each solid colour square separately to get the Red, Green and Blue value for each colour. The colour scheme for the Lovibond comparator disk was created by incoporating the resultant mean RGB values recorded for each calibration standard into the colour developer using the computer desktop colour application (More fill). **Figure 4.16** illustrates the developed colorimetric scheme along with corresponding mean RGB values for the analysis of NaCl. The created colour pattern for the NaCl calibration standards range matched the colours of the solutions and those processed by imageJ, hence, the Lovibond colorimetric device was fabricated using this colour scheme.

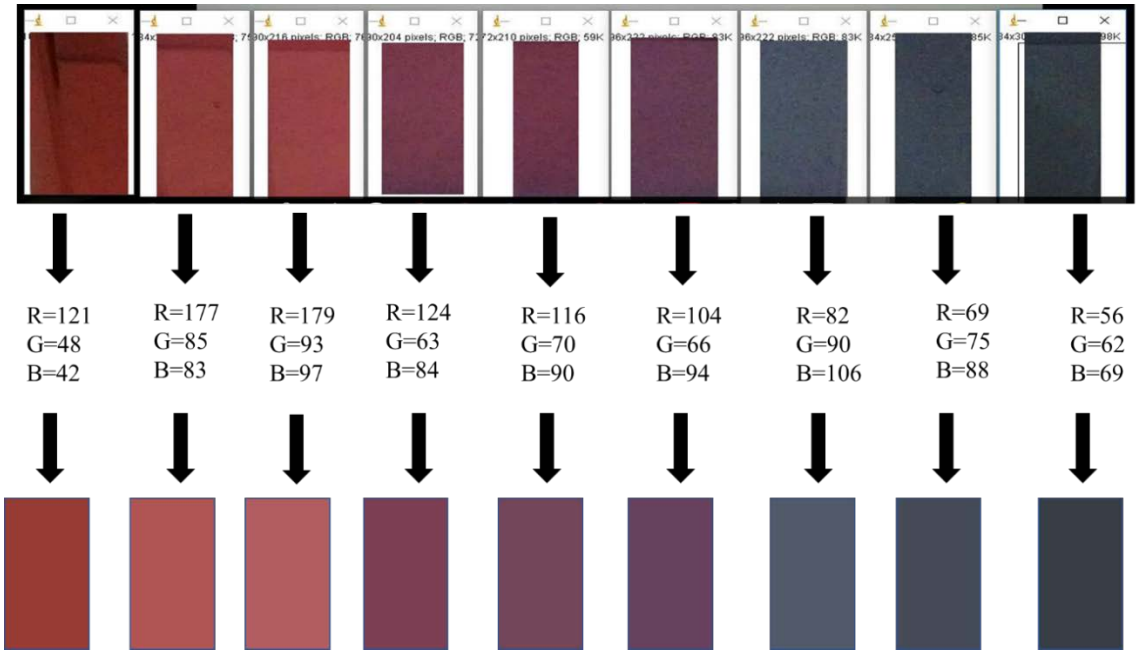

Figure 4. 16: Colorimetric scheme with corresponding calculated mean RGB values.

Figure 4.17 shows the graph of colour development dynamics using the mean R, G, and B values that combine to produce visually stable colour hues that ware easily identified. In **Figure 4.17,** it is clear that the red component varies most significantly as the value of the concentration of NaCl is increased from 10 to 40 ppT, whilst, in contrast, the blue component slowly builds up at all concentration values.

The green and blue colours of the colour model combined at different levels almost parallel to each other to form various strong blue shades which were depending on the intensity of the solution for accurate determination of colour. It was observed in the graph that, at the 30 ppT NaCl concentration the value of B was highest as compared to other points for this colour. The red and blue curves followed the same trend as the graphs in **Figure 4.8** for ionic strength evaluation suggesting a shift of the LSPR peak of the AuNPs to longer wavelengths due aggregation. The domination of the blue colour at this concentration was in agreement with the colorimetric assay in **Figure 4.9** and the UV-Vis LSPR peaks in **Figure 4.10** where maximum aggregation of AuNPs was at its highest. Overall, these results in **Figure 4.17** validated the created colorimetric scheme using RGB colour model values.

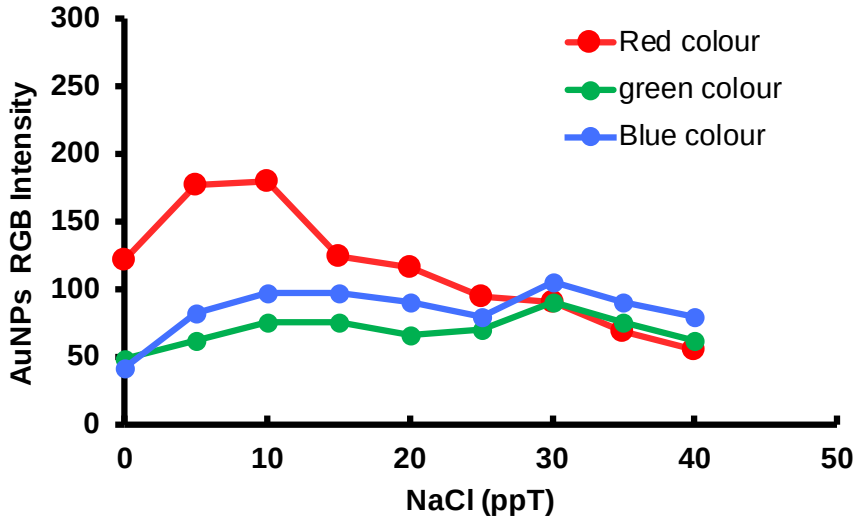

Figure 4. 17: Graph illustrating the R, G, and B colour combination dynamics for the formulation of new colour hues corresponding to NaCl concentration.

4.11. CIELab colour analysis

Delta E was calculated using the CIELab 1976 standard equation (McLaren 1976; Robertson 1977). **Table 4:2 and 4:3** shows the results of the colour differences from the colorimetric assay of the NaCl standard calibration range 5-40 ppT with AuNPs (**Figure 4.18)** Set 1 composes the difference between Line 1 and Line 2, whereas set 2 has the difference between Line 1 and Line 3. The RGB colour model values for each standard colour were converted to L, a and b values using website conversions (http://colormine.org/convert/rgb-to-hunterlab) (McLaren 1976; Yusufu and Mills 2018). The values obtained from the colour difference analysis for set 1 and set 2 gave delta E values which are less than 1 but greater than 0. These results indicated that between each set, there were no significant differences observed in the produced colour patterns for each standard triplicate analysis (McLaren 1976; Robertson 1977; Pointer 1981). The triplicate colour variation test for NaCl produced similar colour pallets for each line for the same NaCl standard, which was a good indication of the stability of the AuNPs used in the developed colorimetric sensor kit. Therefore, CIELab colour management analysis validated colour stability in the presence of the analyte.

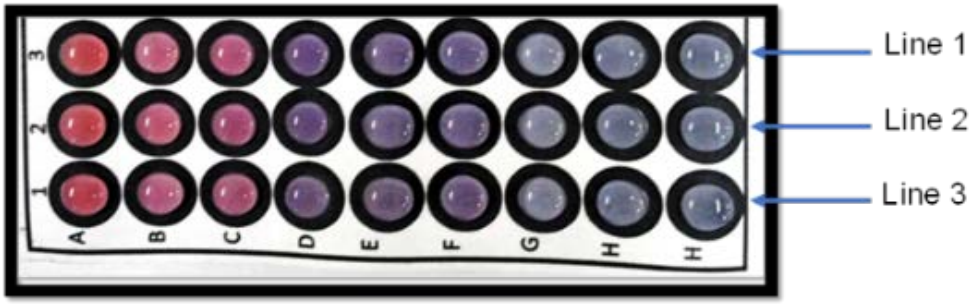

Figure 4. 18: AuNPs colorimetric assay, triplicate analysis used to calculate delta E for colour variations in the NaCl calibration range 5-40 ppT (total volume per sample 100 µL), the volume ratio of AuNPs to NaCl within each hydrophobic circle barrier of the µPAD is 80 µL: 20 µL.

Table 4. 2: Set 1 calculated colour differences (delta E) between the triplicate colorimetric assay of NaCl calibration range 5-40 ppT with AuNPs (N=3).

SET 1									
Concentration (ppT)	*L1	*a1	*b1	$*(L1)^2$	$*(a1)^2$	$*(b1)^2$	ΔE	ΔE status	Comment
0	-0.33	-0.12	-0.03	0.11	0.01	0.001	0.12 ± 0.32	0 <ΔE< 1	Observer does not notice the difference
5	-0.45	0.07	-0.22	0.20	0.01	0.05	0.26 ± 0.05	0 <ΔE< 1	Observer does not notice the difference
10	0.4	-0.06	0.11	0.16	0.004	0.01	0.18 ± 0.39	0 <ΔE< 1	Observer does not notice the difference
15	0.24	-0.35	0.21	0.06	0.12	0.04	0.22 ± 0.02	0 <ΔE< 1	Observer does not notice the difference
20	-0.43	0.48	-0.2	0.18	0.23	0.04	0.46 ± 0.31	0 <ΔE< 1	Observer does not notice the difference
25	0.36	-0.55	0.21	0.13	0.30	0.04	0.48 ± 0. 33	0 <ΔE< 1	Observer does not notice the difference
30	0.05	0.14	0.71	0.003	0.02	0.50	0.53 ± 0.10	0 <ΔE< 1	Observer does not notice the difference
35	-0.48	-0.24	-0.07	0.23	0.06	0.01	0.29 ± 0.71	0 <ΔE< 1	Observer does not notice the difference

Line 1 in photograph (**Figure 4.18**) used as a reference to calculate the colour difference. * and Δ=delta notation.

Table 4. 3: Set 2 calculated colour difference colour (delta E) for NaCl concentration range (5-40 ppT) (N=3).

SET 2									
Concentration (ppT)	*L2	*a2	*b2	$(*L2)^2$	$(*a2)^2$	$(*b2)^2$	ΔE ± SD	ΔE status	Comment
0	-0.49	-0.19	-0.52	0.24	0.04	0.27	0.55 ± 0.03	0 <ΔE< 1	Observer does not notice the difference
5	0.1	0.06	-0.4	0.01	0.004	0.16	0.17 ± 0.06	0 <ΔE< 1	Observer does not notice the difference
10	0.24	-0.84	-0.14	0.06	0.71	0.02	0.78 ± 0.43	0 <ΔE< 1	Observer does not notice the difference
15	0.06	0.1	0.41	0.004	0.01	0.17	0.18 ± 0.03	0 <ΔE< 1	Observer does not notice the difference
20	0.02	0.01	0.06	0.0004	1E-04	0.004	0.004 ± 0.31	0 <ΔE< 1	Observer does not notice the difference
25	0.01	0	0	$1x10^{-4}$	0	0	$1x10^{-4}$ ± 0.34	0 <ΔE< 1	Observer does not notice the difference
30	0.56	-0.27	-0.03	0.31	0.07	0.0009	0.39 ± 0.09	0 <ΔE< 1	Observer does not notice the difference
35	-0.25	-0.4	-0.44	0.06	0.16	0.19	0.42 ± 0.06	0 <ΔE< 1	Observer does not notice the difference
40	-0.46	0.02	-0.08	0.21	0.0004	0.006	0.22 ± 0.10	0 <ΔE< 1	Observer does not notice the difference

Line 1 in photograph (**Figure 4.18**) used as a reference to calculate the colour difference. * and Δ=delta notation.

To further evaluate the resultant colour pattern variations in the optimized NaCl calibration range, CIELab was used to measure the differences between the series of colours developed for the Lovibond device. In order for the colorimetric device to fully function for its intended use which is on-site detection of NaCl in seawater, the engraved optimised NaCl concentrations on the device must be distinguishable by the naked eye for easy comparison with the sample analysed. **Table 4.4,** shows the ∆E calculations of the gold nanoparticles and the NaCl calibration standards (5-40 ppT) with AuNPs. The calculations were based on the mean $(*L)^2$, $(*a)^2$ and $(*b)^2$ values for Line 1, 2 and 3. From the results, the calculated ∆E was found to be above 5 for all colour difference measurements, each calibration standard had a noticeable colour difference as the concentration was increased. These differences did not discriminate towards the unexperienced observer but represent every observer, meaning that everyone could use the developed colorimetric sensor kit and quantify NaCl without any difficulties in comparing the sample colour to the optimized colours on the Lovibond device. Therefore, the AuNPs colorimetric sensor for the analysis of NaCl in seawater was used for on-site detection in real samples.

Table 4. 4: Colour difference measurements between two colours of the increasing NaCl concentration colorimetric assay with AuNPs (N=3).

Concentration	Delta E ± SD	∆E status	Comments
0-5	10.11 ± 4.96	∆E > 5	Observer notices two different colours
5-10	9.99 ± 2.25	∆E > 5	Observer notices two different colours
10-15	19.75 ± 2.29	∆E > 5	Observer notices two different colours
15-20	8.27 ± 2.90	∆E > 5	Observer notices two different colours
20-25	5.53 ± 1.28	∆E > 5	Observer notices two different colours
25-30	25.81 ± 0.40	∆E > 5	Observer notices two different colours
30-35	18.37 ± 0.20	∆E > 5	Observer notices two different colours
35-40	5.44 ± 0.13	∆E > 5	Observer notices two different colours

4.12. Fabrication of Lovibond comparator device

The colour hues obtained from the mean RGB values were used to fabricate the Lovibond comparator disk for quantification of NaCl in environmental samples. Each colour was incorporated into a circular shape design at right angles (90 degrees) to the engraved corresponding optimized concentration on the disk. This was done to allow the Lovibond disk to rotate at 90 degrees to match the colour of the analysed sample with that of the calibrated NaCl concentration. **Figure 4.19** shows the design of the Lovibond device used for the quantification of NaCl in estuarine and seawater. The fabricated Lovibond device was used to measure the concentration of the NaCl calibration standards (5-40 ppT) and the results of the analysis can be seen in **Annexure A**. The concentration of each standard matched the conforming optimized colour on the Lovibond disk estimating the NaCl concentration. The Lovibond device was then used to quantify real samples from the estuary and seawater.

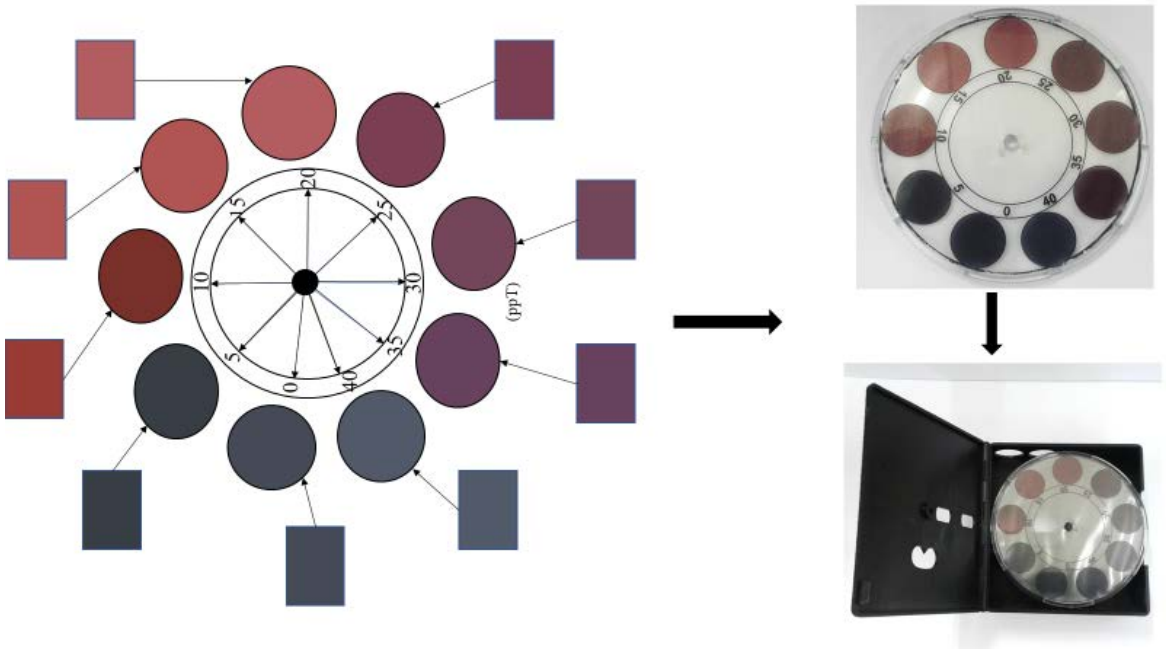

Figure 4. 19: Optimized colorimetric scheme used to fabricate the Lovibond comparative device used for the quantification of NaCl. Colour shade of test strip reveals respective NaCl concentration presence in samples when match with colour wheel.

4.13. Method validation

Validation is essential to determine whether developed methods for the fabricated sensor device are fully appropriate for the aim and objectives designed, or whether the objectives cannot be met with that particular chosen method.

4.13.1. Linearity, detection and quantification limits

The calibration curve given in **Figure 4.20**, shows that the ratio of absorbance recorded at 525 and 660 nm increased linearly (R^2 = 0.998) as the concentration of NaCl was increased in the range of 5-40 ppT. The ratio of the absorbance in two different wavelengths was used for the calibration curve and quantification of NaCl as two separate bands at different absorption wavelength maxima were observed in **Figure 4.10**. This suggested the different physical and chemical changes that the gold nanoparticles would have been undergone in the reaction; therefore, those changes had to be accounted for in the calibration curve for accurate determination of NaCl concentration. In addition, the LOD and LOQ for the developed sensor were calculated based on 3 and 10 times the standard deviation at the minimum NaCl concentration, respectively. LOD and LOQ found for the analysis of NaCl using the proposed method were 1.18 ppT and 3.57 ppT, respectively. The value 3.57 ppT represents the lower LOQ and 40 ppT being the highest calibration standard represents the upper LOQ.

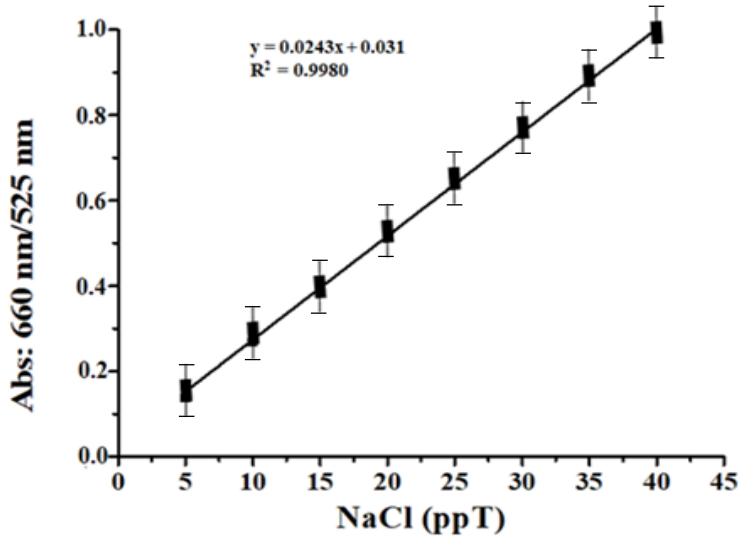

Figure 4. 20: Plot of absorbance ratio at 660 nm/525 nm versus the concentrations of NaCl in the range 5–40 ppT.

4.13.2. Accuracy and precision

The accuracy of the method used to develop AuNPs sensor was determined by calculating the percentage relative error (Bias %) between the mean calculated concentrations and the actual spiked concentrations for the same concentration of NaCl (10, 20 and 30 ppT). The calculated concentration values of the spiked NaCl in **Table 4.5** are in good agreement with the actual values of the spiked concentrations. The results shown in **Table 4.5** for intra-day, the accuracy was between -2.40 to -3.50%, demonstrating high accuracy. The precision test results obtained under optimum conditions for NaCl range of 10, 20 and 30 ppT were analysed and repeated for 5 consecutive days (inter-day) from three measurements of each spiked sample. Additionally, an intra-assay precision value in %RSD was calculated in **Table 4.5** which represented a repeatability test. Repeatability is expressed as the precision under the same operating conditions over a short period of time, usually within a day or within-run (Peters, Drummer and Musshoff 2007). The %RSD was found to be in the range of 0.01-0.03% for the spiked samples. In **Table 4.6**, for inter-day analysis, the precision of the method evaluated by %RSD values was found to be in the range of 0.04-0.06%. The results displayed high precision of the AuNPs based colorimetric sensor method.

Table 4. 5: Accuracy test of the AuNPs for intra-day evaluation. SD = Standard Deviation, SE= Standard Error, % RSD = Relative Standard Deviation, Accuracy bias = [(Calculated - Added) / Added] x 100, (N=9).

Intra-day (same day)			
Added concentration (ppT)	10	20	30
Mean absorbance	0.22	0.36	0.49
Calculated concentration	9.65	19.63	29.29
Recovery (%)	96.53	98.17	97.63
SD	0.01	0.05	0.01
Precision %RSD	0.03	0.13	0.01
Accuracy bias (%)	-3.50	-1.85	-2.40
SE of intercept		0.003	

Table 4. 6: Precision test analysis of the AuNPs for inter-day (5 days) evaluation. SD = standard deviation, SE= Standard Error, % RSD = Relative Standard Deviation. (N=45).

Inter-day (5 days)			
Added concentration (ppT)	10	20	30
Mean absorbance	0.28	0.36	0.48
Calculated concentration	10.67	18.60	30.63
Recovery (%)	106.67	93.02	102.10
SD	0.01	0.02	0.02
%RSD	0.04	0.06	0.04
SE of intercept	0.025		

4.13.3. Robustness

The robustness of the method was examined by varying the absorption wavelength of AuNPs to 530 nm and 550 nm. Gold nanoparticles of different spherical sizes in solution had a capacity to absorb at different wavelength regions in the spectrum (Daniel and Astruc 2004b). This effect had to be accounted for in the developed AuNPs colorimetric sensor to study any variations in the results that could arise due to size effect. Three sets of spiked NaCl concentration of 10, 20 and 30 ppT were analysed and the results of the analysis are presented in **Table 4.7**. The recoveries of the spiked samples were in the range 96.05-101.17% for the 530 nm concentration range and were in the range of 98.63-105.57% for the 550 nm. The %RSD for the 530 and 550 nm wavelengths analysis were 0.004-0.10% and 0.04-0.06% respectively, proving the developed sensor to be highly robust and efficient even at longer absorption wavelengths than 525 nm of the synthesized AuNPs in this study. Therefore, from the results obtained changing the absorption wavelength variables did not affect the colorimetric response of AuNPs.

Table 4. 7: Robustness test of the developed method (N=9).

Wavelength	530 nm			550 nm		
Added concentration (ppT)	10	20	30	10	20	30
Mean Absorbance	0.2789	0.3689	0.4603	0.2819	0.3856	0.4478
Calculated	10.12	19.40	28.81	10.42	21.11	29.59
Recovery (%)	101.17	96.99	96.05	104.23	105.57	98.63
SD	0.009	0.002	0.05	0.01	0.03	0.03
%RSD	0.034	0.004	0.10	0.04	0.06	0.05
SE of intercept	0.0008			0.014		
SD of intercept	0.0024			0.041		

SD = Standard Deviation, SE= Standard Error, %RSD = Relative Standard Deviation.

4.13.4. The effect of interferences on the analysis of sodium chloride

The UV-Vis and colorimetric assay response of AuNPs in the presence of various cations (Ca^{2+}, K^{+}, Mg^{2+}) and anion (SO_4^{2-}) was measured to test the selectivity of AuNPs sensor. These ions were selected as possible competitors as they are known to be present in seawater (Lv *et al.* 2018; Souid *et al.* 2018). The concentrations of Ca^{2+}, K^{+}, Mg^{2+} and SO_4^{2-} in seawater varies between locations in both abundance and concentration due to salinization. Their concentration ranges are reported to be typically from 0.15-0.35 ppT for Ca^{2+} and K^{+}, 0.125-1.5 ppT for Mg^{2+} and 1-3 ppT for SO_4^{2-} (Nielsen *et al.* 2003; Nicolini, Ferraz and Borges 2017; Telahigue *et al.* 2018). In this study, the effect of these ions in the detection of NaCl was investigated where aqueous solutions were spiked with individual ions at levels that are within the concentration ranges usually found in seawater. The spiked concentrations for Ca^{2+}, K^{+}, Mg^{2+} and SO_4^{2-} were in ranges of 0.15-0.35 ppT, 0.15-0.35 ppT, 0.125-1.5 ppT and 1-3 ppT, respectively. The results are depicted in **Figure 4.21** (**1-4**).

The results showed that the addition of these ions into AuNPs gave rise to single LSPR peaks at 525 nm. This is the maximum wavelength (525 nm) for the absorption of AuNPs. This implied that the investigated ions at the aforementioned concentrations did not have the ability to induce aggregation of nanoparticles and shifted the LSPR band of the AuNPs to longer wavelengths to give a resultant colour change from wine red. The results were further corroborated by the accompanying optical images from the colorimetric assay results in **Figure 4.21** (**A, B, C & D**), where the wine-red colour of the AuNPs remained in solution when the AuNPs interacted with the cations and anion solutions.

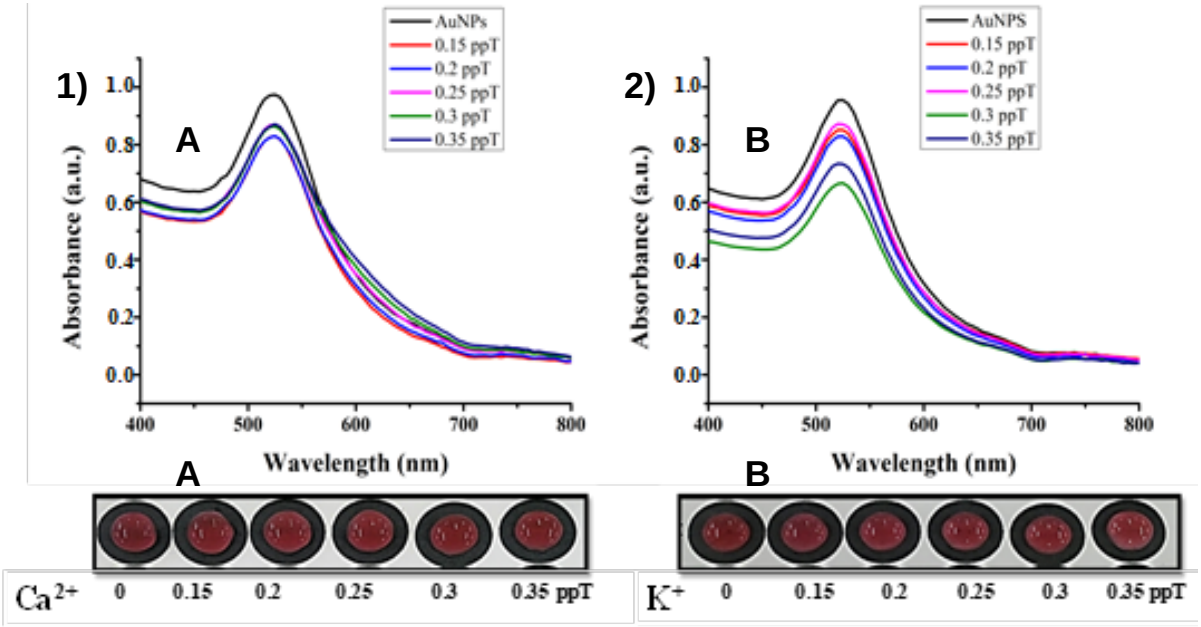

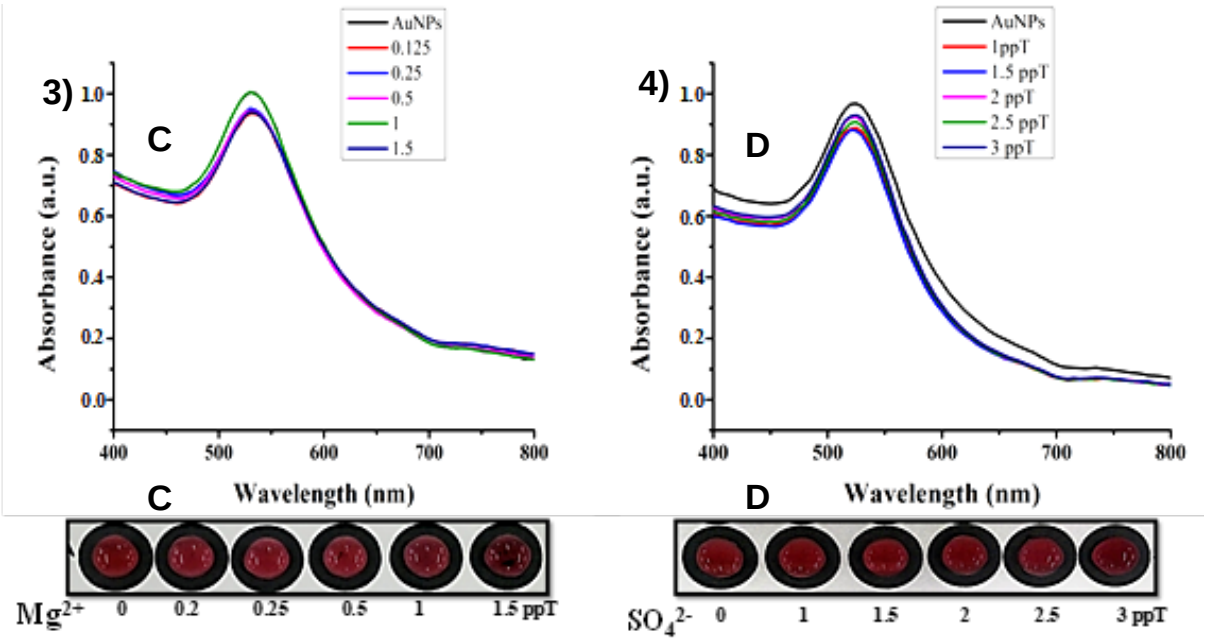

Figure 4. 21: (1-4) The LSPR peaks of AuNPs in presence of interfering ions with different concentrations of (A: Ca^{2+} B: K^{+} C: Mg^{2+} and D: SO_4^{2-}). Corresponding images of the AuNPs in the presence of different concentrations of (A: Ca^{2+} B: K^{+} C: Mg^{2+} and D: SO_4^{2-}).

The same ions were added into the 30 ppT NaCl solution. Resulting solutions were introduced into AuNPs solutions in order to further investigate their effect on detection of NaCl. As presented in **Figure 4.22** (**1-4**) **and 4.22** (**A, B, C & D**), there was a significant shift in the LSPR absorption band of the AuNPs which was accompanied by colour conversion of AuNPs solution from wine red to blue. It was observed that NaCl was capable of inducing the aggregation of AuNPs, regardless of the presence of trace amounts of other ions in solution. Therefore, these results proved that AuNPs exhibited good selectivity for NaCl in the presence of Ca^{2+}, Mg^{2+}, K^{+} and SO_4^{2-} which are known to exist in seawater (Lv *et al.* 2018; Souid *et al.* 2018).

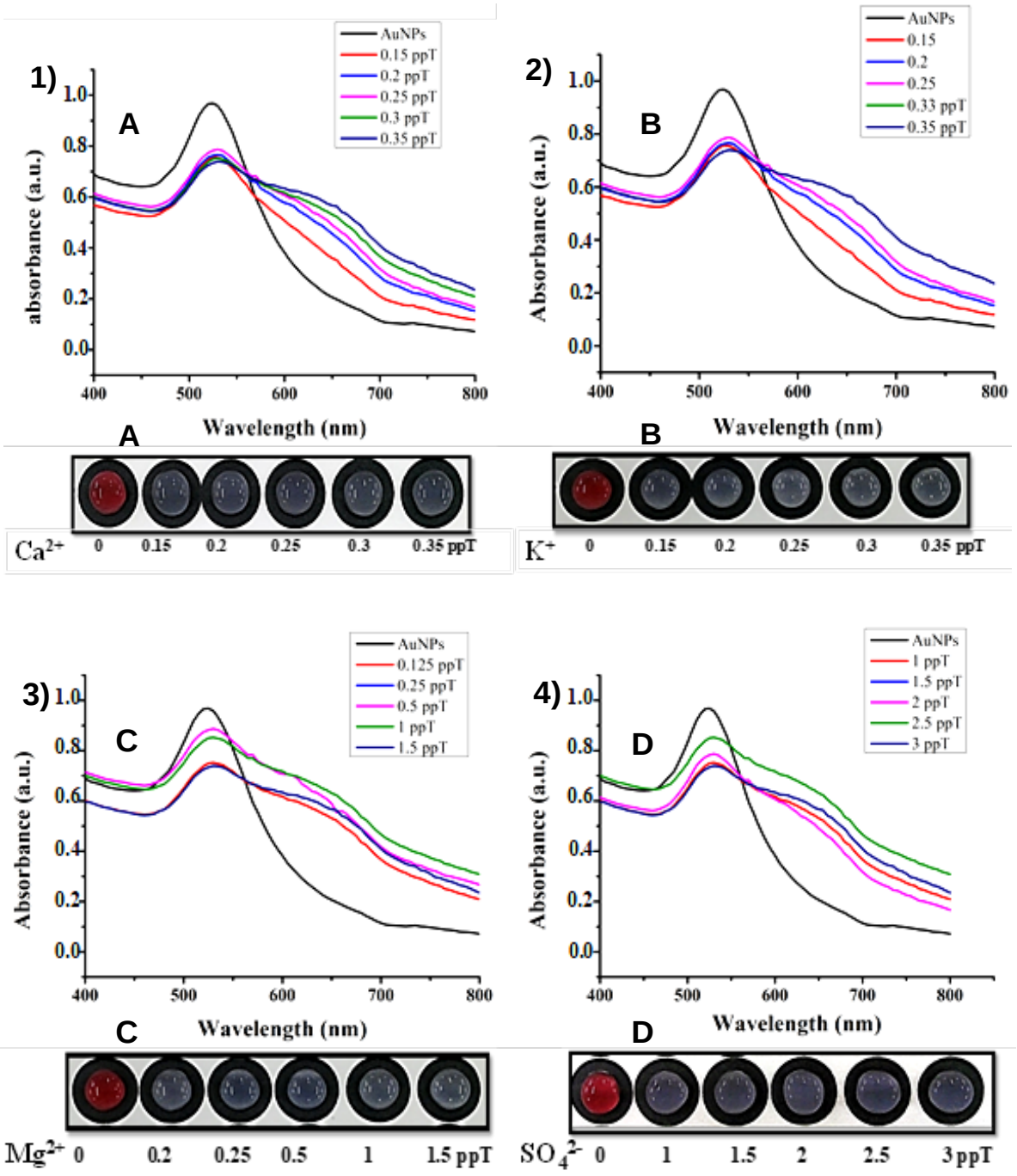

Figure 4. 22: (1-4) The LSPR peaks of AuNPs in presence of interfering ions with different concentrations of (A: Ca^{2+} B: K^{+} C: Mg^{2+} and D: SO_4^{2-}) spiked with 30 ppT NaCl. Corresponding images of the AuNPs in the presence of different concentrations of (A: Ca^{2+} B: K^{+} C: Mg^{2+} and D: SO_4^{2-}) spiked with 30 ppT NaCl.

The selectivity of AuNPs towards NaCl (30 ppT) in the presence of various ions was further studied by comparing the absorbance ratio 660nm/525nm of AuNPs with interference ions Ca^{2+} (0.35 ppT), K^{+} (0.35 ppT), Mg^{2+} (1.5 ppT) and SO_4^{2-} (3 ppT) as observed in **Figure 4.23 and Figure 4.24**. It was observed that the presence of NaCl increased the value of the absorbance ratio 660 nm/525 nm nearly 5 times greater than that of AuNPs with interfering ions which proved that the AuNPs exhibited good selectivity towards NaCl concentration. In order to test the accuracy and precision of the proposed AuNPs sensor towards the determination of NaCl in the presence of interfering ions, the recovered amount of the spiked NaCl concentration in solution was calculated.

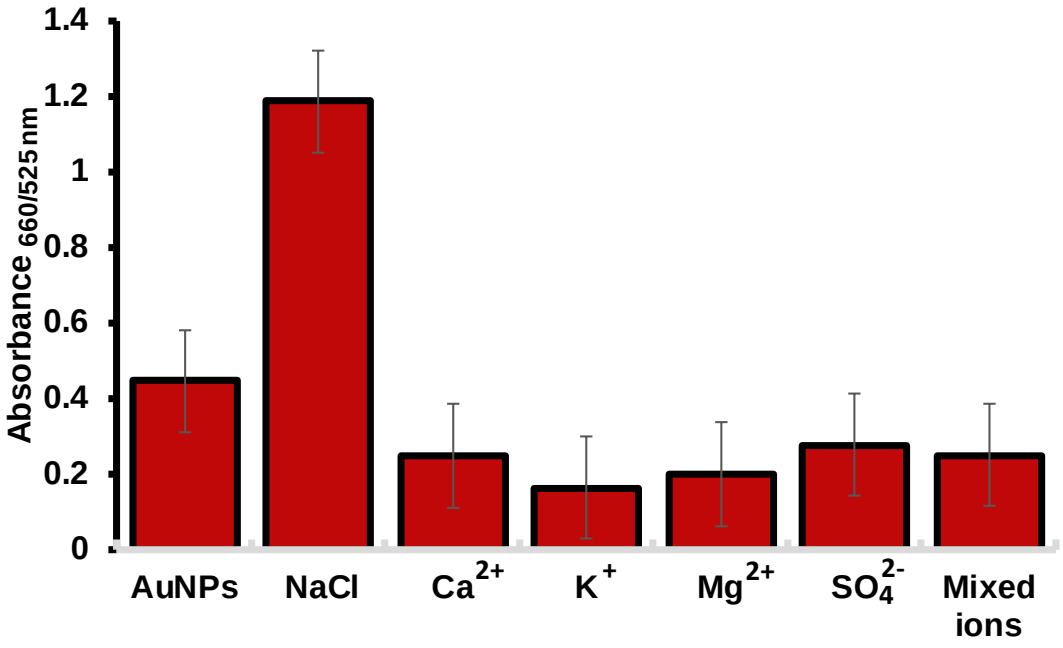

Figure 4. 23: The absorbance ratio (660 nm/525 nm) bar graph of the AuNPs in the presence of interference ions and mixed ions solution, interference ions Ca^{2+} 0.35 ppT, K^{+} 0.35 ppT, Mg^{2+} 1.5 ppT and SO_4^{2-} 3 ppT, 30 ppT NaCl and a mixed ions solution (Ca^{2+} 0.35 ppT, K^{+} 0.35 ppT, Mg^{2+} 1.5 ppT and SO_4^{2-} 3 ppT).

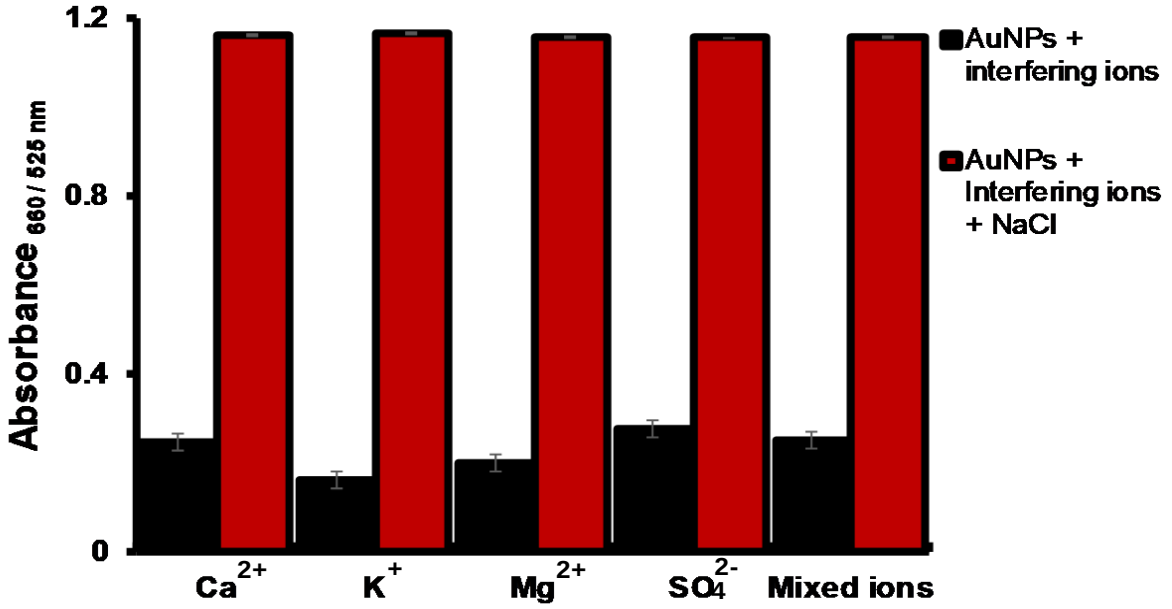

Figure 4. 24: The absorbance ratio (660 nm/525 nm) bar graph of the AuNPs in the presence of interference ions Ca^{2+} 0.35 ppT, K^{+} 0.35 ppT, Mg^{2+} 1.5 ppT and SO_4^{2-} 3 ppT spiked with 30 ppT NaCl and mixed ions solution (Ca^{2+} 0.35 ppT, K^{+} 0.35 ppT, Mg^{2+} 1.5 ppT and SO_4^{2-} 3 ppT) spiked with 30 ppT NaCl vs bar graph of Ca^{2+} 0.35 ppT, K^{+} 0.35 ppT, Mg^{2+} 1.5 ppT and SO_4^{2-} 3 ppT and mixed ions solution (Ca^{2+} 0.35 ppT, K^{+} 0.35 ppT, Mg^{2+} 1.5 ppT and SO_4^{2-} 3 ppT).

In **Table 4.8**, the results of calculated mean, recovery (%) and relative standard deviation (%) of the spiked NaCl concentration (30 ppT) into Ca^{2+}, K^{+}, Mg^{2+} and SO_4^{2-} standard solutions in the ranges of 0.15-0.35 ppT, 0.15-0.35 ppT, 0.125-1.5 ppT and 1-3 ppT, respectively, are presented. The mean concentration of NaCl in spiked solutions was found to be in the range of 29.23-30.30 ppT, which was an indication that the proposed method was accurate for quantification of NaCl in the presence of foreign species. The presence of NaCl in the ionic solutions was easily detected by the AuNPs resulting in the overall recovery of 97-100%. The relative standard deviations were in the range of 1.36-4.71%, which indicated good precision. Therefore, the proposed AuNPs sensor could be employed to detect NaCl without interference from co-existing ions in seawater.

Table 4. 8: Validation of AuNPs sensor method for the analysis of NaCl in seawater in the presence of various concentrations of interfering ions (N=3).

Interfering ions	Concentration range	Measured	Mean	%RSD
Ca^{2+}	0.15-0.35	29.23	97	4.71
K^{+}	0.15-0.35	30.17	100	1.36
Mg^{2+}	0.125-1.5	30.30	100	2.65
SO_4^{2-}	1-3	29.42	98	5.63
Simulated	0.35 (Ca^{2+}),	29.78	98	2.30

4.13.5. Recoveries for the three tested methods

Table 4.9 shows the results of measured concentration, mean recovery (%) and relative standard deviation (%) of the spiked NaCl concentration (30 ppT) in simulated seawater. Simulated seawater using tap water (35 ppT) and spiked deionized water (10, 20 and 30 ppT) for AuNPs sensor, titration and IC method are presented. The mean concentration of NaCl in spiked solutions for AuNPs sensor using the Lovibond device was quite accurate in its quantification for NaCl. The presence of NaCl in the solutions was easily detected by the AuNPs, resulting in the overall recovery of 100% for three replicate measurements showing high accuracy and reliability of the present AuNPs sensor. The relative standard deviations for AuNPs was 0% which indicated high precision to further confirmed that the sensing platform had great potential for the determination of NaCl. For titration and IC relative standard deviations were in the range of 0.33-2.59% and 1.84-4.47% respectively, the precision was good for the other methods but the AuNPs colorimetric analysis was more consistent in its determination for NaCl concentration. Therefore, the proposed AuNPs sensor along with the Lovibond comparator device could be employed to detect NaCl in real samples without deceptive exertion.

Table 4. 9: Validation of AuNPs sensor method for the analysis of NaCl in estuarine and seawater against conventional analytical techniques (N=3).

		Method								
		Lovibond device			**Titration**			**IC**		
Sample	Concentration range (ppT)	Measured conc. (ppT)	Mean Recovery (%)	%RSD	Measured conc. (ppT)	Mean Recovery	%RSD	Measured conc. (ppT)	Mean Recovery (%)	%RSD
Simulated seawater NaCl (3g)	0.35 (Ca^{2+}), 0.35(K^{+}), 1.5 (Mg^{2+}) and 3 (SO_4^{2-})	30	100	0	30.56	101.88	0.33	26.15	87.15	3.31
Tap water seawater NaCl (3.5g)	0.35 (Ca^{2+}), 0.35(K^{+}), 1.5 (Mg^{2+}) and 3 (SO_4^{2-})	35	100	0	33.21	94.89	0.46	33.85	96.72	1.84
NaCl std1	10	10	100	0	11.01	110.07	2.40	10.35	103.53	4.47
NaCl std2	20	20	100	0	20.08	94.17	2.45	18.82	94.12	2.68
NaCl std3	30	30	100	0	29.53	100.39	2.59	26.04	86.81	3.46

Conc. = Concentration, std= Standard.

4.14 Physico-chemical properties of water samples

Physico-chemical parameters results for the tested seawater and estuary water samples in the two different sampling locations are presented in **Table 4.10** for the month of March and in **Table 4.11** for the month of August. The pH values of the overall samples ranged from 8.10 to 8.39 (slightly alkaline). Electrical conductivity varied from 1.29 to 20.80 mS/cm, with high conductivity experienced in seawater (Blue lagoon, Suncoast beach, Umgeni and Amanzimtoti estuary) and estuary water while samples from upstream in the estuaries (Umgeni estuary and Amanzimtoti estuary) had low conductivity. The EC of the tested samples corresponded to the salinity percentage of the samples, where low salinity percentages of 0.54% and 0.56% were observed in the Umgeni and Amanzimtoti estuaries upstream samples, respectively.

Low salinity values are an indicating of low NaCl concentration in the water samples. Total dissolved solids were in the range of 501-10540000 parts per trillion (ppt) being lowest for estuaries upstream and highest at the estuary and seawater, this might be due to solids carried by revolving sea waves. Dissolved oxygen values of all samples laid between 4.30-5.53 mg/L which is within the normal required oxygen range for bottom feeder animals like crabs, oysters and worms in the water (Milstein *et al.* 2006). For sampling No. 2 samples in **Table 4.11**, the highest pH value (8.92) was observed in the Umgeni estuary 400 m upstream sample and highest EC value (26.67 mS/cm) recorded for the Blue lagoon beach sample.

The lowest pH value of 8.01 was observed in the Durban harbour S1 sample and lowest EC value (4.25 mS/cm) was found in the Umgeni estuary 400 m upstream sample, these samples points are far away from the estuary and the sea hence the low levels in pH and EC. Moreover, these values suggested the effect of salinity had been reduced with the distance away from the beach and estuary area. The TDS for the tested samples were ranging between 489-10360000 ppt being high in the samples that were obtained from the sea coastline area and low in estuaries upstream and Durban harbour. The World Health organization (WHO) standards state that, when the TDS value of river water is higher than 600mg/L that water becomes slightly saline whereas moderately saline limit is 1500 – 7000 mg/L (Ngoye and Machiwa 2004; Edition 2011). Therefore, the sample at Umgeni upstream implied that the NaCl

concentration in the water was very low and the water was free from salt intrusion from the sea. The samples at the Durban harbour S1 and S2 were expected to be less or moderately saline as their TDS values were found to be 879-1057 mg/L. These physico-chemical properties for the samples in **Table 4.11** revealed that there was an effect of salinity in the harbour S1 and near to the estuary area with reference to the electrical conductivity, total dissolved solids and salinity % values. The Durban Harbour S2 sample high TDS might be due to the dirt or pollution caused by the boats fuel emission into the water as they depot in this area.

Table 4. 10: Sampling No 1: Physico-chemical parameters of the collected Seawater and Estuary water samples.

Sample	pH	Conductivity (mS/cm)	DO (mg/L)	TDS (ppt)	ORP (mV)	Salinity (%)	Resistivity(Ω)
Blue lagoon Beach	8.26	20.50	5.45	10300000	828	12.27	48.7
Suncoast Beach	8.12	20.80	5.40	10540000	844.3	13.11	48.1
Umgeni estuary	8.39	15.88	4.89	7820000	1009	9.29	62
Umgeni estuary 405.23 m upstream	8.13	1.26	5.53	501	1029	0.54	960
Amanzimtoti estuary	8.36	19.07	4.30	9590000	946.9	11.42	52
Amanzimtoti Estuary 253.05 m upstream	8.10	1.29	5.33	566	879.3	0.56	860

Table 4. 11: Sampling No. 2: Physico-chemical parameters of the collected Seawater, Harbour and Estuary water samples.

Sample	pH	Conductivity (mS/cm)	DO (mg/L)	TDS (ppt)	ORP (mV)	Salinity (%)	Resistivity (Ω)
Blue lagoon Beach	8.26	26.67	6.21	10140000	1062.0	14.23	47.4
Suncoast Beach	8.47	24.32	9.95	10360000	1088.5	11.11	49.3
Durban South Beach	8.56	20.58	6.11	9030000	1032.2	10.02	47.0
Durban Harbour S1	8.01	17.10	6.29	879	808.1	1.77	882
Durban Harbour S2	8.18	5.43	6.33	1057	739.6	0.66	996
Umgeni estuary	8.38	19.67	6.02	8930000	896.1	9.29	48.1
Umgeni estuary 100 m upstream	8.54	19.24	6.73	7505000	883.7	2.74	48.6
Umgeni estuary 200 m upstream	8.76	19.01	6.22	5530000	900.4	1.44	99
Umgeni Estuary 300 m upstream	8.89	17.06	6.31	487000	901.3	1.02	525
Umgeni estuary 400 m upstream	8.92	4.25	6.40	489	856.0	0.58	978

S1 represents sample 1 and S2 represents sample 2.

4.15. NaCl detection by AuNPs through UV-Vis spectroscopy

The developed AuNPs sensor was applied in the detection of NaCl in water samples collected from estuaries and sea around the city of Durban. The AuNPs sensor was calibrated for NaCl analysis in the concentration range of 5-40 ppT, therefore, all water samples collected were analysed without any further dilution. These water samples were expected to contain high amount of NaCl. The source of NaCl in the estuary is known to be due to high tidal waves of the sea that result in salt intrusion (Perera *et al.* 2018; Souid *et al.* 2018). In this study, the concentration of NaCl in two estuaries (Umgeni and Amanzimtoti river mouth) was evaluated. Similar concentrations of 29.63 ppT and 30.42 ppT were found in Umgeni and Amanzimtoti river mouth, respectively (**Table 4.12)**. Further to this, in the same rivers the NaCl concentrations found upstream were less than those in the estuary. This meant that the seawater had a direct influence on the salinity of the river water closer to the sea due to salt intrusion. As shown in **Table 4.12**, the mean concentration of NaCl detected in the seawater samples; Blue Lagoon and Suncoast beaches were 31.68 ppT and 28.43 ppT, respectively. These concentrations were in close agreement with the expected value of 30 ppT NaCl in normal seawater conditions (Millero *et al.* 2008; Papaslioti *et al.* 2018). The slight variations in these two seawater samples could be due to different activities from one point to another by the marine ecosystem or environmental factors.

The above-mentioned results were supported by the UV-Vis LSPR spectra and colorimetric assay detection of NaCl in the samples by AuNPs as shown in **Figure 4.25a and 4.25b**. In **Figure 4.25a**, the intensity of LSPR peaks of Blue lagoon beach, Suncoast beach, Umgeni and Amanzimtoti estuaries showed a decrease in a wavelength of 525 nm. The corresponding LSPR peaks began to emerge in the wavelength of 660 nm, which demonstrated similar LSPR peaks of the optimized NaCl concentration range (5-40 ppT). This observation indicated the aggregation of the AuNPs in the presence of different concentrations of NaCl as discussed for **Figure 4.10.** Umgeni and Amanzimtoti samples collected upstream had a single LSPR peak at 525 nm which corresponded to the LSPR peak of AuNPs. This observation showed minimum aggregation of AuNPs in these samples due to low concentrations of NaCl in the water. The corresponding colorimetric image shown in **Figure 4.25b,** was in line with the analysis of LSPR in the UV-Vis spectra, the blue colour can be observed for

the Blue lagoon beach, Suncoast beach, Umgeni and Amanzimtoti estuaries. The pale red colour was observed for Umgeni and Amanzimtoti samples which were collected from the upstream of respective estuaries.

Table 4. 12: Concentration of water samples by UV-Vis analysis using AuNPs as colorimetric sensors.

Water Samples	Mean concentration ± SD
Sun Coast Beach	28.43 ± 1.36
Blue Lagoon Beach	31.68 ± 0.44
Umgeni estuary	29.63 ± 0.87
Umgeni estuary 405.23 m upstream	10.37 ± 0.03
Amanzimtoti estuary	30.42 ± 0.86
Amanzimtoti estuary 253.05 m upstream	13.15 ± 0.13

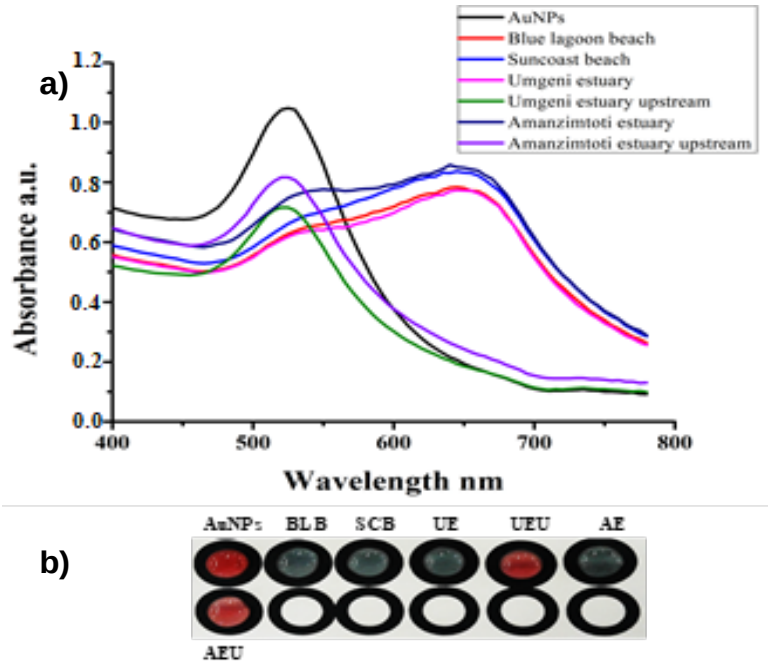

Figure 4. 25: *(*a) UV–Vis absorption spectra of AuNPs after the addition of seawater and estuary water samples. (b) Images of colorimetric detection of NaCl concentration by AuNPs in seawater and estuary water samples. (BLB-Blue lagoon beach, SCB-Suncoast beach, UE-Umgeni estuary, UEU-Umgeni estuary upstream, AE-Amanzimtoti estuary, AEU-Amanzimtoti estuary upstream).

4.16. Statistical analysis

Statistical evaluation of AuNPs based colorimetric assay for the detection of NaCl in the collected samples was done by ANOVA at 95% confidence interval and the results are presented in **Table 4.13**. The ANOVA results showed that the observed data was significant in the entire sample group (P<0.001). In **Figure 4.26**, the Post Hoc test further demonstrated the mean differences in amount of NaCl detected in each sample groups. It was observed that the mean amount of NaCl detected in Blue lagoon beach, Suncoast beach, Umgeni estuary and Amanzimtoti estuary were not statistical different (P >0.05). Significant differences were, however, detected in the NaCl content found in Umgeni and Amanzimtoti estuary and upstream samples (P>0.001) due to the salinization of the estuary by the upward flow of seawater. Overall, the experimental and statistical results authenticated that AuNPs was an excellent detecting sensor for NaCl concentration fluctuations in seawater. AuNPs presented high selectivity, accuracy and precision in determining the NaCl concentration in different samples without limitations to the sample type (estuaries or river water).

Table 4. 13: ANOVA results based on sample group analysis (N = 3).

Sampling location	Mean Concentration (ppT)	Standard deviation	Standard error	95% Confidence Interval	
				Lower Bound	Upper Bound
Blue Lagoon Beach	31.68	0.44	0.25	30.59	32.76
Suncoast Beach	28.43	1.36	0.79	25.04	31.81
Umgeni Estuary	29.63	0.87	0.50	27.48	31.78
Umgeni Estuary	10.37	0.03	0.02	10.30	10.44
Amanzimtoti Estuary	30.42	0.86	0.49	28.30	32.55
Amanzimtoti 253.05 m	13.15	0.13	0.07	12.8321	13.46

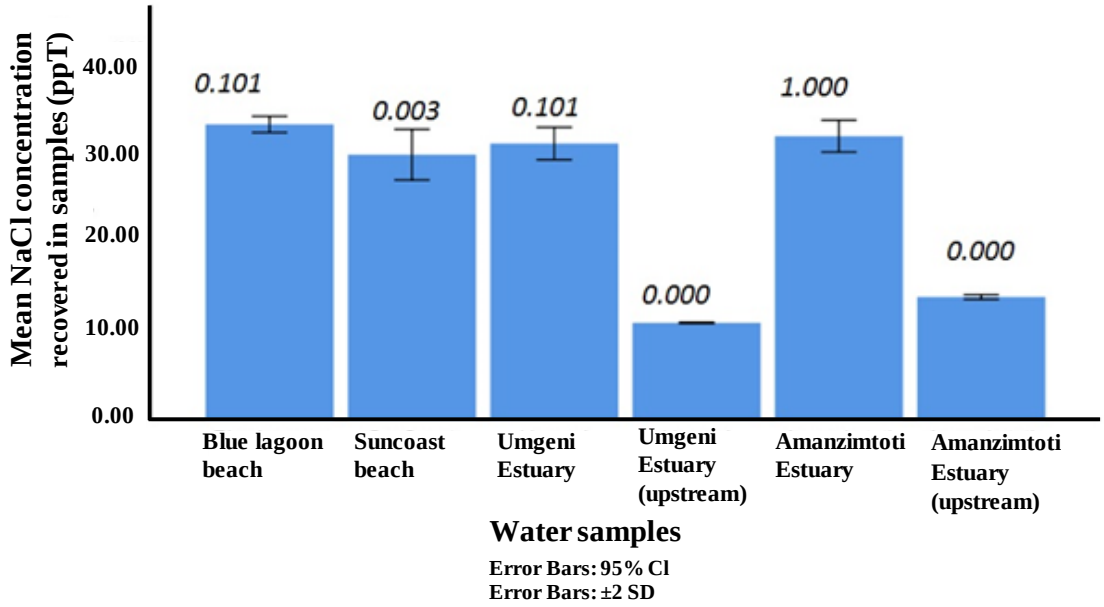

Figure 4. 26: Bar graph of the Post Hoc comparison test using the Bonferroni procedure with corresponding P values shown for the detection of NaCl concentration based on AuNPs.

4.17. Quantification of NaCl in samples

In this study, comparative examination of three different methods was done, namely AuNPs based colorimetric method, titration (Mohr method) and IC method that can be easily applicable for the NaCl/Cl^- analysis in environmental samples. This was done to validate the developed AuNPs colorimetric sensor against the popular traditional analytical methods for quantification of NaCl in water samples. The NaCl concentration results for all methods can be observed in **Table 4.14**. High concentrations of NaCl in estuaries and other still water outlets like in harbours are known to be due to salt intrusion by high tidal waves from the sea (Perera *et al.* 2018; Souid *et al.* 2018; Telahigue *et al.* 2018).

In this study, an on-site detection of NaCl levels was conducted using the fabricated Lovibond device and the colorimetric responses for the quantification of NaCl in samples are shown in **Annexure A**. The concentration of NaCl determined by the proposed sensor device agreed well with that obtained by titration and IC methods. The seawater in Blue lagoon beach had high concentration of NaCl, 35 ppT, as compared to other seawater, with Suncoast beach and Durban South beach at a level of 30 ppT (**Table 4.14**). These results are comparable with the results from titration

and ion chromatography (typical analysis chromatograms can be observed in **Annexure B**) methods in **Table 4.14**. For titration the Blue lagoon seawater had a NaCl concentration of 32.27 ppT and surprising this sample in IC had a lower concentration of NaCl as compared to the other two methods. This might be due to instrumental error causing a problem with analogue simulator convergence and sometimes resulting in inaccurate results. For the two Durban Harbour samples, as expected they had low NaCl concentration with S1 at 15 ppT and S2 at 10 ppT. The water in these areas was still, dirty and had been infected with algae and maybe to some extent by the boats and ships that depot and travel there on daily basis.

The results for these samples using the traditional methods also revealed low salt concentration in the water. Umgeni estuary which connects to the Blue lagoon sea had a NaCl concentration >30 ppT. There was a possibility that the range of NaCl could be from 30-35 ppT as the sea water its connected to is 35 ppT. Since the device was not calibrated for the values between 30 and 35 ppT, the colour wheel results in the Lovibond were assessed using titration and IC. The value of NaCl in titration for Umgeni estuary was 32.42 ppT and in IC was 30.49 ppT, apart from the slight variations in these analytical methods the results suggests that this water outlet is within the 30-35 ppT NaCl range.

In order to further assess the impact of the tides from the sea in the estuary, samples were taken and tested from four different points moving in an upstream direction which are 100 m apart. In the first 100 m from the estuary the water had a 30 ppT concentration of NaCl and also in the 200 m distance, the concentration was 30 ppT measured by Lovibond device. The Lovibond device was clear in its determination in these areas, for titration a NaCl concentration (30.85 ppT) and IC (29.96 ppT) results also agreed with the device for 100 m. At 200 m titration (30.28 ppT) and IC (29.41 ppT) results were in agreement with the Lovibond results.

From the 300 m range the salt concentration seemed to be decreasing with a NaCl concentration of 25 ppT and at 400 m the concentration was 5 ppT, this might be due to the tides not having enough wind force to penetrate through this region. The titration and IC results further confirmed the decrease in salt in these zones in the water as

can be seen in **Table 4.14**. The quantification results of the three methods employed in this study agreed with the physico-chemicals properties predictions for NaCl levels in the water based on electrical conductivity, total dissolved solids and salinity. Overall the results on the analysis of NaCl also suggested that environmental water conditions vary with the seasons, and salinity levels was the reflection of those variations. During rainy weather periods in spring and summer, more fresh water enters the estuary, so salinity is lower at these times, while for dry weather periods less fresh water enters the estuary, higher salinity levels may be found through the influence of seawater mixing with fresh water by high tidal waves. Therefore, the results from the tested areas for NaCl concentration as a representative of salinity in the water especially in estuaries, as they are mostly affected by the sea salinity, urges frequent monitoring of NaCl/salinity with the use of simple, rapid and competent devices similar to the one developed and applied in this study.

Table 4. 14: Concentration of NaCl in water samples collected in the city of Durban measured by Lovibond device, titration and IC method for quantification.

	Lovibond device	IC	Titration
Blue Lagoon Beach	35	28.94	32.27
Suncoast Beach	30	28.98	31.70
Durban South Beach	30	28.27	30.28
Durban Harbour S1	15	14.32	17.24
Durban Harbour S2	10	7.45	8.93
Umgeni estuary	>30	30.49	32.42
Umgeni estuary 100 m upstream	30	29.96	30.85
Umgeni estuary 200 m upstream	30	29.41	30.28
Umgeni estuary 300 m upstream	25	25.65	26.81
Umgeni estuary 400 m upstream	5	5.20	5.06

Analyses were done in triplicate in all tested samples (N=3).

4.18. Cost of analysis and comparison with other chloride testing kits

Chloride test kits based on colorimetric method from Hach Company 1454200 Chlorine free and total test kit Model CN-70 currently costs R3035. LaMotte 3308-01 Model SL-26 Dpd free total and combined Chlorine individual test kit 0.2 0.4 0.6 0.8 1.0 1.5 2.0 3.0 ppm Cl range currently costs R2540. The test kits contain reagents to perform approximately 110 tests for concentration range 0-1 ppT (https://hannainst.com/hi3815-chloride-test-kit.html). Chloride ion test kit from Sigma Aldrich (South Africa) sufficient for 100 colorimetric tests (R4720), tests for concentration range of 0-0.1 ppT. Chloride ion test kit from Sigma Aldrich sufficient for 100 colorimetric tests (R4720), tests for concentration range of 0-0.1 ppT.

The cost of the present developed colorimeter sensor is cost effective compared to the other chloride test kits. Moreover, it gave both qualitative and quantitative information about NaCl. The current cost of chemicals used in the colorimetric kit for NaCl determination for gold (III) chloride trihydrate 1 g ≈ R1200 (DLD Scientific, South Africa) and 500 g tri-sodium citrate ≈ R540 (Sigma Aldrich, South Africa). A mass of 0.4 g of gold (III) chloride trihydrate salt ≈1 L of AuNPs solution (concentrated). A maximum volume of 2 mL AuNPs solution used in experiments ≈ 500 samples analysed. Prices are based on the 2018 year and are subjected to change.

Chapter 5: Conclusion and recommendations

5.1. Conclusion

In conclusion, an interesting colorimetric AuNPs based sensor was successfully constructed for the sensitive and selective determination of sodium chloride in water. The AuNPs were prepared by a simple reduction method in which full advantage of the reducing and protective characteristics of tri-sodium citrate were adopted. The synthesis of materials and the fabricating of the sensors were simple, inexpensive. NaCl flocculation and SPR alteration ability of the AuNPs attributed to the increasing particle size, which endowed the sensor with high selectivity and satisfying interference rejection of about 5 times over other species. The LOQ and LOD of the developed AuNPs were found to be 1.18 ppT and 3.57 ppT respectively. The sensor can reliably identify and quantify the lowest concentration of sodium chloride in water. Statistical validation of the AuNPs using ANOVA confirmed the efficiency and accuracy of the sensor by being able to differentiate between the different NaCl levels (high and low) in the tested samples.

A colour wheel for the Lovibond device fabricated using ImageJ software processing and the RGB values matched the naked eye colorimetric response of the calibration standards. Colorgrab and CIELab colour system confirmed the variation in colour intensities of the colour hues for the Lovibond device. The fabricated device is highly accurate, precise and robust. Furthermore, The AuNPs device worked efficiently in analysis of real seawater samples that are known for its complex matrix. NaCl was successfully detected in real seawater and estuarine water samples for the two city locations in South Africa, Durban and Amanzimtoti, with satisfactory recoveries, both for the AuNPs-UV-Vis detection and the fabricated Lovibond device.

In August, Umgeni estuarine water experienced salt intrusion up to a distance of 300 m upstream. The current study suggested that NaCl concentrations was substantially increasing in dry seasons in estuaries due to salt intrusion from seawater. Therefore, a simple, competent, rapid and cost-effective colorimetric method for the detection of sodium chloride based on gold nanoparticles system in seawater is required for monitoring of this fluctuation of the salinity level. Another advantage of the AuNPs

colorimetric sensor was that it provided an effective platform for practical analysis of NaCl in seawater by overcoming the application of traditional techniques and complicated instrumentation that require highly skilled personnel. Based on these striking properties, the work described herein will open up new avenues for the further design and application of AuNPs along with other noble metals nanoparticles in many fields. Moreover, the developed AuNPs sensor will be a helpful initiative among chemists, nature conservationists, biologists and even to simple people like the life guards at the beaches, it will make a useful tool for field measurements that greatly impacts the environment.

5.2. Recommendations

Highly sophisticated instrumentations such as X-ray photoelectron spectroscopy and Field Flow Fractionation- Zeta nanosizer ZSP for further detailed characterization of the synthesized AuNPs will be necessary for understanding the binding mechanism of NaCl to AuNPs surface, molecular weight and oxidation state of AuNPs confirmation. Studies involving the determination of favourable conditions e.g. weather, seasons etc. for salt generation and the amount of salinization associated with these conditions for different types of environmental waters are recommended.

References

Abbasi-Moayed, S., Golmohammadi, H. and Hormozi-Nezhad, M. R. 2018. A nanopaper-based artificial tongue: a ratiometric fluorescent sensor array on bacterial nanocellulose for chemical discrimination applications. *Nanoscale*, 10 (5): 2492-2502.

Agency, U. S. E. P. 2006. Estuary Monitoring Manual: Salinity. *EPA-842-B-06-003, A methods manual*, Chapter 14, (Second edition): 1-24.

Ajlouni, K., Elshahawy, W., Ajlouni, R. and Sadakah, A. 2018. Color masking measurement for ceramic coating of titanium used for dental implants. *The Journal of Prosthetic Dentistry*, 119 (3): 426-431.

Al-Shammiri, M. 2002. Evaporation rate as a function of water salinity. *Desalination*, 150 (2): 189-203.

Aldewachi, H. S., Woodroofe, N., Turega, S. and Gardiner, P. H. E. 2017. Optimization of gold nanoparticle-based real-time colorimetric assay of dipeptidyl peptidase IV activity. *Talanta*, 169: 13-19.

Alim, S., Vejayan, J., Yusoff, M. M. and Kafi, A. K. M. 2018. Recent uses of carbon nanotubes & gold nanoparticles in electrochemistry with application in biosensing: A review. *Biosensors and Bioelectronics*, 121: 125-136.

Asakai, T. 2018. Chlorate ion standard solution established by multipath titration techniques. *Microchemical Journal*, 142: 9-16.

Barbier, E. B. 2015. Climate change impacts on rural poverty in low-elevation coastal zones. *Estuarine, Coastal and Shelf Science,* 165: 5-13.

Bielmyer-Fraser, G. K., Harper, B., Picariello, C. and Albritton-Ford, A. 2018. The influence of salinity and water chemistry on acute toxicity of cadmium to two euryhaline fish species. *Comparative Biochemistry and Physiology Part C: Toxicology & Pharmacology*, 214: 23-27.

Bonyár, A., Csarnovics, I., Veres, M., Himics, L., Csik, A., Kámán, J., Balázs, L. and Kökényesi, S. 2018. Investigation of the performance of thermally generated gold nanoislands for LSPR and SERS applications. *Sensors and Actuators B: Chemical*, 255: 433-439.

Bornman, T., Schmidt, J., Adams, J., Mfikili, A., Farre, R. and Smit, A. 2016. Relative sea-level rise and the potential for subsidence of the Swartkops Estuary intertidal salt marshes, South Africa. *South African Journal of Botany*, 107: 91-100.

Buchori, I., Pramitasari, A., Sugiri, A., Maryono, M., Basuki, Y. and Sejati, A. W. 2018. Adaptation to coastal flooding and inundation: Mitigations and migration pattern in Semarang City, Indonesia. *Ocean & Coastal Management*, 163: 445-455.

Castro, P. and Huber, M. 2005. Marine Biology Ed ke-5. *New Yor: Mc Graw HillInternational*: 119-125.

Celik, T. 2010. Fast and efficient method for fire detection using image processing. *ETRI journal*, 32 (6): 881-890.

Chen, H., Zhou, K. and Zhao, G. 2018. Gold nanoparticles: From synthesis, properties to their potential application as colorimetric sensors in food safety screening. *Trends in Food Science & Technology*, 78: 83-94.

Cheng, X., Dai, D., Yuan, Z., Peng, L., He, Y. and Yeung, E. S. 2014. Color difference amplification between gold nanoparticles in colorimetric analysis with actively controlled multiband illumination. *Analytical chemistry*, 86 (15): 7584-7592.

Cooper, J. 2001. Geomorphological variability among microtidal estuaries from the wave-dominated South African coast. *Geomorphology*, 40 (1-2): 99-122.

Cox, R. W. 1996. AFNI: software for analysis and visualization of functional magnetic resonance neuroimages. *Computers and Biomedical research*, 29 (3): 162-173.

Daniel, M.-C. and Astruc, D. 2004b. Gold nanoparticles: assembly, supramolecular chemistry, quantum-size-related properties, and applications toward biology, catalysis, and nanotechnology. *Chemical reviews*, 104 (1): 293-346.

Das, A., Justic, D., Inoue, M., Hoda, A., Huang, H. and Park, D. 2012. Impacts of Mississippi River diversions on salinity gradients in a deltaic Louisiana estuary: Ecological and management implications. *Estuarine, Coastal and Shelf Science*, 111: 17-26.

Dorrington, R. A., Lombard, A. T., Bornman, T. G., Adams, J. B., Cawthra, H. C., Deyzel, S. H., Goschen, W. S., Liu, K., Mahler-Coetzee, J. and Matcher, G. F. 2018. Working together for our oceans: a marine spatial plan for Algoa Bay, South Africa. *South African Journal of Science*, 114 (3-4): 1-6.

Doyen, M., Bartik, K. and Bruylants, G. 2013. UV–Vis and NMR study of the formation of gold nanoparticles by citrate reduction: Observation of gold–citrate aggregates. *Journal of colloid and Interface Science*, 399: 1-5.

Du, J., Du, H., Ge, H., Fan, J. and Peng, X. 2018. A plasmonic nano-sensor for the fast detection of Ag+ based on synergistic coordination-inspired gold nanoparticle. *Sensors and Actuators B: Chemical*, 255: 808-813.

Dube, E., Oluwole, D. O., Nwaji, N. and Nyokong, T. 2018. Glycosylated zinc phthalocyanine-gold nanoparticle conjugates for photodynamic therapy: Effect of nanoparticle shape. *Spectrochimica Acta Part A: Molecular and Biomolecular Spectroscopy*, 203: 85-95.

Edition, F. 2011. Guidelines for drinking-water quality. *WHO chronicle*, 38 (4): 104-108.

Ellwood, M. J., Hunter, K. A. and Cunninghame, R. G. 2003. Elimination of equivalence point errors in the potentiometric titration of chloride, bromide and iodide mixtures with silver nitrate. *Microchemical Journal*, 74 (2): 187-192.

Esfahani, M. R., Pallem, V. L., Stretz, H. A. and Wells, M. J. M. 2016. Humic acid disaggregation with/of gold nanoparticles: Effects of nanoparticle size and pH. *Environmental Nanotechnology, Monitoring & Management*, 6: 54-63.

Fang, C., Dharmarajan, R., Megharaj, M. and Naidu, R. 2017. Gold nanoparticle-based optical sensors for selected anionic contaminants. *Trends in Analytical Chemistry*, 86: 143-154.

Feng, Y., Sun, T., Zhu, M. S., Qi, M., Yang, W. and Shao, D. D. 2017. Salt marsh vegetation distribution patterns along groundwater table and salinity gradients in yellow river estuary under the influence of land reclamation. *Ecological Indicators*, 85: 190-200. https://doi.org/10.1016/j.ecolind.2017.09.027

Fisher, B., Naidoo, R., Guernier, J., Johnson, K., Mullins, D., Robinson, D. and Allison, E. H. 2017. Integrating fisheries and agricultural programs for food security. *Agriculture & Food Security*, 6 (1): 1.

Forbes, A. T. and Demetriades, N. T. 2008. *Estuaries of durban*. Second ed. Durban, Republic of South Africa: *eThekwini Municipality*, 66: 1-32.

Gene Chong, Elizabeth D. Laudadio, Meng Wu, Catherine J. Murphy, Robert J Hamers and Hernandez, R. 2018. Density, Structure, and Stability of Citrate and HCitrate on Bare and Coated Gold Nanoparticles. *Journal of Physical Chemistry C*: 1-34.

Gingerich, S. B., Voss, C. I. and Johnson, A. G. 2017. Seawater-flooding events and impact on freshwater lenses of low-lying islands: Controlling factors, basic management and mitigation. *Journal of Hydrology*, 551: 676-688.

Girjatowicz, J. P. and Świątek, M. 2016. Salinity variations of the surface water at the southern coast of the Baltic Sea in years 1950–2010. *Continental Shelf Research*, 126: 110-118.

Gong, X., Wang, S., Moses, D., Bazan, G. C. and Heeger, A. J. 2005. Multilayer polymer light-emitting diodes: white-light emission with high efficiency. *Advanced Materials*, 17 (17): 2053-2058.

Gopinath, S., Srinivasamoorthy, K., Saravanan, K., Suma, C., Prakash, R., Senthilnathan, D., Chandrasekaran, N., Srinivas, Y. and Sarma, V. 2016. Modeling

saline water intrusion in Nagapattinam coastal aquifers, Tamilnadu, India. *Modeling Earth Systems and Environment*, 2 (1): 2.

Gossett, D. R., Millhollon, E. P. and Lucas, M. 1994. Antioxidant response to NaCl stress in salt-tolerant and salt-sensitive cultivars of cotton. *Crop Science*, 34 (3): 706-714.

Gros, N. 2013. Ion Chromatographic Analyses of Sea Waters, Brines and Related Samples. *Water* (5): 659-676.

Gupta, R. C. 2018. Chapter 34 - Sodium Chloride (Salt) A2 In: Thompson, L. J. ed. *Veterinary Toxicology*. Third edn. Academic Press, 479-482. Available: https://www.sciencedirect.com/science/article/pii/B9780128114100000349 (Accessed 05 February 2018)

Habib, A., Tabata, M. and Wu, Y. G. 2005. Formation of gold nanoparticles by good's buffers. *Bulletin of the Chemical Society of Japan*, 78 (2): 262-269.

Han, D., Post, V. E. and Song, X. 2015a. Groundwater salinization processes and reversibility of seawater intrusion in coastal carbonate aquifers. *Journal of Hydrology*, 531: 1067-1080.

Han, D., Post, V. E. A. and Song, X. 2015b. Groundwater salinization processes and reversibility of seawater intrusion in coastal carbonate aquifers. *Journal of Hydrology*, 531: 1067-1080.

Hinrichsen, H. H., Lehmann, A., Petereit, C., Nissling, A., Ustups, D., Bergström, U. and Hüssy, K. 2016. Spawning areas of eastern Baltic cod revisited: Using hydrodynamic modelling to reveal spawning habitat suitability, egg survival probability, and connectivity patterns. *Progress in Oceanography*, 143: 13-25.

Hoggart, S. P. G., Hanley, M. E., Parker, D. J., Simmonds, D. J., Bilton, D. T., Filipova-Marinova, M., Franklin, E. L., Kotsev, I., Penning-Rowsell, E. C., Rundle, S. D., Trifonova, E., Vergiev, S., White, A. C. and Thompson, R. C. 2014. The consequences of doing nothing: The effects of seawater flooding on coastal zones. *Coastal Engineering*, 87: 169-182.

Hondow, N., Brydson, R., Wang, P., Holton, M. D., Brown, M. R., Rees, P., Summers, H. D. and Brown, A. 2012. Quantitative characterization of nanoparticle agglomeration within biological media. *Journal of Nanoparticle Research*, 14 (7): 977.

Hoogendoorn, G., Grant, B. and Fitchett, J. M. 2016. Disjunct perceptions? Climate change threats in two-low lying South African coastal towns. *Bulletin of Geography. Socio-economic Series*, 31 (31): 59-71.

Hossain, A., Canning, J., Ast, S., Rutledge, P. J., Yen, T. L. and Jamalipour, A. 2015. Lab-in-a-phone: smartphone-based portable fluorometer for pH measurements of environmental water. *IEEE Sensors Journal*, 15 (9): 5095-5102.

Jonkman, S. N. 2005. Global perspectives on loss of human life caused by floods. *Natural hazards*, 34 (2): 151-175.

Kandel, E. R., Schwartz, J. H., Jessell, T. M., Biochemistry, D. o., Jessell, M. B. T., Siegelbaum, S. and Hudspeth, A. 2000. *Principles of neural science*. McGraw-hill New York, 4: 1232-1253.

Kang, Y. and Kim, B. 2018. Multiple and periodic measurement of RBC aggregation and ESR in parallel microfluidic channels under on-off blood flow control. *Micromachines*, 9 (7): 318.

Katerji, N., Van Hoorn, J., Hamdy, A. and Mastrorilli, M. 2003. Salinity effect on crop development and yield, analysis of salt tolerance according to several classification methods. *Agricultural water management*, 62 (1): 37-66.

Kennish, M. J. 2002. Environmental threats and environmental future of estuaries. *Environmental conservation*, 29 (1): 78-107.

Khan, M., Singha, K. L. and Panda, S. 2002. Changes in antioxidant levels in Oryza sativa L. roots subjected to NaCl-salinity stress. *Acta Physiologiae Plantarum*, 24 (2): 145-148.

Khezri, S., Bahram, M. and Samadi, N. 2018. Hydrogen bonding recognition and colorimetric detection of isoprenaline using 2-amino-5-mercapto-1,3,4-thiadiazol

functionalized gold nanoparticles. *Spectrochimica Acta Part A: Molecular and Biomolecular Spectroscopy*, 189: 522-527.

Khodaveisi, J., Dadfarnia, S., Shabani, A. M. H. and Saberi, D. 2017. Colorimetric determination of nabumetone based on localized surface plasmon resonance of functionalized gold nanoparticles as a chemical sensor. *Sensors and Actuators B: Chemical*, 239: 1300-1306.

Kijewska, A., Kalamarz-Kubiak, H., Arciszewski, B., Guellard, T., Petereit, C. and Wenne, R. 2016. Adaptation to salinity in Atlantic cod from different regions of the Baltic Sea. *Experimental Marine Biology and Ecology*, 478: 62-67.

Kildow, J. T., Colgan, C. S., Scorse, J. D., Johnston, P. and Nichols, M. 2014. State of the US ocean and coastal economies 2014, Edition 1: 1-10.

Kim, S. C., Jalal, U. M., Im, S. B., Ko, S. and Shim, J. S. 2017. A smartphone-based optical platform for colorimetric analysis of microfluidic device. *Sensors and Actuators B: Chemical*, 239: 52-59.

Knüppe, K. and Meissner, R. 2016. Drivers and barriers towards sustainable water and land management in the Olifants-Doorn Water Management Area, South Africa. *Environmental Development*, 20: 3-14.

Kolesar, K. R., Mattson, C. N., Peterson, P. K., May, N. W., Prendergast, R. K. and Pratt, K. A. 2018. Increases in wintertime PM2.5 sodium and chloride linked to snowfall and road salt application. *Atmospheric Environment*, 177: 195–202.

Kuehni, R. G. 1990. Industrial color difference: progress and problems. *Color Research & Application*, 15 (5): 261-265.

Kumar, T. and Verma, K. 2010. A Theory Based on Conversion of RGB image to Gray image. *International Journal of Computer Applications*, 7 (2): 7-10.

Kusumawati, E. N., Nishio-Hamane, D. and Sasaki, T. 2018. Size-controllable gold nanoparticles prepared from immobilized gold-containing ionic liquids on SBA-15. *Catalysis Today*, 309: 109-118.

Lai, T.-S., Chang, T.-C. and Wang, S.-C. 2017. Gold nanoparticle-based colorimetric methods to determine protein contents in artificial urine using membrane micro-concentrators and mobile phone camera. *Sensors and Actuators B: Chemical*, 239: 9-16.

Laikhtman, M., Riviello, J. and Rohrer, J. S. 1998. Determination of magnesium and calcium in 30% sodium chloride by ion chromatography with on-line matrix elimination. *Journal of Chromatography A*, 816 (2): 282-285.

Langer, M. S. 2001. A model of how interreflections can affect color appearance. *Color Research & Application:* Endorsed by Inter-Society Color Council, The Colour Group (Great Britain), Canadian Society for Color, Color Science Association of Japan, Dutch Society for the Study of Color, The Swedish Colour Centre Foundation, Colour Society of Australia, Centre Français de la Couleur, 26 (S1): S218-S221.

Laux, J., Hemminger, J. and Finlayson-Pitts, B. 1994. X-ray photoelectron spectroscopic studies of the heterogenous reaction of gaseous nitric acid with sodium chloride: Kinetics and contribution to the chemistry of the marine troposphere. *Geophysical research letters*, 21 (15): 1623-1626.

Lazarus, N., Jin, R. and Fedder, G. K. 2014. The use of coated gold nanoparticles in high performance chemical sensors A2. In: *Nanosensors for Chemical and Biological Applications*. Woodhead Publishing, 231-253.

Leon, K., Mery, D., Pedreschi, F. and Leon, J. 2006. Color measurement in L∗ a∗ b∗ units from RGB digital images. *Food research international*, 39 (10): 1084-1091.

Li, F.-M., Liu, J.-M., Wang, X.-X., Lin, L.-P., Cai, W.-L., Lin, X., Zeng, Y.-N., Li, Z.-M. and Lin, S.-Q. 2011. Non-aggregation based label free colorimetric sensor for the detection of Cr (VI) based on selective etching of gold nanorods. *Sensors and Actuators B: Chemical*, 155 (2): 817-822.

Li, G., Deng, L., Cao, Y., Wang, B., Ran, J. and Zhang, H. 2017a. Effect of sodium chloride on fine coal flotation and discussion based on froth stability and particle coagulation. *International Journal of Mineral Processing*, 169: 47-52.

Li, S., Wei, T., Ren, G., Chai, F., Wu, H. and Qu, F. 2017b. Gold nanoparticles based colorimetric probe for Cr(III) and Cr(VI) detection. *Colloids and Surfaces A: Physicochemical and Engineering Aspects*, 535: 215-224.

Li, X., Hu, Z., Ma, J., Wang, X., Zhang, Y., Wang, W. and Yuan, Z. 2018. The systematic evaluation of size-dependent toxicity and multi-time biodistribution of gold nanoparticles. *Colloids and Surfaces B: Biointerfaces*, 167: 260-266.

Lin, S.-Y., Tsai, Y.-T., Chen, C.-C., Lin, C.-M. and Chen, C.-h. 2004. Two-step functionalization of neutral and positively charged thiols onto citrate-stabilized Au nanoparticles. *The Journal of Physical Chemistry B*, 108 (7): 2134-2139.

Little, S., Wood, P. J. and Elliott, M. 2017. Quantifying salinity-induced changes on estuarine benthic fauna: The potential implications of climate change. *Estuarine, Coastal and Shelf Science*, 198: 610-625.

Liu, J., Bai, W., Zhu, C., Yan, M., Yang, S. and Chen, A. 2012. Sensitive colorimetric detection of cyromazine in cucumber samples by using label-free gold nanoparticles and polythymine. *The Royal Society of Chemistry 2012*, 00, 3: 1-3.

Liu, J. and Lu, Y. 2004. Accelerated color change of gold nanoparticles assembled by DNAzymes for simple and fast colorimetric Pb2+ detection. *Journal of the American Chemical Society*, 126 (39): 1298-1300.

Livingstone, M. and Hubel, D. 1988. Segregation of form, color, movement, and depth: anatomy, physiology, and perception. *Science*, 240 (4853): 740-749.

Lv, Q., Zang, X., Li, X. and Li, G. 2018. Effect of seawater ions on cyclopentane-methane hydrate phase equilibrium. *Fluid Phase Equilibria*, 458: 272-277.

Martínez-Barrera, B., Gutiérrez-Arzaluz, M., Montoya de la Fuente, J. A., Romero-Romo, M. and Torres-Rodríguez, M. 2018. Formaldehyde CWO with gold nanoparticles in a forced through flow catalytic-membrane reactor. *Catalysis Today*, 1-5 (Accessed online 18 June 2018)

Martins, L. G. and Mainardes, R. M. 2017. Application of a validated HPLC-PDA method for the determination of melatonin content and its release from poly (lactic acid) nanoparticles. *Journal of pharmaceutical analysis*, 7 (6): 388-393.

Mazzei, V. and Biber, P. 2015. Autotrophic net productivity patterns at four artificial reef sites in the Mississippi Sound. *Hydrobiologia*, 749 (1): 135-154.

McLaren, K. 1976. XIII—The development of the CIE 1976 (L* a* b*) uniform colour space and colour-difference formula. *Journal of the Society of Dyers and Colourists*, 92 (9): 338-341.

Mdluli, P. S., Sosibo, N. M., Revaprasadu, N., Karamanis, P. and Leszczynski, J. 2009. Surface enhanced Raman spectroscopy (SERS) and density functional theory (DFT) study for understanding the regioselective adsorption of pyrrolidinone on the surface of silver and gold colloids. *Journal of Molecular Structure*, 935 (2009): 32-38.

Meade, R. H. 2003. Relations between suspended matter and salinity in estuaries of the atlantic seaboard, U.S.A. *U.S. Geological Survey*, Contribution No. 2003 from the Woods Hole Océanographie Institution: 96-109.

Meng, L., Huang, M., Bi, L., Cai, T. and Huang, Y. 2018. Performance of simultaneous wastewater reuse and seawater desalination by PAO-LPRO process. *Separation and Purification Technology*, 1-33.

Millero, F. J., Feistel, R., Wright, D. G. and McDougall, T. J. 2008. The composition of Standard Seawater and the definition of the Reference-Composition Salinity Scale. *Deep Sea Research Part I: Oceanographic Research Papers*, 55 (1): 50-72.

Milstein, A., Ahmed, A., Masud, O., Kadir, A. and Wahab, M. 2006. Effects of the filter feeder silver carp and the bottom feeders mrigal and common carp on small indigenous fish species (SIS) and pond ecology. *Aquaculture*, 258 (1-4): 439-451.

Mohanraj, V. and Chen, Y. 2006. Nanoparticles-a review. *Tropical journal of Pharmaceutical Research*, 5 (1): 561-573.

Mondal, N., Singh, V. and Saxena, V. 2010. Determining the interaction between groundwater and saline water through groundwater major ions chemistry. *Journal of Hydrology*, 388: 100-111.

Montangero, M. 2015. Determining the amount of copper (ii) ions in a solution using a smartphone. *Journal of Chemical Education*, 92 (10): 1759-1762.

Moorman, B. P., Inokuchi, M., Yamaguchi, Y., Lerner, D. T., Grau, E. G. and Seale, A. P. 2014. The osmoregulatory effects of rearing Mozambique tilapia in a tidally changing salinity. *General and Comparative Endocrinology*, 207: 94-102.

Nehl, C. L. and Hafner, J. H. 2008. Shape-dependent plasmon resonances of gold nanoparticles. *Journal of Materials Chemistry*, 18 (21): 2415-2419.

Nehl, C. L., Liao, H. and Hafner, J. H. 2006. Optical properties of star-shaped gold nanoparticles. *Nano Letters*, 6 (4): 683-688.

Ngoye, E. and Machiwa, J. F. 2004. The influence of land-use patterns in the Ruvu river watershed on water quality in the river system. *Physics and Chemistry of the Earth, Parts A/B/C*, 29 (15-18): 1161-1166.

Nhung, T. T., Le Vo, P., Van Nghi, V. and Bang, H. Q. 2019. Salt intrusion adaptation measures for sustainable agricultural development under climate change effects: A case of Ca Mau Peninsula, Vietnam. *Climate Risk Management*, 23: 88-100.

Nicolini, J. V., Ferraz, H. C. and Borges, C. P. 2017. Effect of seawater ionic composition modified by nanofiltration on enhanced oil recovery in Berea sandstone. *Fuel,* 203: 222-232.

Nielsen, D. L., Brock, M. A., Rees, G. N. and Baldwin, D. S. 2003. Effects of increasing salinity on freshwater ecosystems in Australia. *Australian Journal of Botany*, 51: 655-665.

Nirala, N. R., Saxena, P. S. and Srivastava, A. 2018. Colorimetric detection of cholesterol based on enzyme modified gold nanoparticles. *Spectrochimica Acta Part A: Molecular and Biomolecular Spectroscopy*, 190: 506-512.

Papaslioti, E.-M., Pérez-López, R., Parviainen, A., Sarmiento, A. M., Nieto, J. M., Marchesi, C., Delgado-Huertas, A. and Garrido, C. J. 2018. Effects of seawater mixing on the mobility of trace elements in acid phosphogypsum leachates. *Marine Pollution Bulletin*, 127: 695–703.

Park, J.-W. and Shumaker-Parry, J. S. 2014. Structural study of citrate layers on gold nanoparticles: role of intermolecular interactions in stabilizing nanoparticles. *Journal of the American Chemical Society*, 136 (5): 1907-1921.

Park, S.-C., Yun, S.-T., Chae, G.-T., Yoo, I.-S., Shin, K.-S., Heo, C.-H. and Lee, S.-K. 2005. Regional hydrochemical study on salinization of coastal aquifers, western coastal area of South Korea. *Journal of Hydrology*, 313 (3-4): 182-194.

Paull, B. N., P. N. . 2004. Novel ion chromatographic stationary phases for the analysis of complex matrices. *Journal of Royal Society of Chemistry*: 134-136.

Pawlowicz, R. 2012. The electrical conductivity of seawater at high temperatures and salinities. *Desalination*, 300: 32-39.

Pawlowicz, R. 2015. The Absolute Salinity of seawater diluted by riverwater. *Deep Sea Research Part I: Oceanographic Research Papers*, 101: 71-79.

Pereira, C. S., Lopes, I., Sousa, J. and Chelinho, S. 2015. Effects of NaCl and seawater induced salinity on survival and reproduction of three soil invertebrate species. *Chemosphere*, 135: 116-122.

Pereira, W. E., Domagalski, J. L., Hostettler, F. D., Brown, L. R. and Rapp, J. B. 1996. Occurrence and accumulation of pesticides and organic contaminants in river sediment, water and clam tissues from the San Joaquin River and tributaries, California. *Environmental Toxicology and Chemistry: An International Journal*, 15 (2): 172-180.

Perera, M. D. N. D., Ranasinghe, T. K. G. P., Piyadasa, R. U. K. and Jayasinghe, G. Y. 2018. Risk of seawater intrusion on coastal community of Bentota river basin Sri Lanka. *Procedia Engineering*, 212: 699-706.

Peters, F. T., Drummer, O. H. and Musshoff, F. 2007. Validation of new methods. *Forensic science international*, 165 (2-3): 216-224.

Petersen, L., Moll, E., Collins, R. and Hockings, M. 2012. Development of a compendium of local, wild-harvested species used in the informal economy trade, Cape Town, South Africa. *Ecology and Society*, 17 (2)

Pointer, M. 1981. A comparison of the CIE 1976 colour spaces. *Color Research & Application*, 6 (2): 108-118.

Qin, L., Zeng, G., Lai, C., Huang, D., Xu, P., Zhang, C., Cheng, M., Liu, X., Liu, S., Li, B. and Yi, H. 2018. “Gold rush” in modern science: Fabrication strategies and typical advanced applications of gold nanoparticles in sensing. *Coordination Chemistry Reviews*, 359: 1-31.

Qin, L., Zeng, G., Lai, C., Huang, D., Zhang, C., Xu, P., Hu, T., Liu, X., Cheng, M., Liu, Y., Hu, L. and Zhou, Y. 2017. A visual application of gold nanoparticles: Simple, reliable and sensitive detection of kanamycin based on hydrogen-bonding recognition. *Sensors and Actuators B: Chemical*, 243: 946-954.

Rasmussen, P., Sonnenborg, T., Goncear, G. and Hinsby, K. 2013. Assessing impacts of climate change, sea level rise, and drainage canals on saltwater intrusion to coastal aquifer. *Hydrology and Earth System Sciences*, 17 (1): 421-443.

Ray, P. C., Yu, H. and Fu, P. P. 2011. Nanogold-based sensing of environmental toxins: excitement and challenges. *Journal of Environmental Science Health: Part C*, 29: 52-89.

Rivero, P. J., Ibañez, E., Goicoechea, J., Urrutia, A., Matias, I. R. and Arregui, F. J. 2017. A self-referenced optical colorimetric sensor based on silver and gold nanoparticles for quantitative determination of hydrogen peroxide. *Sensors and Actuators B: Chemical*, 251: 624-631.

Robaina, N. F., Feiteira, F. N., Cassella, A. R. and Cassella, R. J. 2016. Determination of chloride in brazilian crude oils by ion chromatography after extraction induced by emulsion breaking. *Journal of Chromatography A*, 1458: 112-117.

Roberts, D. 2008. Thinking globally, acting locally—institutionalizing climate change at the local government level in Durban, South Africa. *Environment and Urbanization*, 20 (2): 521-537.

Robertson, A. R. 1977. The CIE 1976 color-difference formulae. *Color Research & Application*, 2 (1): 7-11.

Sadak, S., Mervat, Abdelhamid, M. T. and Schmidhalter, U. 2015. Effect of foliar application of aminoacids on plant yield and some physiological parameters in bean plants irrigated with seawater. *Acta Biológica Colombiana*, 20 (1): 141-152.

Salman, A. and Al-Shammiri, M. A. 2007. New Computational Intelligence model for predicting evaporation rates for saline water. *Desalination*, 214 (1): 273-286.

Santos, R. V. S., Ramos, S. and Bonecker, A. C. T. 2017. Can we assess the ecological status of estuaries based on larval fish assemblages? *Marine Pollution Bulletin*, 124 (1): 367-375.

Sappi. 2013. Defining and Communicating Color: The CIELAB System. North America. Available: https://cdn-s3.sappi.com/s3fs-public/sappietc/Defining%20and%20Communicating%20Color.pdf : 2013: 4-5 (Accessed 25 July 2013).

Sapsford, K. E., Berti, L. and Medintz, I. L. 2006. Materials for fluorescence resonance energy transfer analysis: beyond traditional donor–acceptor combinations. *Angewandte Chemie International Edition*, 45 (28): 4562-4589.

Schoeman, J. and Steyn, A. 2003. Nitrate removal with reverse osmosis in a rural area in South Africa. *Desalination*, 155 (1): 15-26.

Seh, Z. W., Liu, S., Low, M., Zhang, S. Y., Liu, Z., Mlayah, A. and Han, M. Y. 2012. Janus Au-TiO2 photocatalysts with strong localization of plasmonic near-fields for efficient visible-light hydrogen generation. *Advanced Materials*, 24 (17): 2310-2314.

Senner, N. R., Moore, J. N., Seager, S. T., Dougill, S., Kreuz, K. and Senner, S. E. 2018. A salt lake under stress: Relationships among birds, water levels, and

invertebrates at a Great Basin saline lake. *Biological Conservation*, (2018), https://doi.org/10.1016/j.biocon.2018.02.003: 1-10.

Shi, L., Buhler, E., Boué, F. and Carn, F. 2017. How does the size of gold nanoparticles depend on citrate to gold ratio in Turkevich synthesis? Final answer to a debated question. *Journal of colloid and Interface Science*, 492: 191-198.

Shiraishi, Y., Tanaka, H., Sakamoto, H., Ichikawa, S. and Hirai, T. 2017. Photoreductive synthesis of monodispersed Au nanoparticles with citric acid as reductant and surface stabilizing reagent. *RSC Advances*, 7 (11): 6187-6192.

Shrivas, K., Maji, P. and Dewangan, K. 2017. Onsite-detection of barium and nickel from river, pond and tap water samples using gold nanoparticles as a chemical sensor. *Spectrochimica Acta Part A: Molecular and Biomolecular Spectroscopy*, 173: 630-636.

Silveira, E. L. C., de Caland, L. B. and Tubino, M. 2014. Simultaneous quantitative analysis of the acetate, formate, chloride, phosphate and sulfate anions in biodiesel by ion chromatography. *Fuel*, 124: 97-101.

Sink, K. 2016. The marine protected areas debate: implications for the proposed Phakisa marine protected areas network. *South African Journal of Science*, 112 (9-10): 1-4.

Sivaraman, S. K., Kumar, S. and Santhanam, V. 2011. Monodisperse sub-10 nm gold nanoparticles by reversing the order of addition in Turkevich method-the role of chloroauric acid. *Journal of colloid and Interface Science*, 361 (2): 543-547.

Souid, F., Agoubi, B., Telahigue, F., Chahlaoui, A. and Kharroubi, A. 2018. Groundwater salinization and seawater intrusion tracing based on Lithium concentration in the shallow aquifer of Jerba Island, southeastern Tunisia. *Journal of African Earth Sciences*, 138: 233-246.

Starnes, D. L., Unrine, J. M., Starnes, C. P., Collin, B. E., Oostveen, E. K., Ma, R., Lowry, G. V., Bertsch, P. M. and Tsyusko, O. V. 2015. Impact of sulfidation on the bioavailability and toxicity of silver nanoparticles to Caenorhabditis elegans. *Environmental Pollution*, 196: 239-246.

Strickland, J. D. H. and Parsons, T. 1972. *A practical handbook of seawater analysis*. Second ed. Department of Fisheries and the Environment Fisheries and Marine Service, Scientific Information and Publications Branch, 116 Lisgar Street, Ottawa, Canada K1A OH3, 167: 320-328.

Sutton-Grier, A. E., Wowk, K. and Bamford, H. 2015. Future of our coasts: The potential for natural and hybrid infrastructure to enhance the resilience of our coastal communities, economies and ecosystems. *Environmental Science & Policy*, 51: 137-148.

Takatsuji, Y., Ikeno, S. and Haruyama, T. 2012. Gold nanoparticles functionalized with peptides for specific affinity aggregation assays of estrogen receptors and their agonists. *Sensors*, 12 (4): 4952-4961.

Tan, F., Li, T., Wang, N., Lai, S. K., Tsoi, C. C., Yu, W. and Zhang, X. 2016. Rough gold films as broadband absorbers for plasmonic enhancement of TiO 2 photocurrent over 400–800 nm. *Scientific reports*, 6: 33-49.

Tang, J., Wu, P.;, Hou, X.,D.;, Xu, K.,L. 2016. Modification-free and N-acetyl-L-cysteine-induced colorimetric response of AuNPs: a mechanistic study and sensitive Hg(2+) detection. *Talanta*, 159: 87–92.

Telahigue, F., Agoubi, B., Souid, F. and Kharroubi, A. 2018. Assessment of seawater intrusion in an arid coastal aquifer, south-eastern Tunisia, using multivariate statistical analysis and chloride mass balance. *Physics and Chemistry of the Earth*, (2018) 10.1016/j.pce.2018.05.001.

Terry, J. P. and Falkland, A. C. 2010. Responses of atoll freshwater lenses to storm-surge overwash in the Northern Cook Islands. *Hydrogeology Journal*, 18 (3): 749-759.

Thambiraj, S., Hema, S. and Ravi Shankaran, D. 2018. Functionalized gold nanoparticles for drug delivery applications. *Materials Today: Proceedings*, 5 (8, Part 3): 16763-16773.

Tsolaki, E., Pitta, P. and Diamadopoulos, E. 2010. Electrochemical disinfection of simulated ballast water using Artemia salina as indicator. *Chemical Engineering Journal*, 156 (2): 305-312.

Turkevich, J., Stevenson, P. C. and Hillier, J. 1951. A study of the nucleation and growth processes in the synthesis of colloidal gold. *Discussions of the Faraday Society*, 11 (0): 55-75.

van Wyk, J.-A. 2015. Defining the blue economy as a South African strategic priority: toward a sustainable 10th province? *Journal of the Indian Ocean Region*, 11 (2): 153-169.

Velez, C., Figueira, E., Soares, A. M. and Freitas, R. 2016. Combined effects of seawater acidification and salinity changes in Ruditapes philippinarum. *Aquatic Toxicology*, 176: 141-150.

Ventura, Y., Wuddineh, W. A., Myrzabayeva, M., Alikulov, Z., Khozin-Goldberg, I., Shpigel, M., Samocha, T. M. and Sagi, M. 2011. Effect of seawater concentration on the productivity and nutritional value of annual Salicornia and perennial Sarcocornia halophytes as leafy vegetable crops. *Scientia Horticulturae*, 128 (3): 189-196.

Vineis, P., Chan, Q. and Khan, A. 2011. Climate change impacts on water salinity and health. *Journal of Epidemiology and Global Health*, 189: 1-10.

Wei, T., Wang, Z., Chen, J. and Li, M. 2018. Non-flood season neap tides in the Yangtze estuary offshore: Flow mixing processes and its potential impacts on adjacent wetlands. *Physics and Chemistry of the Earth, Parts A/B/C*, 103: 127-139.

Wei, X., Wang, Y., Zhao, Y. and Chen, Z. 2017. Colorimetric sensor array for protein discrimination based on different DNA chain length-dependent gold nanoparticles aggregation. *Biosensors and Bioelectronics*, 97: 332-337.

Welch, C. M. and Compton, R. G. 2006. The use of nanoparticles in electroanalysis: a review. *Analytical and bioanalytical chemistry*, 384 (3): 601-619.

Wells, S. and Ravilious, C. 2006. *In the front line: shoreline protection and other ecosystem services from mangroves and coral reefs*. UNEP/Earthprint, 24: 432-450.

Wiegman, A. R. H., Day, J. W., D'Elia, C. F., Rutherford, J. S., Morris, J. T., Roy, E. D., Lane, R. R., Dismukes, D. E. and Snyder, B. F. 2018. Modeling impacts of sea-level rise, oil price, and management strategy on the costs of sustaining Mississippi delta marshes with hydraulic dredging. *Science of The Total Environment*, 618: 1547-1559.

Wolanski, E., Chicharo, L., Chicharo, M. A. and Morais, P. 2006. An ecohydrology model of the Guadiana estuary (South Portugal). *Estuarine, Coastal and Shelf Science*, 70 (1-2): 132-143.

Wu, D., Gao, A., Zhao, H. and Feng, X. 2018. Pervaporative desalination of high-salinity water. *Chemical Engineering Research and Design*, 136: 154-164.

Wulandari, P., Nagahiro, T., Michioka, K., Tamada, K., Ishibashi, K.-i., Kimura, Y. and Niwano, M. 2008. Coordination of carboxylate on metal nanoparticles characterized by Fourier transform infrared spectroscopy. *Chemistry letters*, 37 (8): 888-889.

Xie, H., Tkachenko, A. G., Glomm, W. R., Ryan, J. A., Brennaman, M. K., Papanikolas, J. M., Franzen, S. and Feldheim, D. L. 2003. Critical flocculation concentrations, binding isotherms, and ligand exchange properties of peptide-modified gold nanoparticles studied by UV− visible, fluorescence, and time-correlated single photon counting spectroscopies. *Analytical chemistry*, 75 (21): 5797-5805.

Yakoh, A., Rattanarat, P., Siangproh, W. and Chailapakul, O. 2018. Simple and selective paper-based colorimetric sensor for determination of chloride ion in environmental samples using label-free silver nanoprisms. *Talanta*, 178: 134-140.

Yang, Y. and Chui, T. F. M. 2017. Aquatic environmental changes and ecological implications from the combined effects of sea-level rise and land reclamation in Deep Bay, Pearl River Estuary, China. *Ecological Engineering*, 108: 30-39.

Yuan, Z., Du, Y., Tseng, Y.-T., Peng, M., Cai, N., He, Y., Chang, H.-T. and Yeung, E. S. 2015. Fluorescent gold nanodots based sensor array for proteins discrimination. *Analytical chemistry*, 87 (8): 4253-4259.

Yusufu, D. and Mills, A. 2018. Spectrophotometric and Digital Colour Colourimetric (DCC) analysis of colour-based indicators. *Sensors and Actuators B: Chemical*, 273: 1187-1194.

Zhang, M., Sun, Y., Liu, Y., Qiao, F., Chen, L., Liu, W.-T., Du, Z. and Li, E. 2016. Response of gut microbiota to salinity change in two euryhaline aquatic animals with reverse salinity preference. *Aquaculture*, 454: 72-80.

Zhang, Y., Li, M., Niu, Q., Gao, P., Zhang, G., Dong, C. and Shuang, S. 2017. Gold nanoclusters as fluorescent sensors for selective and sensitive hydrogen sulfide detection. *Talanta*, 171: 143-151.

Zhang, Z.-S., Song, X.-L., Lu, X.-G. and Xue, Z.-S. 2013. Ecological stoichiometry of carbon, nitrogen, and phosphorus in estuarine wetland soils: influences of vegetation coverage, plant communities, geomorphology, and seawalls. *Journal of Soils and Sediments*, 13 (6): 1043-1051.

Žiljak, V., Pap, K., Stanimirović, I. Ž. and Vujić, J. Ž. 2012. Managing dual color properties with the Z-parameter in the visual and NIR spectrum. *Infrared physics & technology*, 55 (4): 326-336.

Zohora, N., Kumar, D., Yazdani, M., Rotello, V. M., Ramanathan, R. and Bansal, V. 2017. Rapid colorimetric detection of mercury using biosynthesized gold nanoparticles. *Colloids and Surfaces A: Physicochemical and Engineering Aspects*, 532: 451-457.

Zuma, J. 2014. Address by President Zuma at the operation Phakisa: Unlocking the economic potential of the ocean economy open day. In: *Proceedings of the International Convention Centre (ICC), Durban*. Retrieved from http://www.presidency.gov.za., 1: 1-7.

Annexures

Annexure A: Lovibond results for the quantification of NaCl in standard solutions and samples.

NaCl Standard concentration	**Quantification of NaCl by Lovibond device**
0 ppT	

5 ppT	
10 ppT	

15 ppT	
20 ppT	

25 ppT	
30 ppT	

35 ppT	
40 ppT	

Samples	Quantification of NaCl by Lovibond device
Blue lagoon beach ≈35 ppT	

Suncoast beach ≈30 ppT	

Durban South beach ≈30 ppT	

Durban Harbour S1 ≈15 ppT	

Durban Harbour S2 ≈10 ppT	
Umgeni estuary	

>30 ppT	
Umgeni estuary 100m upstream ≈30 ppT	

Umgeni estuary 200m upstream ≈30 ppT	

Umgeni estuary 300m upstream ≈25 ppT	
Umgeni estuary 400m upstream ≈5 ppT	

Distilled water Simulated seawater (3g) NaCl ≈30 ppT	

Tap water Simulated seawater (3.5g) NaCl ≈35 ppT	

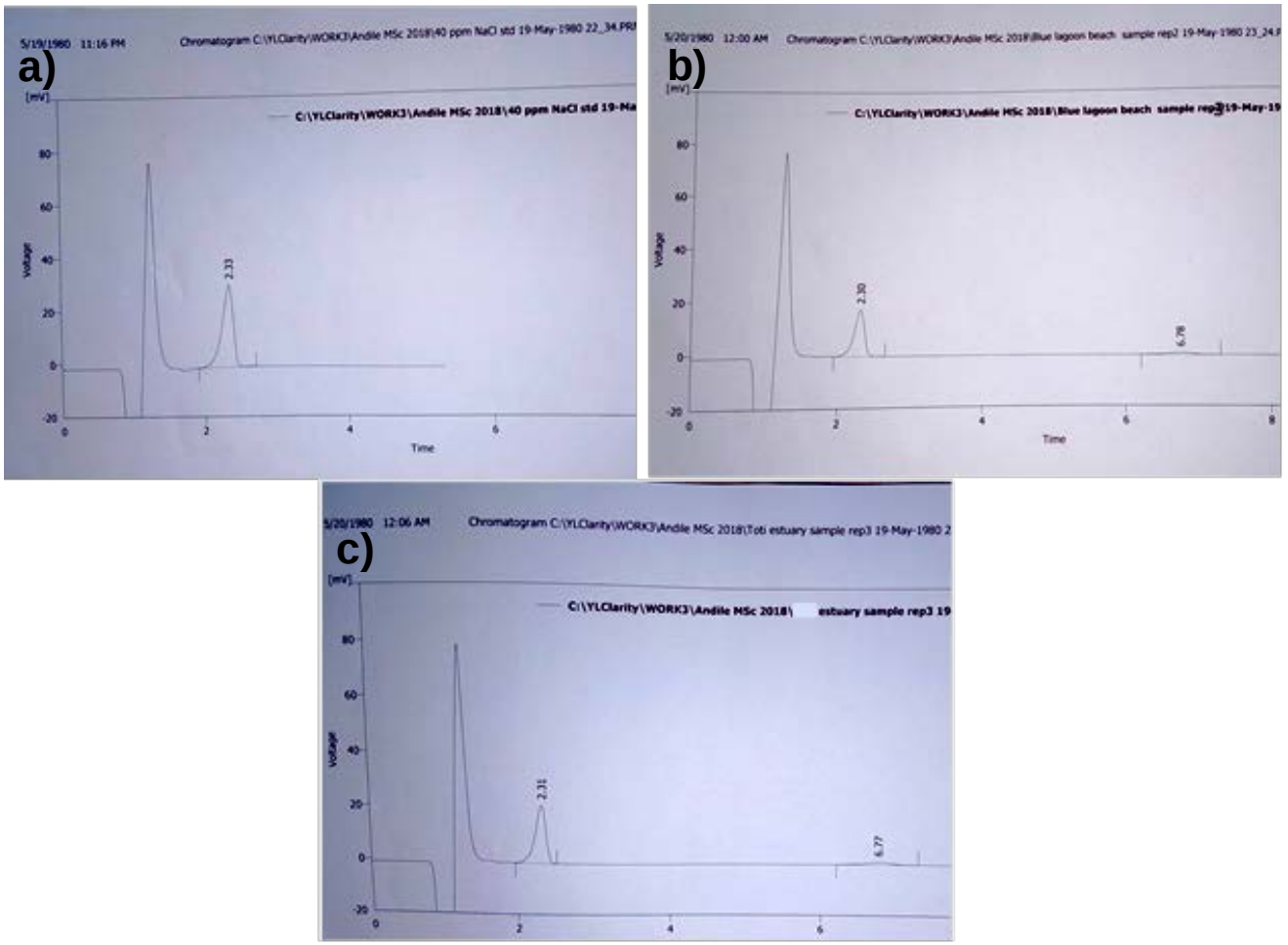

Annexure B: Typical ion chromatograms for NaCl standard 40 ppm, seawater sample and estuarine water sample.

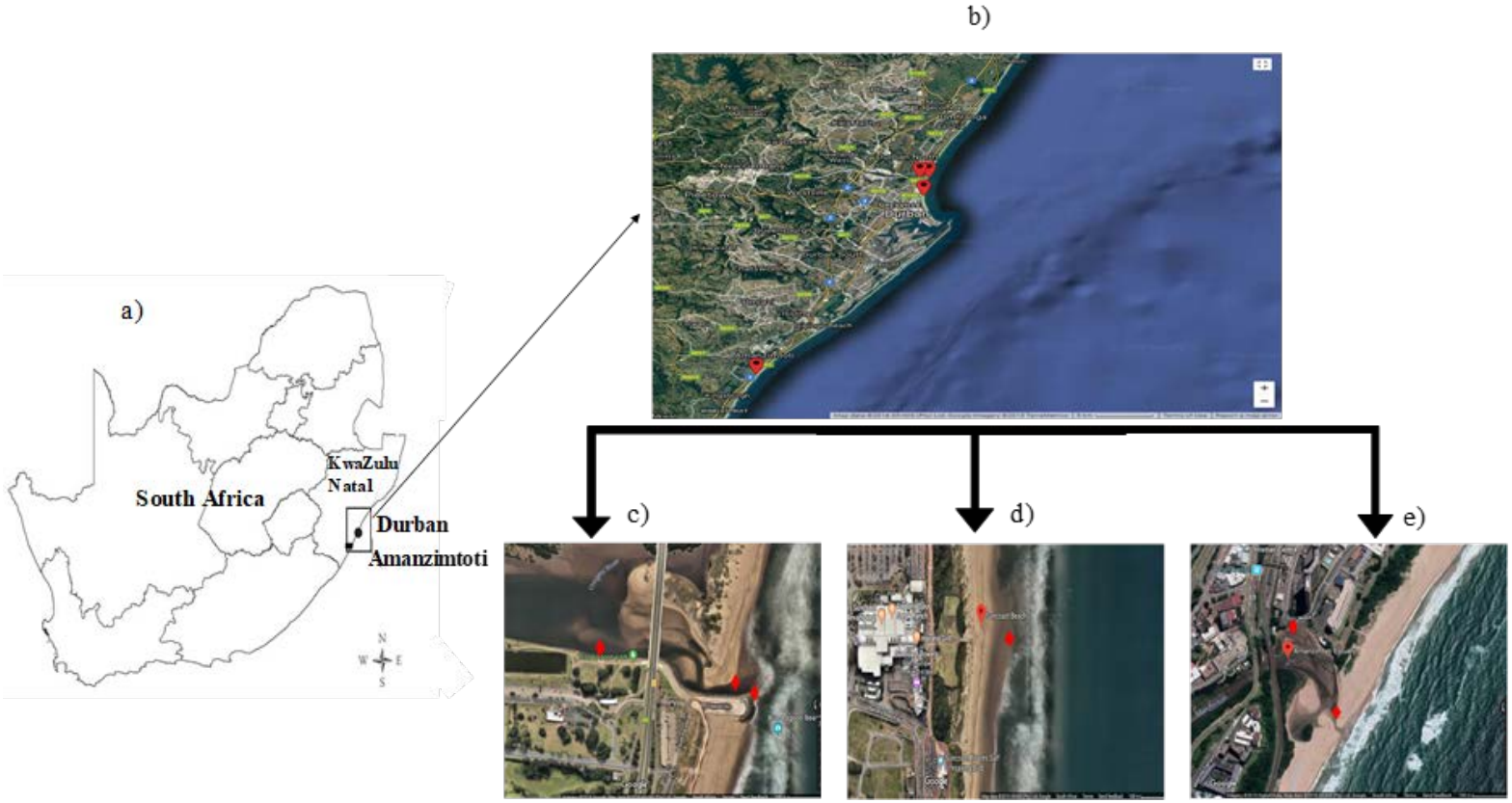

Annexure C: Map and sampling locations

(a) Map of South Africa with sampling locations. (b) Satellite map showing sampling points in Durban and Amanzimtoti along the sea coast areas (c) Umgeni estuary, upstream (405 m away from mouth) and Blue lagoon beach sampling points. (d) Amanzimtoti estuary and upstream (205 m away from mouth) sampling points. (e) Suncoast beach sample point. (The red diamond shape represents the actual sampling position on site).

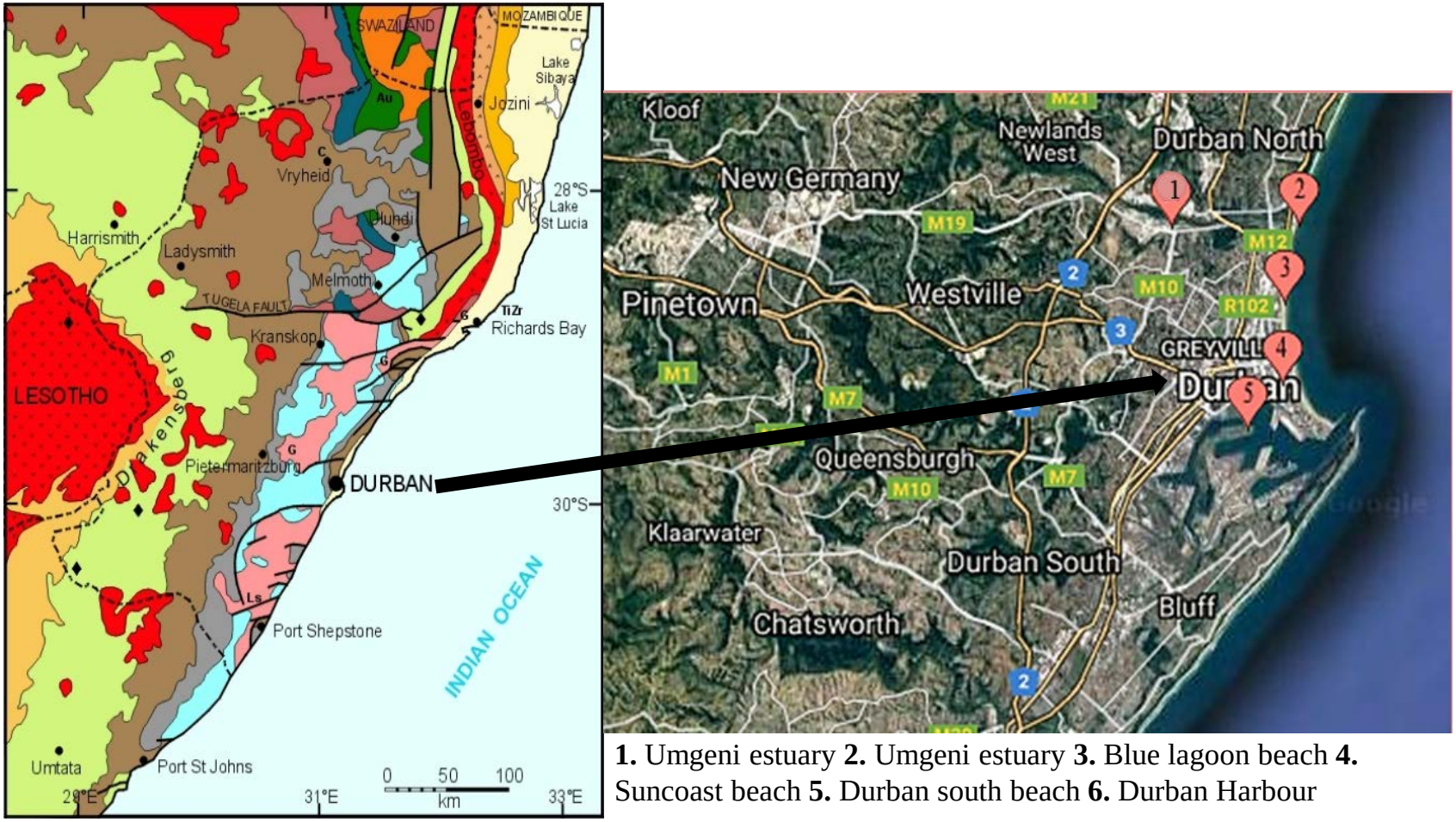

1. Umgeni estuary **2.** Umgeni estuary **3.** Blue lagoon beach **4.** Suncoast beach **5.** Durban south beach **6.** Durban Harbour

Annexure D: Sampling No. 2; map of sample locations in Durban city in South Africa.